UNIVERSIDADE DE ÉVORA

ARCHMAT

(ERASMUS MUNDUS MASTER IN ARCHaeological MATerials Science)

Mestrado em Arqueologia e Ambiente

Morphological and chemical characterization of tintypes and ambrotypes

Leonor Costa 34314

Supervisors:

Professor Teresa Ferreira, Universidade de Évora

Professor Catarina Miguel, Universidade de Évora

Évora, September 2016

A Tese não inclui as críticas e sugestões do Júri

Acknowledgements

I want to acknowledge my supervisors, Professor Teresa Ferreira and Doutora Catarina Miguel, for their much prised advice, guidance and support. I am very thankful to Margarida Nunes for her precious help, patience and availability to clarify (a lot) of things I struggled with. Also, Sónia Costa for the technical photography and Milene Trindade for handling the conservation issues.

I also want to thank my friends and fellow Archmatians, Milan Marković for his kindness and wholehearted friendship; Whitney Jacobs, Diego Badillo and Dauren Adilbekov for their friendships and wide-ranging conversations, sometimes, though rarely, even about our projects; and everyone else for sticking together and having fun wherever we went.

Finally, and most vitally, I want to thank my parents. For so many things they wouldn’t fit.

Table of Contents

Acknowledgements i

Table of Contents ii

List of figures ii

List of tables v

Abstract ii

Chapter I: Introduction

1.1. Introduction to the subject 1

1.2. The basic elements of photography 1

1.3. Historical context 3

1.4. The wet collodion process 4

1.4.1. The Ambrotype 8

1.4.2. The Tintype 11

1.4.3. Retouched photographs 15

1.4.4. Finishing varnishes 17

1.5. Degradation of photographic objects 18

1.5.1. General degradation 18

1.5.2. Degradation of the image forming particles 18

1.5.3. Degradation of the collodion 19

1.5.4. Degradation of the support 20

1.6. Review of the analytical techniques used in the characterization of photographic items 22

1.6.1. Working principles of the analytical techniques used in this work 23

1.6.1.1. Technical photography 23

1.6.1.2. Optical Microscopy (OM) 24

1.6.1.3. Scanning Electron Microscopy coupled with Energy Dispersive Spectroscopy (SEM-EDS) 25

1.6.1.4. Micro-Fourier Transform Infrared Spectroscopy (μ-FT-IR) 26

1.6.1.5. Micro-Raman Spectroscopy (μ-Raman) 27

1.6.1.6. Micro X-ray Diffraction (μ-XRD) 28

Chapter II: Materials and Methods

2.1. Sample selection 32

2.2. Methodology 35

2.2.1. Technical photography 36

2.2.2. Optical Microscopy (OM) 36

2.2.3. Scanning Electron Microscopy coupled with Energy Dispersive Spectroscopy (SEM-EDS) 37

2.2.4. Micro-Fourier Transform Infrared Spectroscopy (μ-FT-IR) 37

2.2.5. Micro-Raman Spectroscopy (μ-Raman) 38

2.2.5. Micro X-ray Diffraction (μ-XRD) 38

Chapter III: Results and Discussion

3.1. Morphological and chemical characterization 40

3.1.1. Technical photography 40

Ambrotypes 40

Tintypes 43

3.1.2. Optical Microscopy (OM) 45

Ambrotypes 45

Tintypes 51

3.1.3. Scanning Electron Microscopy coupled with Energy Dispersive Spectroscopy (SEM-EDS) 56

Ambrotypes 56

Tintypes 66

3.1.4. Micro-Fourier Transform Infrared Spectroscopy (μ-FT-IR) 73

Ambrotypes 73

Tintypes 74

3.1.5. Micro-Raman Spectroscopy (μ-Raman) 75
Ambrotypes 75
Tintypes 77
3.1.6. Micro X-ray Diffraction (μ-XRD) 79
Ambrotypes 79
Tintypes 81
Brass mats 83
Chapter IV: Conclusions 85
References 87
Appendices 93

List of figures

Figure 1: steps in the formation of a silver halide image. 2
Figure 2: Niépce's first photograph. Source: hrc.utexas.edu 3
Figure 3: iodized collodion being poured onto the plate (top) and the excess being poured back into the bottle (bottom). Source: americanhistory.si.edu 5
Figure 4: example of a thumb mark left on a wet plate collodion negative. Source: graphicatlas.org 5
Figure 5: example of an ambrotype with drip lines. Source: graphicatlas.org 6
Figure 6: scheme of the disposition of the elements of a cased daguerreotype, identical to cased tintypes and ambrotypes. Source: www.phototree.com 7
Figure 7: example of a cased ambrotype (front and back). Source: americanantiquarian.org 8
Figure 8: thin section of an ambrotype on which varnish was applied as background. 9
Figure 9: example of an ambrotype with the black varnish applied on the opposite side of the collodion. Source: graphicatlas.org 9
Figure 10: ambrotype with a dark fabric as background. Source: graphicatlas.org 9
Figure 11: example of an ambrotype made on a dark glass, substituting the dark background. Positive image (left) and negative image (right). Source: graphicatlas.org 10
Figure 12: cross-section of a tintype. Source: graphicatlas.org 11
Figure 13: example of pinholes. Source: graphicatlas.org 12
Figure 14: example of a tintype in a case (left) and in a paper mat (right). 13
Figure 15: example of a tintype presented in a frame (left) and in a passe-partout (right). 13
Figure 16: example of a bon ton tintype, with two clipped corners (left) and of a *vignetted* bon ton tintype with clipped corners (right). Source:graphicatlas.org 14
Figure 17: a four lens camera used to produce bon tons. Adapted from [7] 14
Figure 18: example of a retouched tintype. Source: graphic atlas.org 16
Figure 19: example of a painted ambrotype. Source: graphicatlas.org 17
Figure 20: example of a photograph with silver mirroring. Source: notesonphotographs.org 18
Figure 21: example of an ambrotype with reticulation of the collodion. Source: graphicatlas.org 19
Figure 22: Example of mould on a collodion based object (50x specular light). Source: graphicatlas.org 19
Figure 23: example of the phenomenon of bleaching of the glass. Source: graphicatlas.org 20
Figure 24: example of cracking of the background varnish. Source: graphicatlas.org 21
Figure 25: example of abrasion and detachment of the binder and formation of rust. 22
Figure 26: the electromagnetic spectrum showing the different regions, measured in nanometres. Source: www.nailsmag.com 24
Figure 27: Scheme of the dark-field and bright-field modes on a microscope. 25
Figure 28: Structure of a scanning electron microscope (SEM). Adapted from [42] 25
Figure 29: interaction zone of electrons and specimen atoms below a specimen surface. Source: [42] 26
Figure 30: optical diagram of a simple specular reflectance accessory for FTIR instrument. 27
Figure 31: Optical diagram of a Raman microscope. Source: [42] 28
Figure 32: Bragg's diffraction by crystal planes. Source: [42] 29
Figure 33: Scheme of an X-ray diffractometer that follows the Bragg-Brentano geometry. 29

Figure 34: ambrotype A (AA) and ambrotype B (AB); tintype A (TA) and tintype B (TB) before the removal of the frame. 32
Figure 35: two ambrotypes from 1859 (estimated date). Source: phototree.com © 33
Figure 36: ambrotype dated from 1856 (estimate) (left) and tintype dated from 1858 (estimate) (right). Source: phototree.com© 34
Figure 37: Stereomicroscopic images of the inscriptions on the mat of Tintype A. 34
Figure 38: [Union Soldier and Barber] (American) 1861–1865 (left) and Unidentified Photographer, ca. 1863, United States (right). Source: icp.org 35
Figure 39: Tintype dated from 1862 (estimated). Source: phototree.com© (left) and Unidentified Photographer, ca. 1863, United States. Source: icp.org (right) 35
Figure 40: mapping of the areas observed with optical microscopy on ambrotypes A (AA) and B (AB) 45
Figure 47: mapping of the areas observed with optical microscopy on tintypes A and B. 51
Figure 42: mapping of the analysed areas with SEM-EDS on ambrotypes A and B. 57
Figure 43: mapping of the areas analysed with SEM-EDS on tintypes A and B. 66
Figure 44: μ-FTIR spectrum of ambrotype A. The inset, detail from the analysed spot. 74
Figure 45: μ-FTIR spectrum of ambrotype B. The inset, detail from the analysed spot. 74
Figure 46: μ-FTIR spectrum of tintype A. The inset, detail from the analysed spot. 75
Figure 47: μ-FTIR spectrum of tintype B. The inset, detail from the analysed spot. 75
Figure 48: mapping of the areas analysed with μ-Raman spectroscopy on ambrotypes A and B. 76
Figure 49: μ-Raman spectrum of ambrotype A (areas 1 and 2). 76
Figure 50: μ-Raman spectrum of ambrotype B. The inset, detail from the analysed spot. 77
Figure 51: mapping of the areas analysed with μ-Raman spectroscopy on tintypes A and B. 77
Figure 52: μ-Raman spectra of tintype A. The inset, detail from the analysed spots. 78
Figure 53: μ-Raman spectra of tintype B (areas 1 and 2). The insets, details from the analysed areas 78
Figure 50: μ-XRD diffractogram of the analysis of ambrotype A. The inset, detail of the analysed spot. 79
Figure 51: μ-XRD diffractogram of the analysis of ambrotype B. The inset, detail of the analysed spot. 80
Figure 52: μ-XRD diffractogram of the analysis of tintype A. The inset, detail of the analysed spot. 81
Figure 53: μ-XRD diffractogram of the analysis of tintype B. The inset, detail of the analysed spot. 82
Figure 54: μ-XRD results of the analysis of the four brass mats. 83
Figure 59: stick patterns of Cu (reference code: 00-004-0836) and Zn (reference code: 00-004-0831). 84

List of tables

Table 1: Daguerreotype typical formats. Adapted from [19]. 10
Table 2: typical tintype formats. Source: graphicatlas.org 13
Table 3: finishing varnishes used for collodion images, adapted from [33] 17
Table 4: normal and raking light, ambrotypes. 41
Table 5: transmitted light and UV radiation, ambrotypes. 42
Table 6: normal light, tintypes. 43
Table 7: raking light and UV radiation, tintypes. 44
Table 8: red pigment particles on the cheeks. Ambrotypes A and B, areas 2 and 2. 46
Table 9: image forming particles and the interface between highlights and a dark areas on ambrotypes A and B, areas 3 and 3. 46
Table 10: abrasion caused by the frames on ambrotypes A and B, areas 1 and 1. 47
Table 11: cracks (a) and gaps (b) on the varnish and the emulsion on ambrotype A, area 3. 48
Table 12: *drip line* and degraded areas on ambrotype A, area 4. 49
Table 13: cracks on the varnish and emulsion (a), varnish layers of different thickness (b) on ambrotype A, area 5. Gaps (c) and cracks (d, transmitted mode) on the dark varnish on the back side of ambrotype B. 50
Table 14: *drip line* with cracks, tintype A, area 1. Abrasion and gaps on the varnish, tintype B, area 2. 52
Table 15: abrasion and green degradation compound on tintype A, area 2 and tintype B, area 5. 53
Table 16: gold retouch on tintype A, area 3. Red pigment on tintype B, area 3 54
Table 17: *drip lines* on tintype A, area 5 and tintype B, area 1. 55
Table 18: back sides of the tintypes, showing a red degradation compound and varnish layers. 56
Table 19: VP-SEM images of highlights on ambrotype A (A and B) and on ambrotype B (C and D); dark areas on ambrotype A (E and F) and on ambrotype B (G and H). 58
Table 20: VP-SEM images interfaces on ambrotype A (A and B) and on ambrotype B (C and D). 59
Table 21: VP-SEM image of the areas 1, 2 and 3 showing the points analysed (a, b, c and d); elemental point analysis of a particle showing the presence of silver on the image forming particles (a); of the glass surface (b), showing the support to be a soda-lime-silica (Na-Ca-Si) glass; of a particle of the red pigment, probably iron oxide (c); and of a particle containing Ba and S (d). 60
Table 22: VP-SEM images of areas 1 and 2 showing the points analysed (a, b and c); elemental point analysis of a particle showing the presence of silver on the image forming particles (a); of a particle on a tarnished area with Ag and S, suggesting the presence of silver sulphide (b); on the dark area, showing that the support is a soda-lime-silica glass (c). BSE, backscattered electrons; elemental maps (Ag, S). 62
Table 23: VP-SEM images of area 2 showing the points analysed (d and e); elemental point analysis of a particle containing Ag and I (d); and of a particle containing Na and S. 63
Table 24: VP-SEM image of area 3 showing the points analysed (a and b); elemental point analysis on a particle containing Ag and Cl (a); and on a particle containing Cu, S and Cl (b). 64
Table 25: BSE, backscattered electrons; elemental maps (Cu, S, Cl and Ag). VP-SEM image of area 4 showing the point analysed (c); elemental point analysis on a pigment particle containing Fe (c). 65

Table 26: VP-SEM images of highlights on tintype A (A and B) and on tintype B (C and D); dark areas on tintype A (E and F) and on tintype B (G and H). 67
Table 27: VP-SEM images interfaces on tintype A (A and B) and on ambrotype B (C and D). 68
Table 28: VP-SEM images of areas 1 and 2 showing the points analysed (a, b and c) and of the golden particles (i); elemental point analysis on a particle containing Ag (a); on a particle containing Au (b); and on particle containing Ag and S (c). 69
Table 29: VP-SEM images of area 3 showing the points analysed (a and b); elemental point analysis on a particle containing Ag and I (a) and on a particle containing Fe (b). 70
Table 30: VP-SEM images of areas 1 and 2 showing the points analysed (a and b); elemental point analysis on a particle containing Ag (a); and on a particle containing Ag, S and Na (b). . 71
Table 31: VP-SEM images of area 3 showing the point analysed (a); elemental point analysis on a particle containing Fe (a). BSE, backscattered electrons; elemental maps (C, Fe). 72

Abstract

The present work was done on two ambrotypes and two tintypes. It aimed evaluate their chemical and physical characteristics, especially their degradation patterns. Moreover, to understand the materials used for their production and cross-check analytical and historical information about the production processes. To do so multi-analytical, non-destructive methods were applied. Technical photography highlighted the surface morphology of the objects and showed the distribution of the protective coatings on their surfaces through UV radiation, which were very different between the four pieces. OM allowed for a detailed observation of the surfaces along with the selection of areas of interest to be analysed with SEM-EDS. SEM-EDS was the technique used most extensively and the one that provided the most insightful results: it allowed to observe the morphology of the image forming particles and the differences between highlights, dark areas and the interfaces between them. Also, elemental point analysis and elemental maps were used to identify the image forming particles as silver and to detect the presence of compounds related to the production, particularly gold used to highlight jewellery, iron as the red pigment and traces of the compounds used in the photographic process containing Ag, I, Na and S . Also, some degradation compounds were analysed containing Ag, Cu, S and Cl. With μ-FT-IR the presence of collodion was confirmed and the source of the protective varnishes was identified, particularly mastic and shellac, in either mixtures of the two or only one. μ-Raman detected the presence of metallic silver and silver chloride on the objects and identified one of the red pigments as Mars red. Finally, μ-XRD showed the presence of metallic silver and silver iodide on both ambrotypes and tintypes and hematite, magnetite and wuestite on the tintypes.

Resumo

O presente estudo foi desenvolvido sobre dois ambrótipos e dois ferrótipos. O propósito consiste em estudar as suas características químicas e físicas, dando particular ênfase aos padrões de degradação. Também é pretendido compreender os materiais usados na sua produção e relacionar esta informação analítca com dados históricos de manuais técnicos contemporâneos à produção dos objectos. Para tal foram utilizadas técnicas multi-analíticas e não destrutivas. O uso da fotografia técnica permitiu uma observação da morfologia das superficies dos objectos e da distribuição das camadas de verniz através da radiação UV, muito diferente entre os quatro. A microscopia óptica proporcionou uma observação detalhada das superfícies assim como a selecção de pontos de interesse para serem analisados com SEM-EDS. SEM-EDS foi a técnica usada mais extensivamente e a que proporcionou os resultados mais detalhados: observação da morofologia das partículas formadoras da imagem e as diferenças entre zonas de altas luzes, baixas luzes e as interfaces entre elas. A análise elemental e os mapas elementares foram usados para detectar prata nas partículas formadoras da imagem e a presença de compostos relacionados com a produção, em particular ouro utilizado para realçar joalharia, ferro no pigmento vermelho e vestígios de compostos utilizados no processo fotográfico incluindo Ag, I, Na e S. Do mesmo modo, alguns compostos de degradação foram analisados contendo Ag, Cu, S e Cl. Com μ-FT-IR a presença de colódio foi confirmada e identificada a origem dos vernizes, mástique e goma-laca, tanto em misturas dos dois como apenas um. Com μ-Raman foi detectada a presença de prata metálica e de cloreto de prata e identificado um dos pigmentos vermelhos como Mars red. Finalmente, μ-DRX revelou a presença de prata metálica e iodeto de prata tanto nos ambrótipos como nos ferrótipos e hematite, magnetite e wuestite nos ferrótipos.

CHAPTER 1: INTRODUCTION

1.1. Introduction to the subject

Since its discovery, photography has gained an increasing importance in cultural heritage. Although disregarded as an actual art form on the first decades of its existence, it is now solidly established as one. Archives, museums and private collections comprise large amounts of photographs, which can be a testimony of our ancestors and their lifestyles as well as objects of artistic expression. Thus the importance of this medium and the keenness to study and understand these objects. Although photography had a profound social presence and influence in the last 150 years, the conservation of photographic objects has been developed relatively recently in the last 30 years. This has been done through the chemical characterisation and historical research of photographic objects [1]. Regarding the subjects of this study, tintypes and ambrotypes, the scientific literature is still rare. During the period of their production, a great variety of materials was used, because photographic processes were evolving very quickly and a lot of materials were being tried to achieve better results. Also, sometimes materials were used besides the ones documented on manuals of the time. Therefore, when analyzing these objects, different materials can be encountered, with different chemical and physicochemical characteristics. They are multilayered items, composed of organic and inorganic compounds and their degradation phenomena are strictly related to the composition of their layers: hence the importance of their physical and chemical analysis.

1.2. The basic elements of photography

Photographic objects are composite items, typically composed of three layers: the support, which can be glass, metal or paper, or another; the emulsion, which comprises a binder and the image forming particles; and additional layers such as colour particles and finishing coatings [2].

Black and white photographic images, in particular, are usually made up of an emulsion which includes silver particles embedded in a thin layer of binder, a transparent compound such as gelatine, collodion or albumen. This emulsion rests on a support, which can be made out of glass, paper, metal or film, among others. The image is obtained through several steps. First, a support with a light sensitive emulsion has to be acquired. This emulsion typically contains crystals of a soluble silver halide salt, such as silver

bromide, suspended on the binder. Then, this film is exposed to light. During the exposure, a latent image is formed by a group of silver particles over the emulsion. These are usually formed by a small number of atoms, undetectable by optical means. The interaction between the light and the silver halide grains induces the photo reduction of AgX:

$$AgX\ (crystal) + h\vartheta\ (radiation) \rightarrow Ag^{+} + X + e^{-}$$

Then, the image is developed. The *developer bath* is composed of a developing agent, a base (e.g. sodium carbonate, Na_2CO_3), an anti-oxidizing agent (e.g. sodium sulphite, Na_2SO_3) and a restrictor (e.g. potassium bromide, KBr). When the plate is immersed, the reaction that formed the latent image is amplified in the order of 10^9, so that it becomes visible by naked eye. This is achieved through the reduction of the Ag^+ ions to metallic silver: redox reaction in which the silver ions are reduced and the developing agent, ionized in a basic environment, is oxidized:

$$Ag^{+} + developing\ agent\ (reduced\ form) \rightarrow Ag^{0} + developing\ agent\ (oxidized\ form)$$

After the development, a s*top bath* is used to stop the developing process. Because the non-sensitive crystals that contain silver halides are still active after the developing step, they might slowly react with the developing agent. The bath consists of a water solution with a weak acid, such as acetic acid (CH_3COOH). After, a *fixing bath* is used to remove the active silver ions from the emulsion. Usually potassium cyanide (KCN) is used, which reacts with the silver halides forming complexes ($[Ag(S_2O_3)_2]_3^-$ and $[Ag(CN)_4]_3^-$) that are easily washed with water. It can also contain sodium sulphite, acetic acid and boric acid (H_3BO_3). Lastly, the image is washed and dried and the final product is obtained (Figure 1) [3, 4].

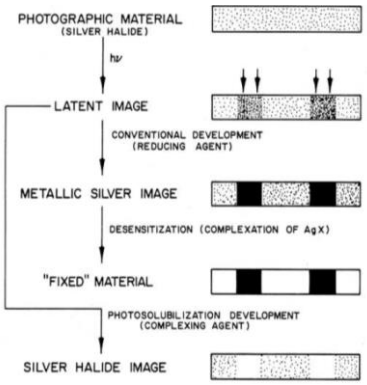

Figure 1: steps in the formation of a silver halide image.
Source: MRV Sahvun J. Chem. Educ., 1974, 51 (2), p 72

1.3. Historical context

The interest in exploring light sensitive compounds to produce images begun in the late 1700s. The first photographic processes were published in 1839, one in Paris and another in London: the daguerreotype and the calotype [5]. The daguerreotype is a monochromatic image on a metal plate, unique and not duplicable. It was first published in January 1839 in the French Academy of Sciences bulletin, by Louis Jacques Mande Daguerre. It was the outcome of a research led by Daguerre and Joseph Nicephore Niépce since 1920. In 1827, Niépce managed to produce an image by exposing a treated metal plate to light in a *camera obscura* for over 8 hours, using bitumen, a varnish ingredient that hardens and becomes insoluble once exposed to light (Figure 2). Through a common goal, Niépce and Daguerre started working together, and after Niépce's death in 1833, Daguerre continued the work. His definite step towards the creation of the daguerreotype was taken in 1835, when he discovered latent development, i.e., the fact that the images formed by exposure can be chemically developed after a relatively short exposure time. In this case he used mercury vapour as developer. He also found that the action of light could be stopped after the development of the image, using a bath of sodium thiosulphate to wash the unexposed silver salts. The daguerreotype process was logistically challenging as well as expensive and time consuming. Despite this, it attracted numerous operators and the news of its discovery spread around Europe. It was published in foreign scientific papers, but was not significantly commercially successful anywhere except for France, England and the USA [6].

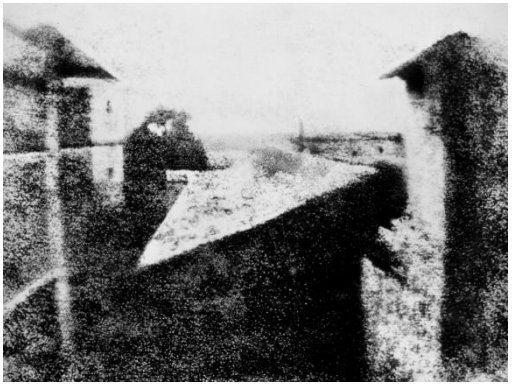

Figure 2: Niépce's first photograph. Source: hrc.utexas.edu

The calotype or talbotype, is a monochromatic image on paper, laterally reversed, i.e., a negative. It can be placed in contact with another photo sensitive surface to transfer the reversed image, obtaining one with normal spatial and tonal values. It was made

public in February 1839, in London, by William Henry Fox Talbot. He used paper treated with a solution of silver nitrate and gallic acid, which was also used to develop the image. His process had advantages over the daguerreotype but it was neglected by the public, possibly because the process of replication seemed hard to grasp. Despite this possibility of reproduction offered by the negative, the paper support had limitations regarding sharpness, definition and fading. Thus, succeeding attempts in replacing the paper for a glass support were conducted by various researchers. A process using albumen as the binder was published both in France and in the USA, in 1847. It produced images without grain but the process was complicated and the exposure time too long. The definite alternative came in 1850, both from Robert Bingham's *Photogenic Manipulation* and Gustave Le Gray's formula for iodized collodion in his photographic method on paper and glass. However, it was Frederick Scott Archer who introduced formulas with practical results in *The Chemist*, in London 1851. The process was cheap, had a short exposure time and produced high quality images. This opened doors for an era of commercial expansion of photographic portraiture and the beginning of amateur photography [6]. In 1871, Richard Leach Maddox introduced the use of gelatine as a binder, which had advantages over the previous materials. In fact, after the First World War, the production of albumen and collodion papers was discontinued and silver bromide gelatin on paper lead the market until the Second World War, after which resin-coated papers and chromogenic materials were introduced [7].

1.4. The wet collodion process (1851-1885)

Collodion is a solution of nitrocellulose in ether and alcohol. It was discovered independently in 1847 by Louis Menard, in France, and by John Parker Maynard, in Boston [8]. The first recipes to produce nitrocellulose, or nitrated cotton, used a mixture of potassium nitrate or nitric acid, sulphuric acid and pure cotton, at 140ºC. Then, collodion could be made by mixing nitrocellulose with ether and alcohol, as mentioned above [9]. When applied to several materials, collodion adheres firmly in a thin and clear film. The compound was originally used as a consolidant for medical cloths but was soon adopted to photography, having ideal functions as a binder for light-sensitive silver halides: is transparent and clear; does not turn yellow with aging; does not swell when in contact with water; and is waterproof after drying [10, 11].

The general photographic formula consists of a 2% solution of collodion with small amounts of potassium, cadmium, ammonium or zinc halides (usually iodides or bromides) and hydrochloric acid, applied directly on a glass plate, forming a thin and clear film [12, 13]. The steps for the wet collodion process are typically the following: preparing the plate, coating it with collodion, sensitizing, exposing, developing and fixing the image [14]. The plate was cleaned with a solution of water, alcohol and calcium carbonate in equal proportions, or a mixture of nitric acid with a thin powder like calcined lamp black [8]. Then, the collodion solution was applied on the plate, holding it between the thumb and forefinger, tilting it until an even coating was obtained and pouring the excess collodion into a bottle (Figure 3). This process left thumb marks in one of the corners of the plates (Figure 4). It is also common to observe bluish or whitish lines, *drip lines*, in the corners of the images, as a consequence of the accumulation of collodion when it was poured back into the bottle (Figure 5) [15].

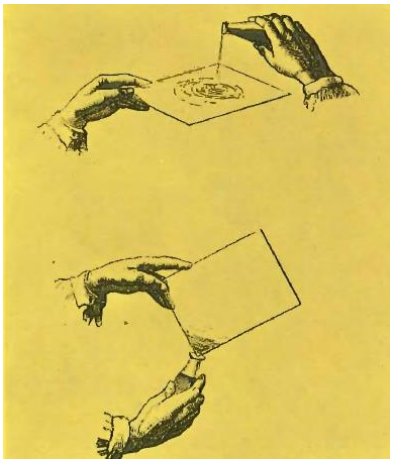

Figure 3: iodized collodion being poured onto the plate (top) and the excess being poured back into the bottle (bottom). Source: americanhistory.si.edu

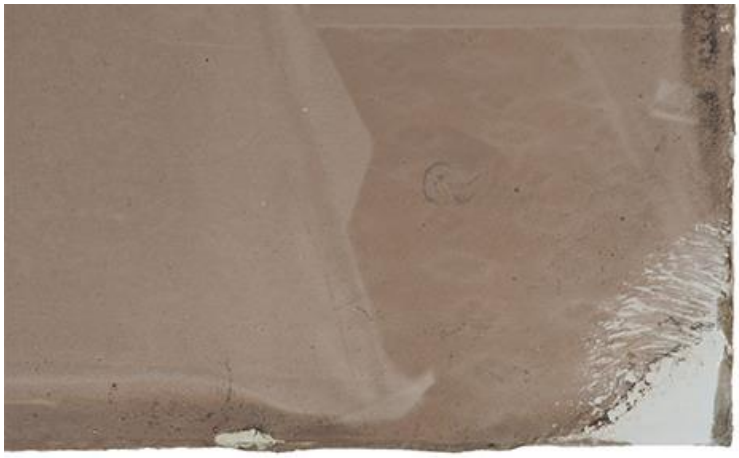

Figure 4: example of a thumb mark left on a wet plate collodion negative. Source: graphicatlas.org

Figure 5: example of an ambrotype with drip lines. Source: graphicatlas.org

After the application of the collodion solution, the plate was immersed in an aqueous solution of silver nitrate ($AgNO_3$), to precipitate silver halides from the salts within the upper layer of the plate. Consequently, the collodion enclosed light-sensitive silver iodide and, sometimes, silver bromide. Then, the plate was exposed while still wet (hence the term wet collodion) for 20 seconds to 3 minutes, depending on the light. The exposure induced a photo reduction of the silver halides, creating a latent image. After, the image was developed under red light with a solution of a silver salt (silver nitrate e.g.) and a reducing agent (pyrogallic acid $C_6H_6O_3$ e.g.), which reduces the silver salt to metallic silver. The acid was washed off with water and the plate exposed to sunlight and sodium thiosulphate ($Na_2S_2O_3$), a fixator that solubilizes the unexposed light sensitive silver salts [8, 16]. Then, the plate was washed to remove the compounds used during the fixing process, and dried. After that, it could be coated with a protective varnish, such as gum sandarac or shellac, for protection and to prevent oxidation [8]. The varnish was applied in the same way as the collodion layer. Sometimes, it is possible to observe exposed collodion areas, usually along the edges and corners of the plates, when the photographer did not even the varnish coverage [15].

The wet collodion method underwent some developments, which perfected the technique. First, it was found that using smaller amounts of bromides improved the sensitivity to blue-green hues. The introduction of a ferrous sulphate ($FeSO_4$) developer rather than pyrogallic acid reduced exposure times, making studio portraiture easier. By the end of the 1850s, all studio photographers were using ferrous sulphate. Also, by this time potassium cyanide was being used as the fixing agent, instead of sodium thiosulfate. The combination of the iron development and the cyanide fixing produced a light yellowish brown image that contributed to spectral density when making negatives [10]. In conclusion, for the development, pyrogallic acid or ferrous sulphate could be used, the

first giving a darker and the second a lighter hue. As fixating agents, sodium thiosulphate or potassium cyanide were used, the first giving a darker brownish-grey image and the second a lighter, milky tone [8]. In the 1850s, dry collodion plates were introduced, due to some difficulties associated with the wet collodion method, particularly when working outdoors [17]. First, these were done by coating the sensitized plate with hygroscopic materials such as beer, honey or glycerine. Then, in 1856, the practice of sealing the sensitized wet-plate with albumen was introduced, which allowed photographers to sensitize the plate several weeks before use. Dry collodion plates, however, were substantially less sensitive than wet plates and were used almost exclusively in outdoor photography [15].

As for additional layers, collodion images were easier to paint than daguerreotypes, accepting several dry and wet materials. The images could be painted with dry powdered, oil- or water-based paints, applied on top of the emulsion [18]. The images made with this process include ambrotypes, on glass, and tintypes, on japanned iron [10]. These could be presented in cases, such as the ones used for daguerreotypes. The cases were made with wood covered in leather, and velvet on the inside. They typically enclose the photograph covered with a glass and a brass mat, enclosed by a thin preserver frame (Figure 6 and Figure 7) [15].

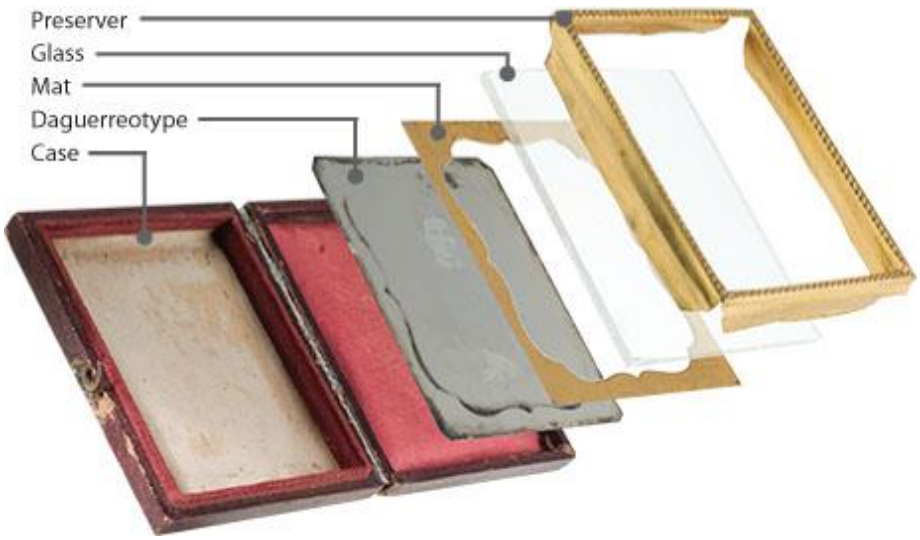

Figure 6: scheme of the disposition of the elements of a cased daguerreotype, identical to cased tintypes and ambrotypes. Source: www.phototree.com

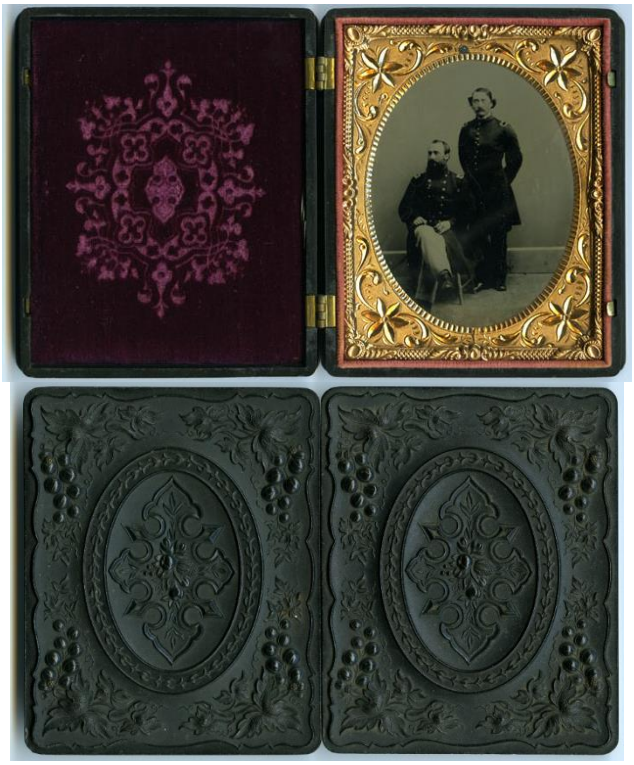

Figure 7: example of a cased ambrotype (front and back). Source: americanantiquarian.org

1.4.1. The Ambrotype (1852-1880)

Ambrotypes are wet collodion images on glass. They are *direct positives*, i.e., deliberately underexposed negative images that appear as positives when placed against a dark surface. This effect occurs because the areas of the collodion which were not impressed by light are transparent and appear dark when laid on a dark background. These contrast with the areas impressed, which reflect light and appear bright [7]. Ambrotypes could be mounted in different ways: with the collodion layer facing downwards, without the need for a protective glass; or with the collodion layer facing upwards, with a protective glass on top of it, with or without a case [11]. The dark background could be in the form of a black varnish applied directly on the collodion layer or on the opposite side of it (Figure 8 and Figure 9) [9]. Instead, it could also be a dark paper, metal or fabric on the back of the picture (Figure 10). Also, a dark glass could be used without the need of a background to achieve the positive effect (Figure 11) [11]. The ambrotypes which used the black varnish as background were cheaper than the other options. Although they were negatives, the image was not necessarily reversed from right to left: if the image was mounted with the image facing downwards, it would represent the actual order.

However, this way of mounting the picture made it loose brightness and detail, so most photographers preferred to lay the image side facing upwards, although it was inverted [7].

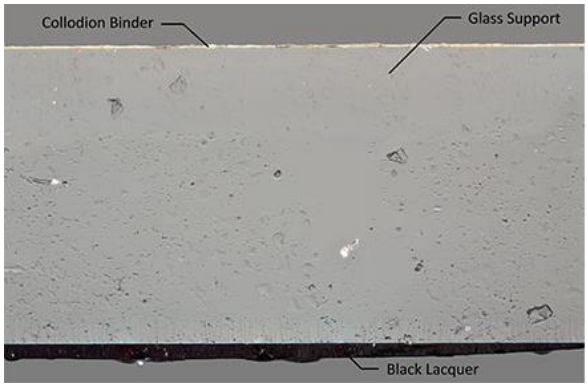

Figure 8: thin section of an ambrotype on which varnish was applied as background. Source: graphicaltas.org

Figure 9: example of an ambrotype with the black varnish applied on the opposite side of the collodion. Source: graphicatlas.org

Figure 10: ambrotype with a dark fabric as background. Source: graphicatlas.org

Figure 11: example of an ambrotype made on a dark glass, substituting the dark background. Positive image (left) and negative image (right). Source: graphicatlas.org

Regarding the support, the glass used for photography in the 19th century was made with sodium or potassium/sodium silicates and produced with an excess of fluxing agents, which made them chemically unstable [11]. The formats used for ambrotypes correspond to the ones used for daguerreotypes, which are the following, being the sixth and the fourth the most popular [7]:

Table 1: Daguerreotype typical formats. Adapted from [19].

Designation	Inches	Centimetres
Whole	6 ½ x 8 ½	16.5 x 21.5
Half	4 ¼ x 6 ½	10.5 x 16.5
Quarter	3 ¼ x 4 ¼	8.3 x 10.5
One-sixth	2 ¾ x 3 ¼	7.0 x 8.3
One-eight	2 1/8 x 3 ¼	5.3 x 8.3

According to photography manuals of the time, the back varnish could be made using a mixture of turpentine, asphaltum and Canada balsam; benzole, asphaltum and India rubber; camphene, white wax, bitumen and lampblack; camphor, shellac, alcohol and Canada balsam; or sandarac, lavender oil, alcohol and chloroform. Also, a clear varnish used on top of the image, for a finishing effect could be applied [14, 20]. The technique was introduced in 1852, but the process was first published in 1854 by James Anson Cutting through a patent for an *Improved Process of Taking Photographic Pictures upon Glass*. It consisted on a method for adding camphor to the nitrocellulose used for the collodion, and sealing the image with a balsam and a cover glass. Once the process was understood and perfected, it was quickly adopted as a popular studio portrait technique, replacing the daguerreotype. Although ambrotypes were produced in the same

size and with similar treatment (hand coloured, framed with glass, and encased), they had the advantage of being cheaper, having shorter exposure times and being less reflective and easier to see than the daguerreotype, which was made on a polished silver plate [10]. Whereas by definition a true ambrotype would be made by the Cutting technique, the word quickly became a generic term for all collodion direct positives on glass that were made in the camera, most of them produced without the sealing [21]. In fact, the Cutting method was found to be unnecessary because the finishing varnish provided the needed protection to the picture. Also, ambrotypes made with the Cutting method typically exhibit a yellowish-green hue presumably caused by the balsam [15]. Although the ambrotype was produced until 1880, its most popular period was between 1856 and 1858, from when they substituted the daguerreotypes until they were replaced by the tintype, cheaper and more resistant.

1.4.2. The Tintype (1856-1930)

Tintypes, or ferrotypes, are also *direct positives*. They are positive wet collodion images on a metal support coated with a black varnished layer on which the emulsion was applied (Figure 12). In this case, the positive effect is obtained by applied the collodion on a dark support, which will make the transparent areas of the collodion appear black [10].

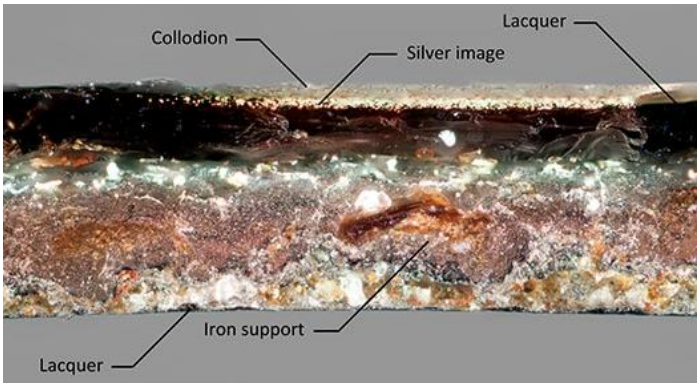

Figure 12: cross-section of a tintype. Source: graphicatlas.org

The first mention of the process was in 1855, by the French photographer Adolphe A. Martin, but had little impact. In the same year, a similar experiment was conducted by Hamilton Smith of Gambier, in Ohio, USA. He patented his product in 1856, introducing a new method to obtain "[…] positive impressions upon a jappaned surface previously prepared upon an iron or other metallic or mineral sheet or plate by means of collodion

and a solution of a salt of silver and a camera […] " [22]. Contemporarily, the process was also patented in England by William Kloen and Daniel Jones [10]. The technique is virtually the same as for the ambrotypes, but with a metal plate as support. Specifically, both *The Ferrotype and How to Make it* (1880) and *Practical Ferrotyper* (1872) mention the use of iodide of ammonium and cadmium as well as cadmium bromide for the preparation of the collodion solution [17, 23]. The base varnish layer, called japan or jappaned, was made with a mixture of "one quart of raw linseed oil […] two ounces of asphaltuin and sufficient umber or lamp-black to give the desired shade" but other ingredients could be used, such as "mastic, lac or copal varnish – and other shades of coloring-matter […]" The term comes from a popular Asian technique of lacquer work [24]. Regarding the exposure, tintypes require a very specific light, about the double amount than what is required for other negatives, otherwise the image is dull and smoky. The manuals also mention *metallic stains on plates*, a problem encountered on tintypes. These are composed of metallic silver transformed from the silver nitrate by some agent. This agent could be iron or copper; iron oxide (rust) in particular will cause a rapid transformation of silver nitrate to metallic silver. Another defect reported are *pinholes* in the picture, black spots caused by the presence of impurities on the plate before the application of the collodion layer (Figure 13) [23].

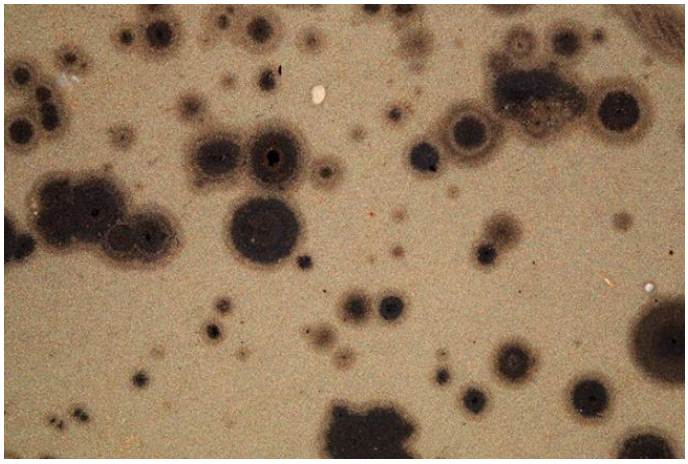

Figure 13: example of pinholes. Source: graphicatlas.org

Early ferrotypes were presented in the same style of protective cases used for daguerreotypes and ambrotypes [23]. Around 1863 and until 1866, they were presented in paper mats (Figure 14). They could also be put in frames, which were used between 1865 and the early 1870s, and *passe-partouts* (Figure 15) [15].

Figure 14: example of a tintype in a case (left) and in a paper mat (right).
Source: ohiohistory.files.wordpress.com

Figure 15: example of a tintype presented in a frame (left) and in a passe-partout (right).
Source: ohiohistory.files.wordpress.com

The formats were variable, because they could be made in any size, but the following were the most popular:

Table 2: typical tintype formats. Source: graphicatlas.org

Designation	Inches	Method
Bon tons	2 ½ x 3 ½	4 images on a 5x7 in plate
	2 ½ x 4 or 4 ¼	8 images on a 8x10 in plate
	2 x 2 ½	16 images on an 8x10 in plate
	1 ¾ x 2 ½	8 images on a 5x7 in plate
Gems	¾ x 1	
	$1\ ^{3}/_{8}$ x $1\ ^{2}/_{3}$ and smaller	
Large plates	5x7	
	8 ½ x 6 ½	
	8x10	

Alternatively, these large plates could be used in multiplying cameras, obtaining multiple images in one plate, which were then cut into individual images. This resulted in sharp and irregular edges, which the photographers clipped (Figure 16). Typically, four-lens cameras were used, producing four images, or 8x10 multiplying boxes (Figure 17) [10, 15, 23]. In the case of the four-lens cameras, the images produced were called bon tons (Figure 16). Finally, *vignetting* was popular technique used in tintypes and other processes, which consisted in gradually fading the edges of the image. In tintypes, it was done by placing a mask in front of the lens (Figure 16) [15]. In the 1880s, dry gelatine tintypes were introduced. These were sold already sensitized and ready to use [17]. Subsequently, street photography emerged with the creation of a camera that allowed the operator to take the plate out of the package inside and place it into the focal plane. After the exposure, the plate was dropped through a slit into the developer/fixer bath [10].

Figure 16: example of a bon ton tintype, with two clipped corners (left) and of a *vignetted* bon ton tintype with clipped corners (right). Source:graphicatlas.org

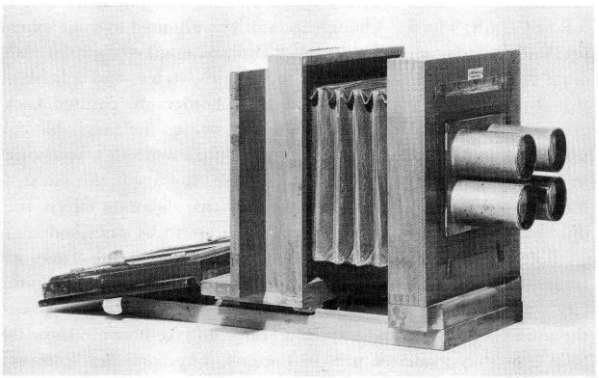

Figure 17: a four lens camera used to produce bon tons. Adapted from [7]

Tintypes became so popular that they turned into a mass production industrial product: the plates were produced in factories and sold to the photographers already coated on both sides. Because they were so easy to make, tintypes were sold by many

photographers, some of which itinerant, most unknown. This makes their production process hard to standardize: the ingredients used for sensitizing, developing and fixing could vary a lot [25]. According to manuals of the time, developers used in tintypes included: ferrous sulphate, sugar and lead nitrate; ferrous sulphate, potassium nitrate, acetic acid and alcohol; ferrous sulphate and barium nitrate; pyrogallic acid, nitric acid and alcohol; sulphite of soda, carbonate of potash, ammonium bromide, hydroquinone, potassium carbonate, sodium sulphite, glycine and hypo [26, 27].The finishing varnishes were similar to those used in ambrotypes, such as copal, sandarac, dammar and amber [14]. The tintype was the easiest and cheapest photographic process at the time, because iron plates were less expensive than sheets of glass. They were also more resistant, so they could be easily transported sent through the mail, thus the occasional term *letter types* for them. Both these factors contributed to the commercial success of the product, making it the most popular photographic technique in the USA between 1865 and 1900 [16]. In fact, this process had huge impact, allowing access to portraiture to virtually everyone. It was a definite step in the democratization of photography, extending the cultural possibilities of portraiture to a mass audience, witnessing the true American lifestyle. The individual portrayed on a tintype likely belongs to the low or middle income part of the population, due to the circulation of this medium mainly among the working class. In fact, the process was established as the opposite of the daguerreotype, a typically bourgeois item. Furthermore, tintypes were popular during the industrial era and can be considered evidences of America's industrial history, comprising social and economic proof. Overall, they present a panorama of modernization and are a testimony of a democratic culture that challenges the bourgeoisie – an all-inclusive medium, with which any citizen created a self-image that affirms their equality [25].

1.4.3. Retouched photographs

The fact that photography could not reproduce colours was one of the main criticisms it faced. Although attempts were done to achieve colour photography, while this was not possible colours were hand-painted with dry pigments, watercolours, oil paints, crayons, and pastels [28]. They could be painted lightly and on specific spots, or completely over painted [29]. Hand colouring kits could be purchased in shops and comprised brushes, mixing plates, binders and dry pigments. The pigments could be

labelled as to where they should be applied [30]. After the application, the excess of dry pigments was removed with a rubber air bulb and a transparent varnish was applied on top. This procedure could be repeated if necessary, on top of the varnish layer [18].

Tintypes were one of the most painted photographic processes and the prices varied according to how long it would take to colour them (Figure 18) [31]. Although there is a good record of the techniques used to apply paint on daguerreotypes, there is a lack of documentation when it comes to tintypes. There is some information about colouring tintypes in the book *Practical Ferrotyper* (1872), in which the author refers the use of "[…] equal part of dry carmine and flesh color […]" [23]. From the information found on contemporary studies, tintypes are mainly painted with oil paints, which have a good adherence to the surface. Watercolours and gouache could be used for details on the face, due to their transparency [31]. Also, crayon and pastel were applied, but needed to be protected with a glass due to their fragility [29]. The metal plate could also be coloured by coating it with India red and linseed oil via electrolytic processes, or *chemical colouring*, before the paint was applied; chocolate, blue and yellow tones could be achieved [32].

Figure 18: example of a retouched tintype. Source: graphic atlas.org

Regarding ambrotypes (Figure 19), the book *The Photograph and the Ambrotype Manual: a Practical Treatise* (1861) gives some information about the types of paints used to colour these images. Chinese vermillion, chrome green and yellow, Chinese blue and a mixture of venetian red and blue for purple. The colours were applied on top of the emulsion, after drying. Because sometimes a white varnish was applied, the colouring had to be done intensely as to avoid the removal of colour by the varnish. If needed, the colour could be applied once again on top of the varnish. Additionally, to remove an

excess of brightness sometimes found on highlights, lampblack could be applied on these spots with a wet brush [9].

Figure 19: example of a painted ambrotype. Source: graphicatlas.org

1.4.4. Finishing varnishes

As mentioned above, images were often covered with a white, clear varnish for protection purposes. Photographic manuals from the collodion era mention the used of shellac, sandarac, or a mixture of these two compounds; and white copal, gum dammar, amber, benzoin, india rubber and lavender. These were diluted in turpentine, chloroform or alcohol [14, 17, 20]. These can be divided into glossy, matt or durable varnishes:

Table 3: finishing varnishes used for collodion images, adapted from [33]

Glossy	Matt	Durable
White shellac	Ether	Benzol
Castor oil	Benzol	Oil of lavander
Sandarac resin	Sandarac resin	Rubber
Benzoin gum	Ether	
	Benzol	
	Mastic	

The finishing varnish could be omitted and the image left unprotected because the varnish darkened the final image [9]. It is important to notice that this data was published at the time, but there probably were other recipes used that were not published.

1.5. Degradation of photographic objects

1.5.1. General degradation

The degradation of photographs can be divided in three types: physical, chemical and biological. Physical degradation involves structural and mechanical damages and is usually caused by poor handling, storage or display. Chemical degradation is usually due to either intrinsic characteristics of the materials used to produce the photograph or external agents present in the atmosphere or in the surrounding materials. If related with the production process, it can occur due to insufficient fixing time or spoiled fixing solution, for example, or to improper washing, which leaves residues of the fixer on the image, these residues will alter the tone of the image to yellow or brown, and fade the image. Biological degradation can be active or inactive and refers to the action of animals, fungi or bacteria, and depends on the composition of the object [2, 5]. Below, the most relevant degradation phenomena for this study are described.

1.5.2. Degradation of the image forming particles

One of the most common types of degradation of the silver image forming particles is silver mirroring. It appears as a bluish iridescent metallic deposit on the surface of the emulsion, with a mirror-like effect (Figure 20). It tends to appear on the darker areas of the image or in certain patterns, related to external agents, such as the case on which the object is stored. It has been defined as a four-step process, starting with the oxidization of the image forming silver particles. Then, the migration of the silver ions towards the top of the binder, their reaction with atmospheric sulphur compounds, and their growth in size creating a deposit formed by silver sulphide, metallic silver and other products. Its exact chemical composition, however, is still a subject of debate [11, 34].

Figure 20: example of a photograph with silver mirroring. Source: notesonphotographs.org

1.5.3. Degradation of the collodion

Collodion is unstable in high humidity conditions, where free nitrogen oxides can attack the cellulose chain and the silver imaging particles. This makes the collodion turn yellow and gradually crumble [33]. The lack of varnish makes the collodion layer more fragile and susceptible to degradation, especially abrasion and oxidation [8]. Another pattern observed in this kind of photographs is the reticulation of the collodion. It is characterized by the shrinkage of the collodion layer which becomes more fragile and develops capillary fissures (Figure 21). It can also lead to detachment, abrasion, chipping or loss of material. This phenomenon can be caused by several factors such as the loss of solvents in low relative humidity conditions; the presence of impurities on the glass where the collodion is applied, which lead to a loss of its adherence to the support; or the loss of plasticizers added to the collodion solution to improve flexibility (ricin oil and glycerine). Finally, because collodion is organic it can suffer biological attack, especially through the formation of mould (Figure 22) [11].

Figure 21: example of an ambrotype with reticulation of the collodion. Source: graphicatlas.org

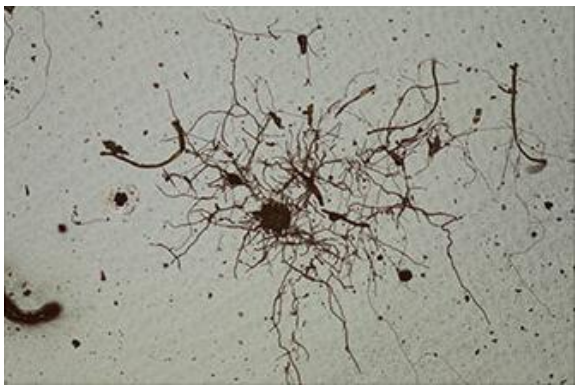

Figure 22: Example of mould on a collodion based object (50x specular light). Source: graphicatlas.org

1.5.4. Degradation of the support

The degradation of ambrotypes differs from tintypes when it comes to the support. The most typical glass degradations are loss of transparency, milky appearance and roughening of the surface (Figure 23). Usually these occur on the side of the emulsion, making it detach from the support. This happens due to the process of *bleaching*, i.e., the formation of a very thin hydrated layer on the surface: the glass surface exchanges K^+ and Na^+ ions, which are dragged onto the glass surface, with the H^+ ions from water on the atmosphere. When humidity drops, an alkaline deposit is left on the glass surface. These make the glass look less bright and less transparent. This process is catalytic, because the deposits are hygroscopic, absorbing water and triggering more *bleaching* [11]. In particular, during the collodion era, some glasses had high proportions of sodium and/or potassium oxide. This made them more susceptible to chemical decay resulting in a softening of the binder and loss of adherence of the emulsion to the glass. This loss of adherence can also be caused by incorrect production methods, particularly the improper cleaning of the glass surface before the setting of the collodion layer [8]. When a black varnish was applied on the glass, it is common to observe cracking (Figure 24) or loss of this layer, revealing the negative image. Alternatively, if the support was separated from the glass, such as a metal plate, it can suffer degradation. Regarding the finishing varnish, unvarnished ambrotypes will have a higher tendency to exhibit silver oxidation in the form of fading and mirroring.

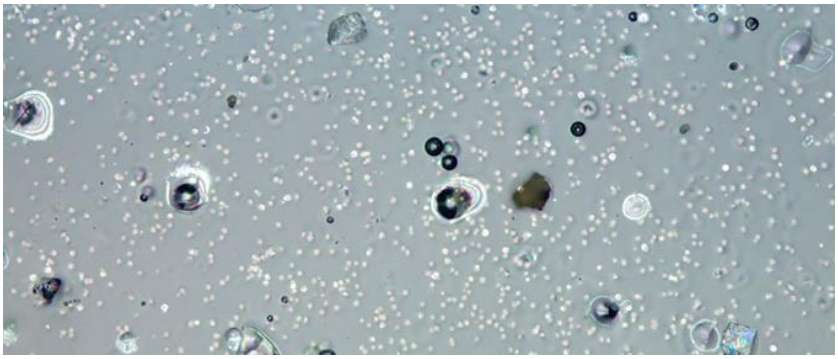

Figure 23: example of the phenomenon of bleaching of the glass. Source: graphicatlas.org

Figure 24: example of cracking of the background varnish. Source: graphicatlas.org

Glass is a non-crystalline amorphous material, made of three main components: network formers, modifiers and stabilisers, fired at temperatures between 1000ºC and 1500ºC. Silica, used in the form of amorphous silicon dioxide (SiO_2), is the network former, and can come from potassium, sodium or calcium silicates. Modifiers are sodium and potassium oxides, used to lower the melting temperature of silica; and stabilizers are magnesium and calcium oxides, used to make the glass more stable chemically. Upon cooling, the components do not crystallize, unlike metals, thus glass is not a crystalline material but amorphous. Glass properties can be modified by varying the fusion temperatures or by adding different materials to its composition [19].

As stated above, the degradation patterns of tintypes and ambrotypes differ according to the support. In the case of tintypes, the most frequent degradation is the formation of rust, which can cause the collodion binder or the black varnish to blister, lift and detach (Figure 25). Also, because tintypes often lack protective housing and were handled frequently, they typically present mechanical damages, such as abrasion, bending and deformation [11].

Figure 25: example of abrasion and detachment of the binder and formation of rust.
Source: graphicatlas.org

1.6. Review of the analytical techniques used in the characterization of photographic items

When it comes to the morphological and chemical characterization of photographic objects, the tendency is to focus either on daguerreotypes, silver gelatine prints or negatives. In fact, only three papers were found specifically about tintypes and one on ambrotypes. However, because these objects have the same image formation process as daguerreotypes, some of the papers on daguerreotypes can be used as references for this study. Regarding the papers that focus specifically on tintypes and ambrotypes, A. Chipman conducted the study *Inexcusable but Appropriate: The Technical Analysis of Hand-painted Tintypes (…)* presented in 2011 [28]. This, however, is more focused on the hand-painted elements rather than on the tintype as a whole. C. Rogge published the paper *The varnished truth: The recipes and reality of tintype coatings* (2012) [35], which focuses on the types of varnishes used on tintypes and how they correlate to the recipes published at the time of their production. E. Carretti *et al* published the paper *Non-invasive physicochemical characterization of two 19th century English ferrotypes* (2009) [16] which deals with the evaluation of the conservation status of the objects and the chemical composition of their constituent materials. Finally, a technical study of five ruby ambrotypes was found, by L. Duncan in 2009 [36], focusing on the characterization of the constituting materials of the ambrotypes. Other papers of relevance to this study include the use of FTIR techniques for the study of the composition and degradation of photographic materials [37], the use of non-invasive micro-Raman spectroscopy for the investigation of historical silver salt gelatine photographs [38], micro-Raman

characterisation of silver corrosion products [39], and a SEM-EDS study on the formation of chlorine-induced alterations in daguerreotypes [40]. Most papers use optical microscopy, ultraviolet induced visible fluorescence, X-ray fluorescence (XRF) spectroscopy, Fourier-transform infrared spectroscopy (FT-IR), Raman spectroscopy, scanning electron microscopy with energy-dispersive spectroscopy (SEM-EDS) and pyrolysis gas chromatography-mass spectroscopy (Py-GC/MS).

Optical microscopy is used to observe the surface of the object, analyse surface defects and understand the stratigraphy. Ultraviolet induced visible fluorescence shows which parts of the surface of the object fluoresce, emphasising the presence of organic compounds and some types of degradation. The colour and type of fluorescence can give clues about the type of organic compound. It is particularly useful to detect the presence of varnishes, for example Chipman (2011) found the presence of a varnish in one of the tintypes. It was selectively applied (the fluorescence was present in only some parts of the image) and the colour of fluorescence (bright orange) suggested that the varnish was shellac based. SEM-EDS and XRF can be used for elemental analysis. SEM-EDS backscattering mode can also be used for imaging and surface analysis. Raman can be used to complement the chemical analysis, especially when it comes to inorganic compounds, e.g. silver degradation compounds. FT-IR and GC/MS are typically used for the identification and characterization of organic compounds, mainly coatings.

1.6.1. Working principles of the analytical techniques used in this work

1.6.1.1. TECHNICAL PHOTOGRAPHY

Technical photography is used for the photographic documentation of the samples. It can be done with several illumination settings and light sources, to gather different information about the surface of the samples. Among these, the ones used for this work were: reflected natural light, artificial, transmitted and raking lights and reflected ultraviolet (UV) radiation. Reflected natural light allows to observe the object as it can be seen with the naked eye; raking light allows to observe the morphology of the surface of the object; and transmitted light to understand which parts of the object are opaque and emphasise losses of material. UV radiation allows to observe and register

surface phenomena not visible to the human eye. On the electromagnetic spectrum (Figure 26), visible light radiates between 400 and 700 nm and UV between 180 and 400 nm. It can be divided into three regions: UVA or longwave UV (320-400 nm); UVB or middle wave UV (280-320 nm); UVC or shortwave UV (180-280 nm). In the study of cultural objects, the observation under UV radiation has been a common procedure since 1925 and the most common UV radiation source is long-wave. In the study of photographic objects, in particular, it can be helpful to identify different compounds present on the surface, because non-fluorescent materials will appear black under radiation of this wavelength, while fluorescent materials display different colours and intensities. By varying the wavelength of the UV radiation used to illuminate the samples, different materials phenomena will be observed [41].

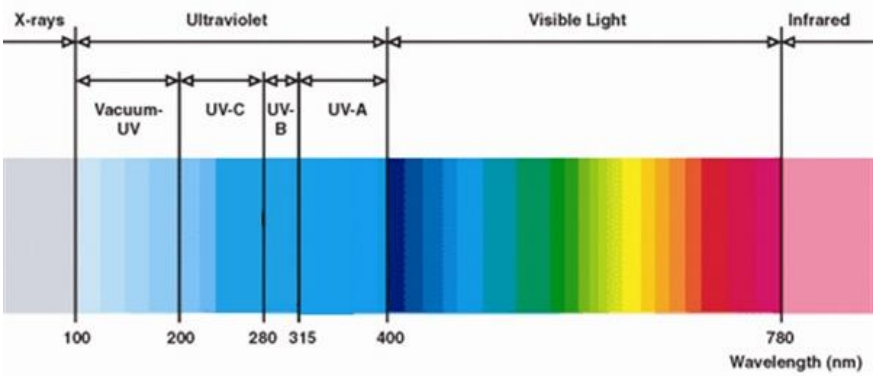

Figure 26: the electromagnetic spectrum showing the different regions, measured in nanometres. Source: www.nailsmag.com

1.6.1.2. OPTICAL MICROSCOPY (OM)

Optical microscopy is used for the microstructural examination of materials: the different ways the samples reflect or transmit light allow the observation of their morphology. Light microscopes are composed essentially by an illumination system, an eyepiece, objective lenses and a holder for the specimen (Figure 27). Also, a photo micrographic system is used to obtain the images observed. They have two illumination modes, *transmitted* or *reflected light*. *Transmitted light* is used for transparent or semi-transparent samples and *reflected light* for opaque or transparent samples. There are also different examination modes available on this kind of equipment: *bright-field* and *dark-field*. With the *bright-field* mode the specimen is evenly illuminated by a light source, while with the *dark field* mode a device blocks the core of the light source, producing a hollow cone of light. This uneven beam of light illuminates the sample causing light to

scatter as it hits the specimen, and only this light scattered by the sample enters the objective lens [42].

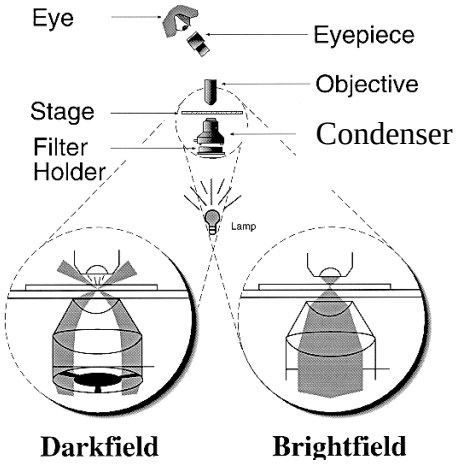

Figure 27: Scheme of the dark-field and bright-field modes on a microscope.
Source: http://public.wsu.edu

1.6.1.3. SCANNING ELECTRON MICROSCOPY COUPLED WITH ENERGY DISPERSIVE SPECTROSCOPY (SEM-EDS)

Scanning electron microscopy has much higher resolution and magnification than regular optical microscopy. Also, it offers a wider depth field which allows for a tri dimensional aspect of the images obtained. When coupled with an X-ray energy dispersive spectrometer, it can give elemental analysis of the specimen along with the microstructure. A scanning electron microscope is composed of an electron gun and electromagnetic lenses and apertures (Figure 28).

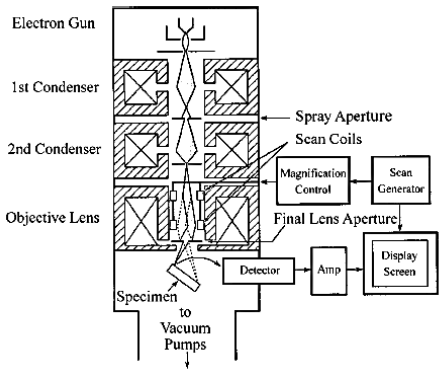

Figure 28: Structure of a scanning electron microscope (SEM). Adapted from [42]

The image is formed by scanning the surface of the specimen with the focused electron beam. When the electrons interact with the surface of the sample, secondary electrons (SE) and backscattered electrons (BSE) are produced, both used for imaging. SE and BSE escape from different locations of the specimen and thus provide different

information (Figure 29). The intensity of SEs depends on the surface topography of the specimen, so these produce an image that shows the surface morphology, while BSE provide information about the elemental distribution within the sample. SEs are a product of inelastic scattering and have an energy level of several keV; they escape from under the surface of the specimen, at a depth of about 5-50 nm. BSEs result from elastic scattering and an energy closer to the incident electrons, escaping from a deeper level under the surface, between 50-300 nm.

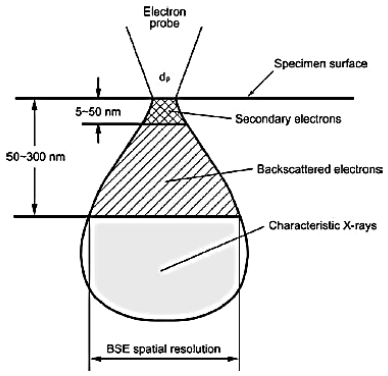

Figure 29: interaction zone of electrons and specimen atoms below a specimen surface. Source: [42]

The interaction of the electrons with the sample also generates the emission of characteristic X-rays. From the energy of these characteristic X-rays, chemical elements can be identified with energy dispersive spectroscopy (EDS). The intensity of these X-rays is plotted against their energy range in a spectrum. The EDS is equipped with a software capable of identifying the possible elements from a spectrum. By coupling EDS with an electron microscope, elemental analysis can be obtained while examining the microstructure of the sample. Typically, SEM is operated at high vacuum and only works on conductive specimens. So, variable pressure SEM has been developed in order to work with nonconductive specimens, such as biological samples.

1.6.1.4. MICRO-FOURIER TRANSFORM INFRARED SPECTROSCOPY (μ-FT-IR)

FT-IR is a vibrational spectroscopy that analyses the structure of molecules through their interaction with electromagnetic radiation, particularly infrared radiation [43]. The energies of infrared radiation match the vibrational energies of molecules allowing the FT-IR spectrometer to detect the molecular vibrations that occur from the absorption of infrared light by the sample. It can be used on gas, liquid or solid samples and on inorganic and organic materials. It cannot be used on metallic materials because they strongly reflect electromagnetic waves. The FT-IR system, or interferometer, is composed of one beam-splitter and two mirrors (Figure 30). The beam-splitter transmits

half of the infrared beam from the source and reflects the other half. These two beams strike a fixed mirror and a moving mirror, combine at the beam-splitter again, irradiate the sample and are finally received by the detector. The moving mirror changes the optical path lengths to generate light interference between the two split beams. When it is located at the same distance from the beam splitter as the fixed one, the optical paths of the two split beams are the same and there is *zero path difference*. Path difference (δ) occurs when the moving mirror moves away from the beam splitter. This leads to something like what happens in diffraction by crystalline structures. The two beams will show constructive and deconstructive interference along with the changing of the δ value. *Completely constructive interference* will occur when $\delta = n\lambda$ and completely destructive when$\delta = \left(\frac{1}{2} + n\right)\lambda$. The light interference is plotted as a function of optical path difference in an interferogram. The Fourier transform method is used to obtain an infrared spectrum from an interferogram, plotting the light intensity versus wavenumber instead of intensity versus optical path difference. The optical path difference can be considered in the time domain because it is obtained by multiplying time with the speed of a moving mirror and the wavenumber can be considered frequency domain because it is equal to frequency divided by the light speed [42].

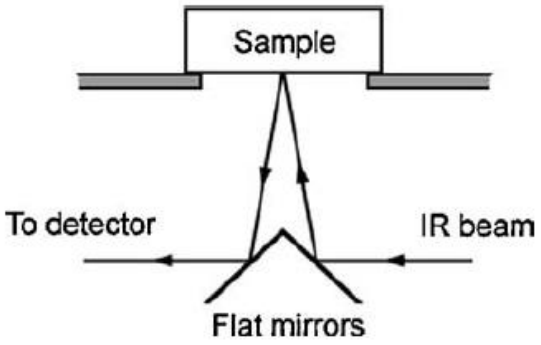

Figure 30: optical diagram of a simple specular reflectance accessory for FTIR instrument. Source: [42]

1.6.1.5. MICRO-RAMAN SPECTROSCOPY (μ-RAMAN)

Micro-Raman spectroscopy works coupled with a microscope by focusing a laser beam, in the order of micrometres, directly on the sample surface (Figure 31), without the need of sample preparation. It has resolution of 1-2 μm and a spectral range of 4000-50 cm^{-1}. Like FT-IR, the working principle of Raman spectroscopy is based on vibrational spectroscopy and identifies functional groups based on their characteristic vibrational energies.

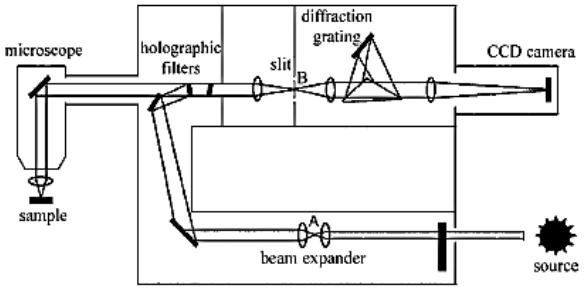

Figure 31: Optical diagram of a Raman microscope. Source: **[42]**

The technique is dispersive, requiring a spectrum at each wavenumber separately. The equipment is composed of a monochromatic, continuous-wave laser source, such as Ar^+, Kr^+ or He-Ne; a microscope for sample illumination and collection; a spectral analyser; and a detection and computer control and processing system. The laser generates beams with wavelengths in the range of visible light, exciting valence electrons in the molecules of the sample. It passes through a filter to become a single wavelength beam and is then focused onto the sample surface. Then, the scattered light is collected by the microscope and sent to the detector. The purpose is to analyse only Raman light, which results from inelastic scattering, and not elastic scattering. So, a *notch filter* is used to prevent the elastic scattered radiation from entering the detector. Also, a *diffraction grating* system is used to select the wavelength before entering the detector [42].

1.6.1.6. MICRO X-RAY DIFFRACTION (μ-XRD)

X-ray diffraction is used in the identification of materials through the determination of their crystalline structure. Thus, only crystalline materials can be analysed with this technique. It allows to distinguish different compounds with the same mineralogical structure. Crystalline materials have orderly periodic arrangements of atoms, defined by unit cell, a repeating pattern. The wavelength of X-rays is about equal to interatomic distances, so crystals act as scattering graters for X-rays, scattering them in a pattern that shows the positions of their atoms. The diffraction from different planes of atoms produces a diffraction pattern which contains information about the atomic arrangement of the crystal. The working principle of an X-ray diffractometer is based on the phenomenon of wave interference: two X-ray beams incident on a crystalline material will be diffracted by the crystallographic planes of the material and they will not be in phase except when *Bragg's Law* is satisfied:

$$n\lambda = 2d\sin\theta$$

For parallel planes of atoms, with *d* space between them, constructive interference occurs only when *Bragg's Law* is satisfied (Figure 32). In diffractometers, λ is fixed, so a family of planes will produce diffraction only at a certain angle θ. X-ray diffractometers are usually constructed according to the Bragg-Brentano geometry (Figure 33). Where the incident angle (ω) is defined by the X-ray tube and the sample and the diffracted angle (2θ) between the diffracted beam and the detector. The incident angle is always ½ of the diffracted angle.

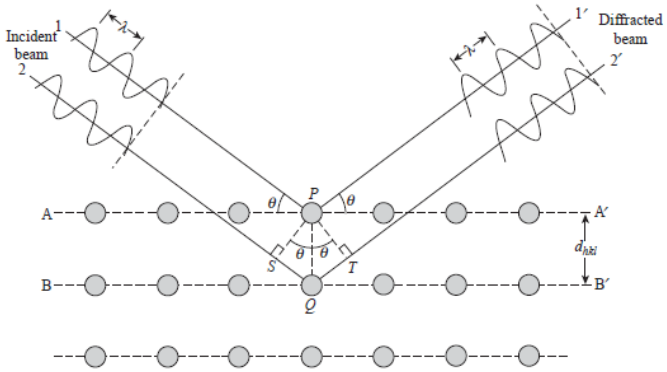

Figure 32: Bragg's diffraction by crystal planes. Source: [42]

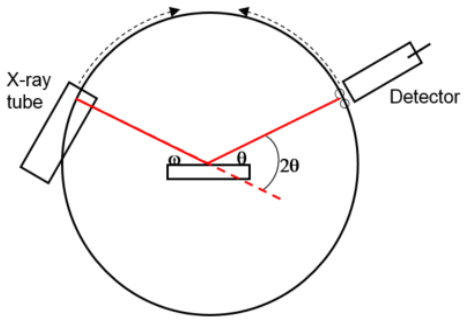

Figure 33: Scheme of an X-ray diffractometer that follows the Bragg-Brentano geometry. Source: http://nptel.ac.in

By plotting the intensity versus the position of the detector (2θ), the position, intensity, width and shape of the peaks can be analysed to identify the compounds present. The space between the planes determines the peak position and the atoms on the planes determine the intensity [42].

CHAPTER 2: MATERIALS AND METHODS

2.1. Sample selection

The samples analysed for this study were purchased on ebay.com (Figure 34). The pieces are probably American although their specific origin or date cannot be presented due to lack of documentation. Because of this and because they do not belong to a museum or archive collection, it could be stated that they lack some historical and artistic value because their context is unknown. However, they serve the purpose of identifying the materials used in their production and characterise the degradation patterns they present. One ambrotype and one tintype were chosen for this study because both are hand painted, framed, and female portraits, since it could be interesting to compare two similar pieces made with different techniques. Then, one tintype was chosen because it was on a case, which is quite rare to come across. The other ambrotype was chosen due to its severe state of degradation, potentially illustrating common degradation mechanisms on this kind of objects. In order to proceed with the study of the objects, it was necessary to remove them from their cases. This was done by a professional conservator and documented.

Figure 34: ambrotype A (AA) and ambrotype B (AB); tintype A (TA) and tintype B (TB) before the removal of the frame.

Regarding their production dates, some elements can be used to try to estimate their production period: the clothes and posing of the subjects; any items that can be seen on the background; and their casings, especially the design of the mats and preservers. Also, it can be useful to compare the object with other pieces of collections which have a documented or estimated date. Observing two objects (Figure 35) from the PhotoTree© collection, two objects with an estimated date of 1859 are very similar to Ambrotype A: the pose is similar, the subjects have tinted cheeks, the hairstyle is similar, and the preservers have more or less the same level of design.

Figure 35: two ambrotypes from 1859 (estimated date). Source: phototree.com ©

Ambrotype B was preserved with a mat, a preserver and a protective glass. Its mat is rather simple, but the preserver shows some level of design, which does not allow for an approximation of the date based on these characteristics. Two pieces were found, one dated around 1856 and the other around 1858 (Figure 36). They both match the subject in Ambrotype B regarding hairstyle and clothing. The first piece has a mat identical to the one on Ambrotype B and the second piece is a tintype with very similar mat and preserver, dated from 1858. Thus, the production of Ambrotype B could be placed between 1856 and 1858.

Figure 36: ambrotype dated from 1856 (estimate) (left) and tintype dated from 1858 (estimate) (right). Source: phototree.com©

Tintype A's mat displays the following inscription "Holmes Booth & Haydens Superfine / Waterbury. Conn. No.41." (Figure 37); it refers to the name of a manufacturer, Holmes, Booth & Hayden. The company was founded in 1853 in Waterbury, Connecticut, as a manufacturer of photograph cases, lens, daguerreotype silver plates and other photographic apparatus. They were one of the major makers of cases and by the 1860s, they dominated the retail market for photographic equipment in New York City, along with three other companies, Scovill, Anthony and J. W. Willard & Co. The firm operated independently until 1901, when it became a part of the American Brass Company [44].

Figure 37: Stereomicroscopic images of the inscriptions on the mat of Tintype A.

Because it was presented in a case, it could be placed from 1855 to the early 1860s, when cased tintypes fell out of common use. Two pieces were found, with very similar preservers and mats, dated between 1861 and 1865, which allows to estimate the date of Tintype A to be between 1855 and 1865 (Figure 38).

Figure 38: [Union Soldier and Barber] (American) 1861–1865 (left) and Unidentified Photographer, ca. 1863, United States (right). Source: icp.org

Tintype B was found with only a mat. Comparing the piece with other two, with mats with an identical aspect, it can be estimated to have been produced between 1862 and 1863 (Figure 39).

Figure 39: Tintype dated from 1862 (estimated). Source: phototree.com© (left) and Unidentified Photographer, ca. 1863, United States. Source: icp.org (right)

2.2. Methodology

The purpose of the study was to do chemical and morphological characterization of the objects: identify the materials used in their production and compare them with historical sources and similar contemporary studies; identify the degradation patterns they exhibit and understand their composition; moreover, to make a connection between the techniques and the deteriorations they exhibit. This way, it was expected to contribute to a better understanding of these objects, which have been scarcely studied; and give an input to conservation initiatives of these items and similar ones. The visual inspection of

the samples was first conducted to evaluate the conservation status and general morphological aspects, followed by the used of the different techniques available and whose results were expected to give answers to the several questions raised.

2.2.1. TECHNICAL PHOTOGRAPHY

Technical photography was used as the first step in the study of the objects, with the purpose of documenting the items, understanding their structure and evaluating their conservation status. The pieces were photographed with a Nikon D3200 camera with a micro-Nikkor 40 mm f/2.8DX lens fixed on a column stand. A Black Light Eastern Corp™ 158A X-4 lamp was used as the UV radiation source. ISO 100 was used for normal and raking modes and 200 for UV mode. They were documented using the following modes: reflected natural light; artificial raking and transmitted light; and reflected UV radiation. Reflected natural light allows for a general observation of the object, including the subject, macroscopic surface morphology and main degradation patterns; raking light is used to observe the morphology of the surface of the object: deposits, deformations, etc.; transmitted light, to understand which parts of the object are opaque and emphasise losses of material; UV radiation is used to observe the characteristics that are not detectable with visible light by highlighting the organic compounds on the surface of the object: in this case, it was expected to detect the areas covered with varnish and areas without varnish, as well as organic degradation compounds.

2.2.2. OPTICAL MICROSCOPY (OM)

Optical microscopy was used to observe the object with high magnifications and analyse morphological characteristics not detectable by naked eye. It served to better understand the inherent characteristics and the pathologies of the objects. The areas chosen included inherent characteristics of the object that are representative of the whole object, related to the production process. Special attention was given to image forming particles, to gather some insight on their morphology. Also, areas including the most relevant degradation patterns of the object were chosen. These areas were documented with both stereomicroscope and dark field microscope. A Leica M205C stereomicroscope

and a Leica DM2500M dark-field microscope were used, both coupled with a Leica DFC 290 HD digital camera.

2.2.3. SCANNING ELECTRON MICROSCOPY-ENERGY DISPERSIVE X-RAY SPECTROSCOPY COUPLED (SEM-EDS)

SEM analyses were carried out to obtain images with very high magnification and higher depth of field than in OM, for the observation of the surface morphology. Coupled with EDS it also provided elemental analysis. The analysis were focused on the areas comprising interfaces between highlights and shadows, to understand the morphology of the silver particles forming the image. Also, elemental analysis was used to identify the image forming elements and the composition of some degradation patterns. Finally, the analyses were also done on the areas of the image displaying colour, to try to identify the compounds used for this effect. The equipment used was a variable pressure Hitachi Scanning Electron Microscope S-3700N coupled with a Bruker Xflash 5010 energy dispersive X-ray spectrometer. The resolution of the EDS detector is 123 eV at the Mn Kα line energy. It allows reliable chemical point analysis and mapping from Na Kα X-ray emission energy up to the L emissions of the heaviest elements. Backscattering mode was used for imaging, with an accelerating voltage of 15 kV or 10 kV and the elemental analysis was done with 20 kV. The Esprit 1.9 software from Brüker Corporation was used. The analyses were done directly on the samples, without any previous preparation and due to the fact that the SEM microscope holds a large chamber were small objects can be placed. So, the variable pressure mode was chosen due to the organic coating present on the surfaces of the objects.

2.2.4. MICRO-FOURIER TRANSFORM INFRARED SPECTROSCOPY(μ-FT-IR)

Micro-FT-IR was applied to detect the presence of collodion as a binder, and to identify the varnish layers and the pigments used for colouring. The samples were analysed in the FT-IR-ATR mode. A Brüker HYPERION 3000 FT-IR spectrometer equipped with a MCT detector cooled with liquid nitrogen and an x20 ATR objective (Germanium crystal with 80 μm of diameter) was used. The spectra were acquired in the range of 4000-650 cm^{-1}, with 4 cm^{-1} spectral resolution and 64 scans. To ensure

reproducibility, at least two points were analysed for each area. In some cases the spectra obtained are identical, so only one is presented. In areas of interface or heterogeneous areas, two different spectra were obtained.

2.2.5. Micro-Raman spectroscopy (μ-Raman)

Micro-Raman spectroscopy was aimed to identify the compounds used to colour the images and to identify silver degradation products. The equipment allowed for in-situ analysis, without prior treatment of the specimens. The analyses were done with an XPlora Horiba Jobin-Yvon spectrometer equipped with high stability OLYMPUS BX41TF optical microscope and an Ivac CCD detector. A laser HeNe of 28 mW power operating at 785 nm was used. The laser beam was focused either with a 10x (numerical aperture: 0.25) or a 50x (numerical aperture: 0.75) Olympus objective lens. The laser power was adjusted with a neutral density filter (optical density of 10%). The spatial resolution was *ca.* 1 μm. The samples were scanned at 10% laser power during 15s and 10 cycles. The higher acquisition time was chosen to minimize the signal-to-noise ratio. The analyses were done at room temperature without humidity control. The identification of bands was done by comparison with the equipment database (Spectral ID, 2009) and with published spectra. The points chosen for each object were the coloured areas, to try to identify the material used for that purpose; at least one point on the, to try to identify the compounds used on the photographic process, such as silver halides, and the presence of degradation compounds; and degraded areas, if any, to identify the composition of the degradation products. In some cases, the points chosen did not present any peaks probably due to the action of the washing and fixing baths during the photographic process: these steps remove the unreacted silver salts, leaving only the organic binder which produces only fluorescence with μ-Raman spectroscopy [38]. Also, this effect could be caused by the presence of a varnish layer on top of the emulsion, an organic compound without Raman activity.

2.2.6. Micro X-ray diffraction (μ-XRD)

Micro-XRD was used to identify materials with a crystalline such as some silver compounds or other degradation products caused by the interaction of the surface of the

image with the metallic frames. Also, the equipment was used to identify the materials composing the mats and preservers. The analyses were performed directly on the samples with a DAVINCI Brüker AXS D8 Advance diffractometer, a Cu Kα radiation source, a Göbel mirror assembly and a LynxEye 1D detector, and the DIFFRAC.SUITE software. A 0.3 mm diameter pinhole collimator was used. The diffraction patterns were collected from 3º to 75º 2θ at a step size of 0.05º 2θ, with a time per step of 1s, with a working voltage and current of 40 kV and 40 mA, respectively. The identification was done with DIFFRAC.EVA software using the ICDD PDF X ray pattern database. To ensure reproducibility, more than two spots were analysed for each area.

CHAPTER 3: RESULTS AND DISCUSSION

3.1. Morphological and chemical characterization

3.1.1. Technical photography

- **AMBROTYPES**

With normal light, on ambrotype A it was possible to verify that the object is overall well preserved, but displays abrasion of the emulsion on the margins as well as two *drip lines* on the bottom and right margin (this one is only observable on the back), and very subtle surface tarnish on the left margin. As for ambrotype B, it can be verified that the object is fragmented in three parts and shows an advanced state of degradation mainly due to abrasion and gaps on the background varnish as well as on the emulsion, which also displays surface tarnish. There is a clear difference between the backs of the ambrotypes, as one used a dark metal plate for the background (A) and its image can be seen in reverse on the back of the object; and the other has a dark varnish on the back, which prevents the image to be seen on the back. With the raking light mode, abrasions and impurities present on the surface can be observed clearly on both ambrotypes (Table 4). The transmitted mode evidences mostly the losses of the varnish on the background and the consequent loss of the positive effect. Finally, the ultraviolet induced visible fluorescence shows minimal fluoresce in the left and right margins, which is not sufficient to draw any conclusions about its origin (Table 5).

Table 4: normal and raking light, ambrotypes.

NORMAL LIGHT

AMBROTYPE A

AMBROTYPE B

RAKING LIGHT

AMBROTYPE A

AMBROTYPE B

Table 5: transmitted light and UV radiation, ambrotypes.

TRANSMITTED LIGHT

AMBROTYPE A		
AMBROTYPE B		

UV RADIATION

AMBROTYPE A		
AMBROTYPE B	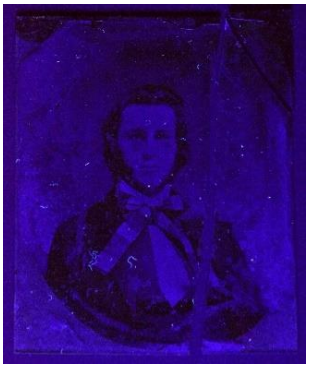	

- **TINTYPES**

With normal light tintype A displays some degradation patterns visible to the naked eye such as the abrasion of the emulsion on the area covered by the frame (oval shape around the couple), mainly on the lower part of the object; a *drip line* on the bottom; and some spots with a different colour suggesting a degradation of the varnish. On the back, some oxidation spots are visible as well as abrasion and the presence of varnish was detected on the left margin. As for tintype B, it displays few degradation patterns visible to the naked eye such as slight abrasion of the emulsion on the area covered by the frame (oval shape around the woman) with higher intensity on the lower left corner of the object; a *drip line* on the upper and left margins. On the back, several oxidation spots can be observed (Table 6). With the raking light, it is possible to observe more clearly abrasions and impurities present on the surface of both objects. Finally, with the ultraviolet radiation tintype A shows a discrete fluorescence concentrated on the area of the face and none on the back. Tintype B shows some strong fluorescent areas in the left margin and over the subjects; and on the lower margin on the back side. The differences in fluorescence might be related to degradation compounds present on the surface but not visible under the normal illumination mode (Table 7).

Table 6: normal light, tintypes.

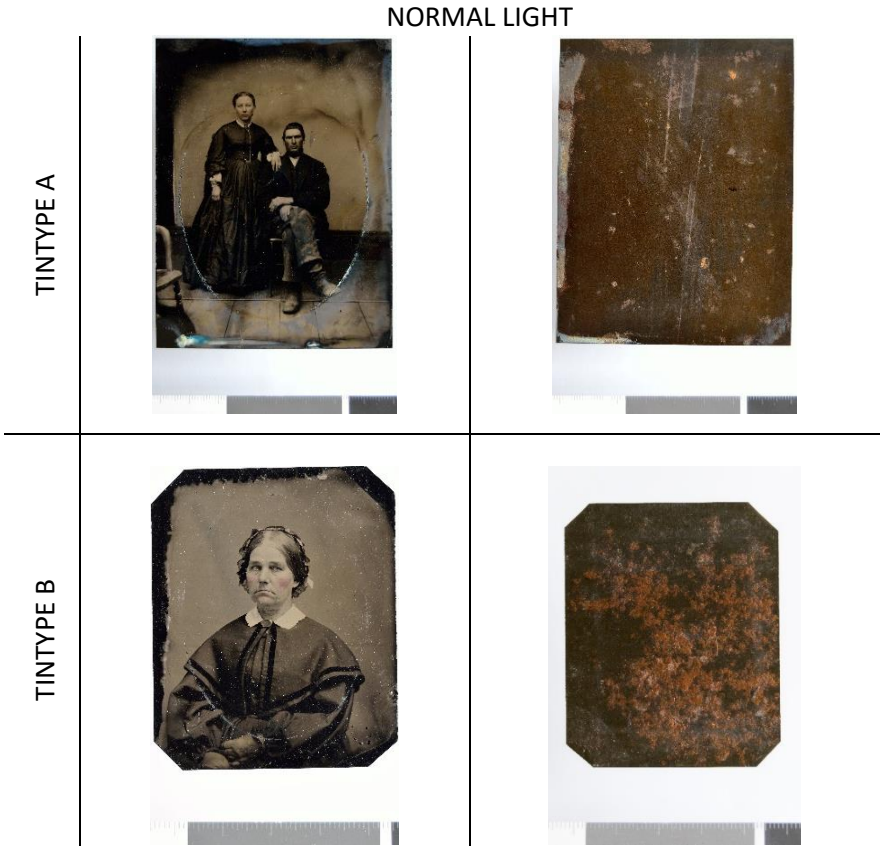

Table 7: raking light and UV radiation, tintypes.

	RAKING LIGHT	
TINTYPE A		
TINTYPE B		
	UV RADIATION	
TINTYPE A		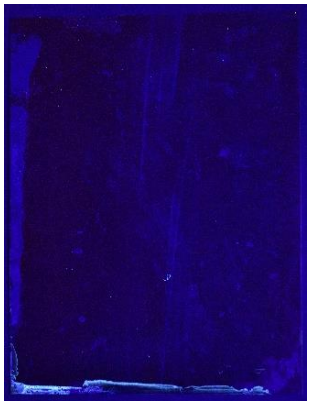
TINTYPE B		

3.1.2. Optical microscopy (OM)

- **AMBROTYPES**

On ambrotype A, five areas were chosen to be observed by optical microscopy. These include factors that were formed or used upon production: the red compound used to colour the cheeks (Figure 40, AA, 2); the *drip line* on the bottom of the object (Figure 40, AA, 4); the interface between highlights and shadows (Figure 40, AA, 3) that allows a clear observation of the image forming particles; and an unevenness of distribution of the finishing varnish (Figure 40, AA, 5). They also include the following degraded areas: abrasion of the varnish and the emulsion, due to contact with the frame (Figure 40, AA, 1) and to lack of protection or incorrect handling or storage (Figure 40, AA, 3).

On ambrotype B, the following areas were chosen: one with an abrasion caused by the frame (Figure 40, AB, 1); another including a painted area on the left cheek (Figure 40, AB, 2); one including both a degraded area, where the background varnish is missing, and an interface area between highlight and shadow (Figure 40, AB, 3); and finally one including a degradation compound that is spread in several areas of the surface, which appears to be *silver mirroring* (Figure 40, AB, 4). Also, two areas of the back side of the object are shown, one of the glass support and another of the dark varnish applied as a background for the image.

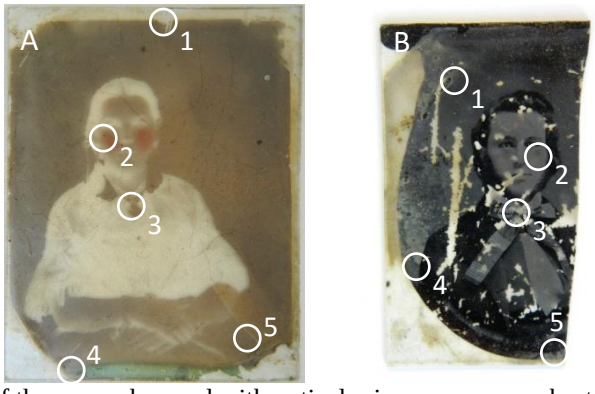

Figure 40: mapping of the areas observed with optical microscopy on ambrotypes A (AA) and B (AB).

Table 8 comprises the retouches of the ambrotypes, with red pigment particles. On a larger scale, these are clearly seen on ambrotype A, but ambrotype B does not seem to be painted and this characteristic is only observable with the dark field microscope. Perhaps the colours have fainted through time, only visible with high magnifications currently. With the dark field microscope, the red pigment particles can be observed with

great detail and are clearly more abundant on ambrotype A. They are present on the cheeks and lips of both ambrotypes.

Table 8: red pigment particles on the cheeks. Ambrotypes A and B, areas 2 and 2.

	STEREOMICROSCOPE	DARK FIELD MICROSCOPE
AMBROTYPE A	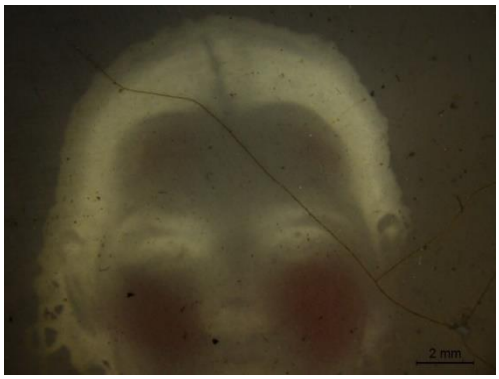	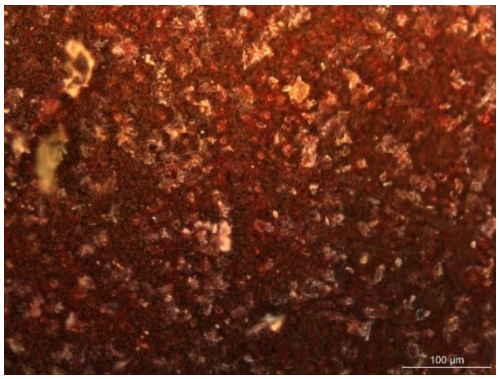
AMBROTYPE B		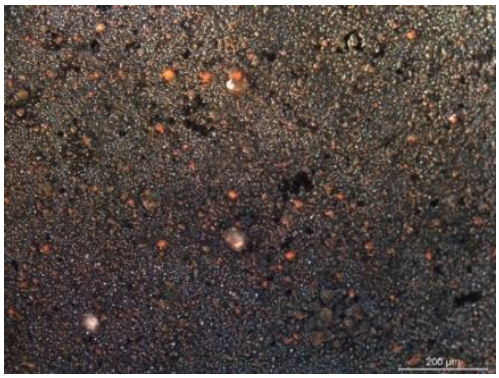

Table 9 includes areas of both ambrotypes where the image forming particles can be seen as well as the interface between highlights and dark areas.

Table 9: image forming particles and the interface between highlights and a dark areas on ambrotypes A and B, areas 3 and 3.

	AMBROTYPE A	AMBROTYPE B
DARK FIELD MICROSCOPE	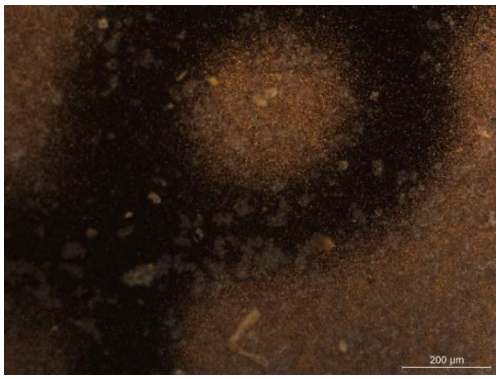	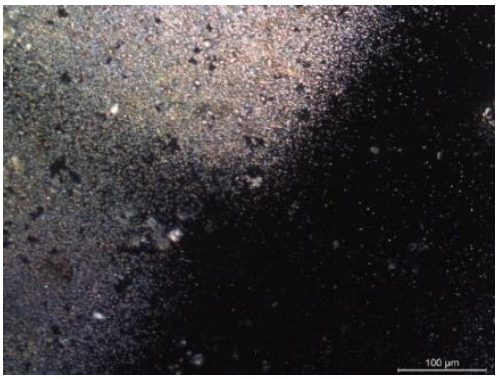

Table 10 covers areas on both ambrotypes with abrasions probably caused by the frames, because they coincide with the areas on which they rest. These abrasions removed parts of the finishing varnish and the emulsion, exposing the glass support. It can be observed that the supports also suffered abrasion. It can also be observed that, on ambrotype B, around the edges of the abraded area the image has a different colour. This could be a consequence of the interaction of the compounds from the frame and the ones from the image.

Table 10: abrasion caused by the frames on ambrotypes A and B, areas 1 and 1.

	STEREOMICROSCOPE	DARK FIELD MICROSCOPE
AMBROTYPE A	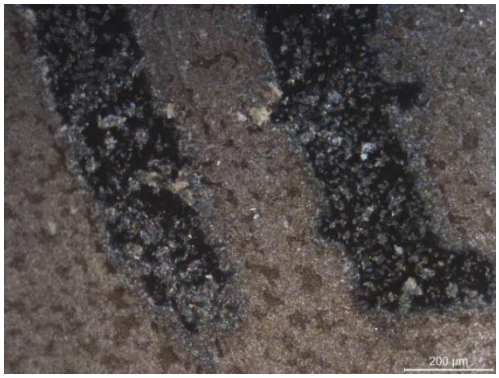	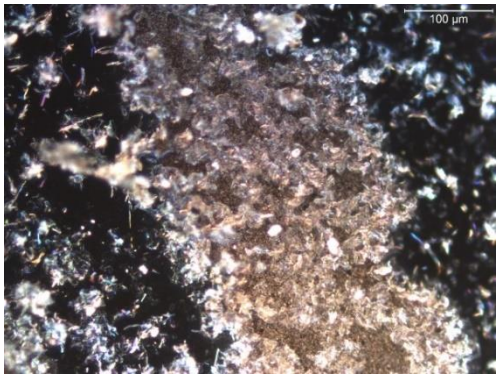
AMBROTYPE B	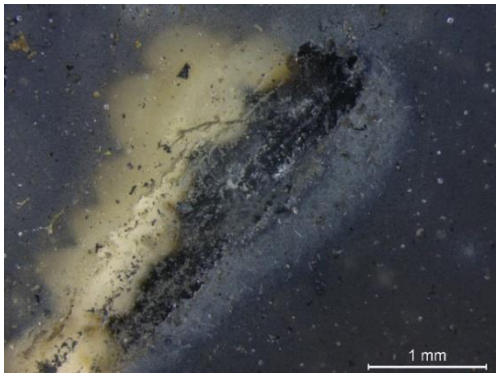	

Table 11 contains abraded areas of the ambrotypes. On ambrotype A, there are cracks (a) and gaps (b) in the varnish and the emulsion, which have led to the exposure of the support. Because this area was not in contact with the frame, the abrasions were probably caused either by mishandling or inadequate housing of the object. It also includes some areas of ambrotype B where the background varnish is missing (c), making it seem that the image is missing can be observed. In fact, it is not, but without the contrast with the dark varnish the image cannot be seen. The areas that appear black on the image are areas are the ones that did not reflect light and therefore did not cause the formation of any or very few image forming particles. Also, the back of the glass support is shown, particularly an area without varnish with physical and chemical damages (d).

Table 11: cracks (a) and gaps (b) on the varnish and the emulsion on ambrotype A, area 3. Gaps (c) on the background varnish and physical and chemical degradation of the glass (d) on ambrotype B, areas 3 (c) and 5 (d).

	STEREOMICROSCOPE	DARK FIELD MICROSCOPE
AMBROTYPE A	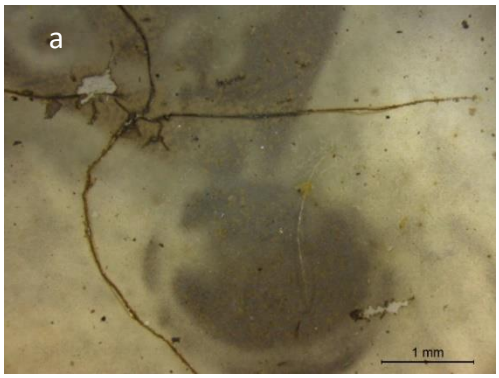	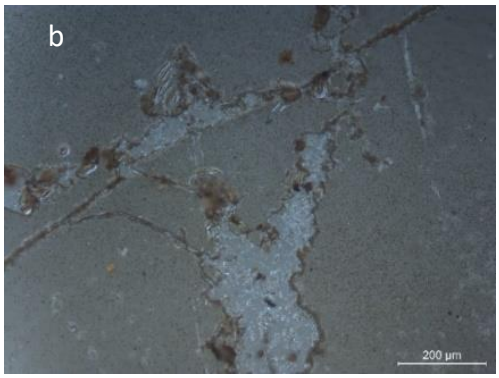
AMBROTYPE B	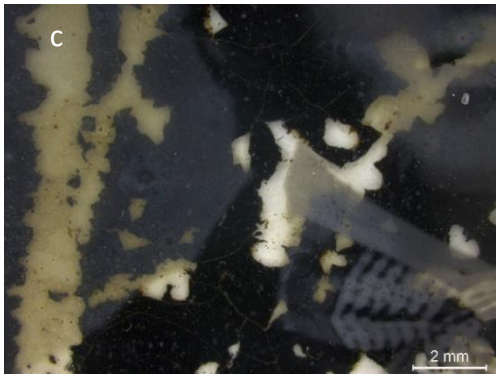	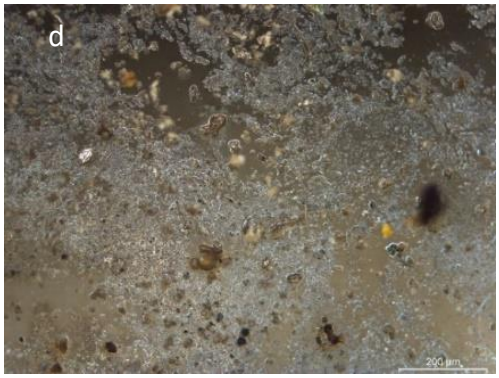

Table 12 comprises degradation compounds on both ambrotypes. On ambrotype A details of a *drip line* can be seen, with some degraded spots which were probably formed either by external agents or by the interaction of compounds in the emulsion. Ambrotype B shows a degradation compound which aspect suggests that it to be a silver degradation compound, probably *silver mirror*, which will be identified with chemical analysis. This compound is present in several areas of the object.

Table 12: *drip line* and degraded areas on ambrotype A, area 4.
Silver degradation compound on ambrotype B, area 4.

	STEREOMICROSCOPE	DARK FIELD MICROSCOPE
AMBROTYPE A	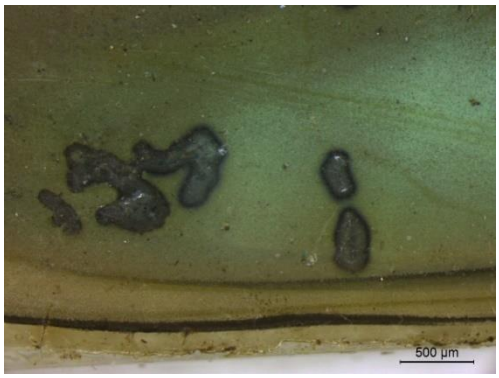	
AMBROTYPE B	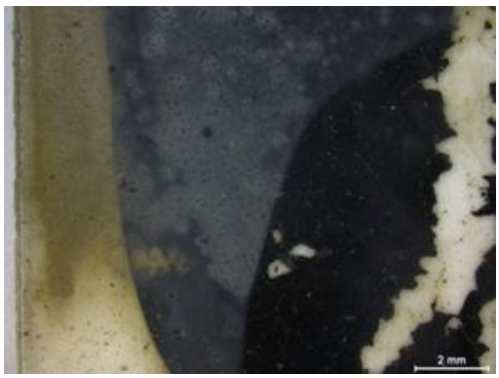	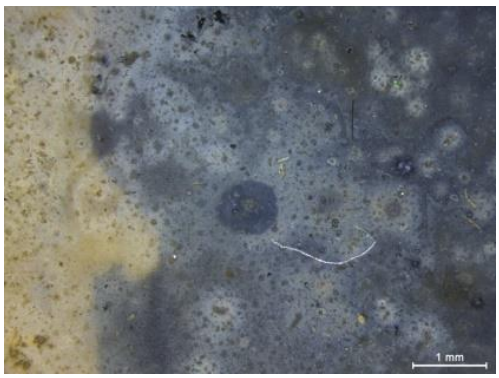

Table 13 shows the back of both ambrotypes. Ambrotype A shows cracks on the varnish and the emulsion (a) and yellowing and an uneven distribution of the varnish layer (b). On ambrotype B it can be seen that the dark varnish applied as a background as suffered physical damages, particularly gaps (c) and cracks (d).

Table 13: cracks on the varnish and emulsion (a), varnish layers of different thickness (b) on ambrotype A, area 5. Gaps (c) and cracks (d, transmitted mode) on the dark varnish on the back side of ambrotype B.

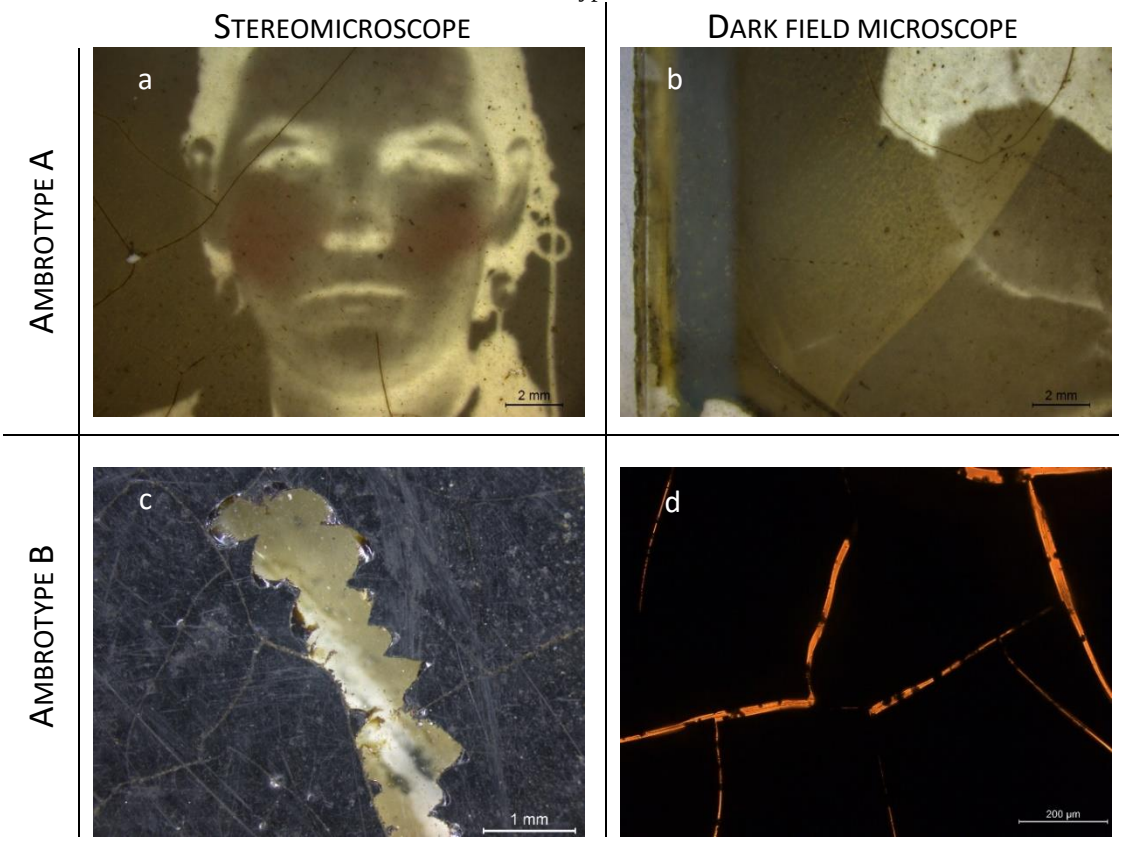

- **TINTYPES**

On tintype A, the following five areas were chosen for analysis with optical microscopy: an edge of the support, were there is a *drip line* with cracks, that expose the support (Figure 41, TA, 1); an area degraded by the contact with the frame, consisting of abrasion and the formation of a green degradation compound (Figure 41, TA, 2); an area including a gold retouch on the woman's hand (Figure 41, TA, 3); the *drip line* on the lower margin of the object (Figure 41, TA, 4); and one area on the back.

On tintype B four areas were selected for analysis with optical microscopy. One displaying a *drip line* (Figure 41, TB, 1); two areas with abrasion caused by the frame, on one of these the support is exposed (Figure 41, TB, 2 and 4) and on another a green degradation compound was formed (Figure 41, TB, 4). Finally, an area on the face of the subject was chosen including a red colouring compound (Figure 41, TB, 3); and one area on the back.

Figure 41: mapping of the areas observed with optical microscopy on tintypes A and B.

Table 14 shows abraded areas on the tintypes. The one on tintype A is on a *drip line* which has cracks that expose the painted metallic support, clearly visible on the dark field image. On tintype B, the area is more abraded, also exposing the support.

Table 14: *drip line* with cracks, tintype A, area 1. Abrasion and gaps on the varnish, tintype B, area 2.

	STEREOMICROSCOPE	DARK FIELD MICROSCOPE
TINTYPE A	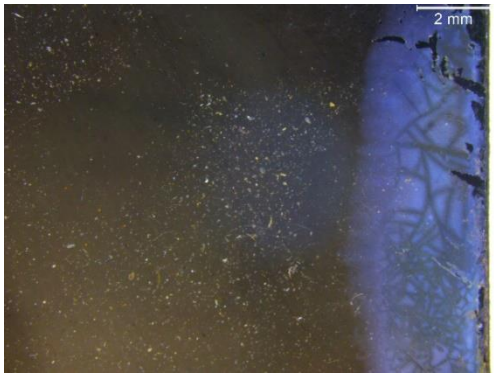	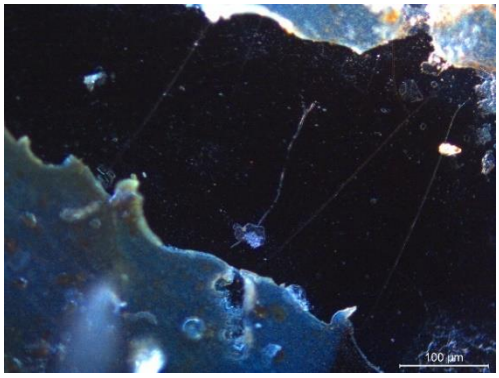
TINTYPE B	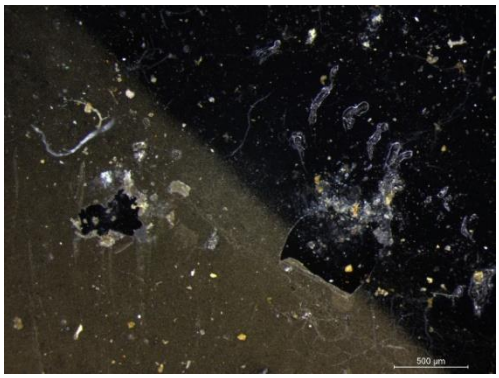	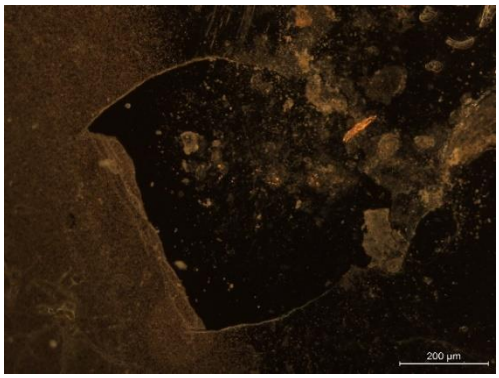

Table 15 contains abrasions caused by the frames of the tintypes, along with green degradation contacts formed probably due to the interaction of the image layers with the metallic compounds of the frames. From tintype A its shown a part of the oval abrasion line surrounding the subjects where it can be observed that the image is damaged and a green degradation product was formed. Tintype B displays an area abraded by the frame exposing the support.

Table 15: abrasion and green degradation compound on tintype A, area 2 and tintype B, area 5.

	STEREOMICROSCOPE	DARK FIELD MICROSCOPE
AMBROTYPE A	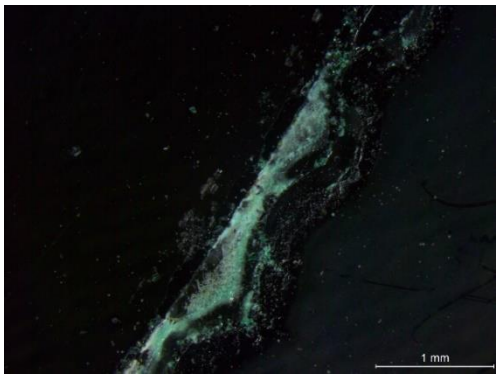	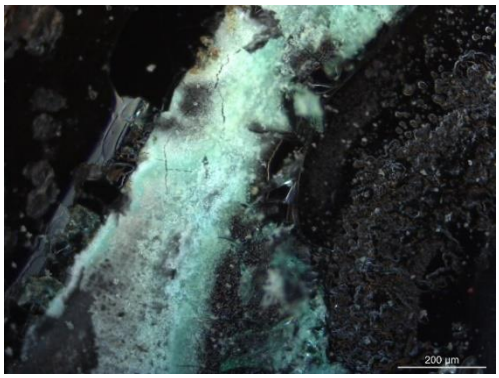
AMBROTYPE B	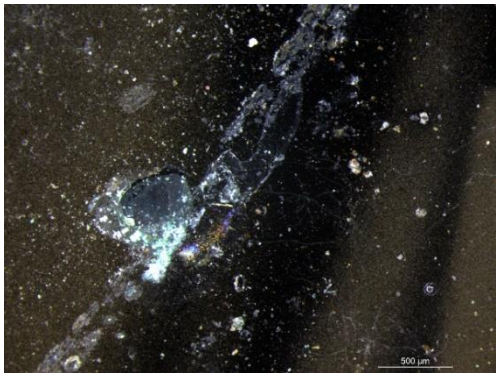	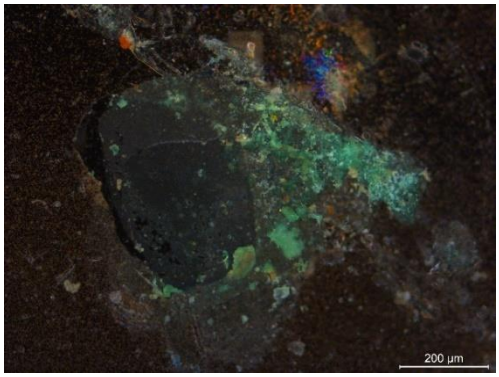

Table 16 contains retouches done on the tintypes. On tintype A, the gold retouch on what should be a ring on the woman's hand. And on tintype B, the red pigment used to colour the cheeks and lips. On the stereomicroscope images, interfaces between highlights and shadow can also be seen.

Table 16: gold retouch on tintype A, area 3. Red pigment on tintype B, area 3

	STEREOMICROSCOPE	DARK FIELD MICROSCOPE
AMBROTYPE A	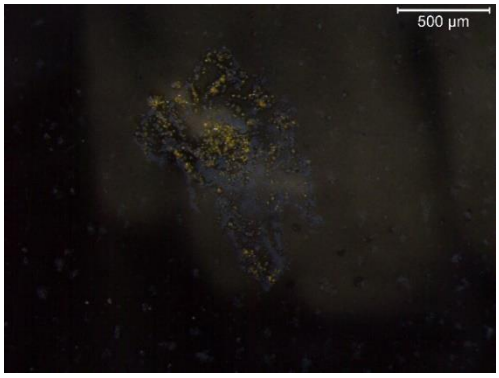	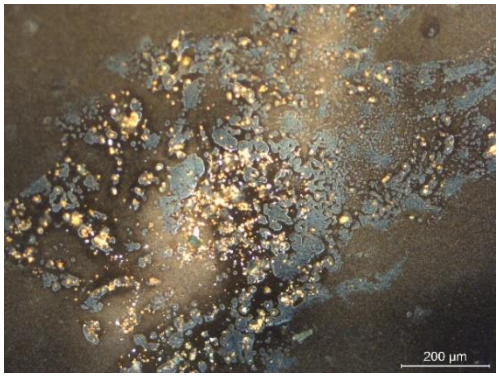
AMBROTYPE B	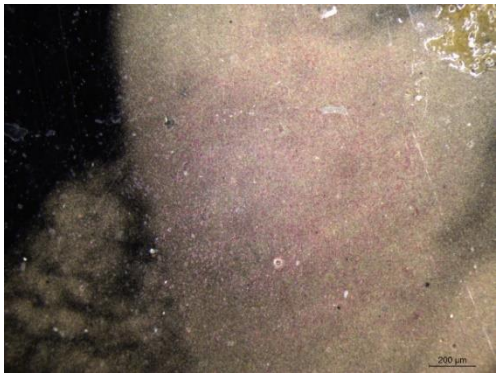	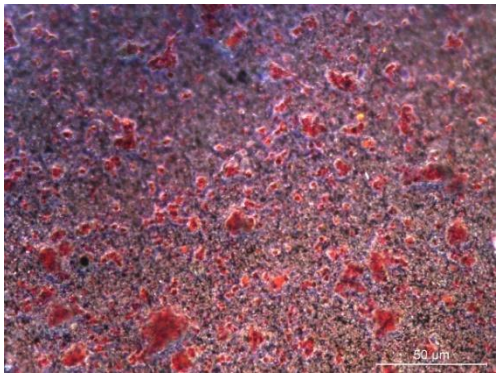

Table 17 includes *drip lines*. On tintype A the *drip line* displays several colours, such as white, yellow and blue, as seen on the stereomicroscope image; and is somewhat transparent, as seen on the dark field image. The one on tintype B is different, it is smaller, white, and opaque and surrounded by particles and impurities.

Table 17: *drip lines* on tintype A, area 5 and tintype B, area 1.

	STEREOMICROSCOPE	DARK FIELD MICROSCOPE
AMBROTYPE A	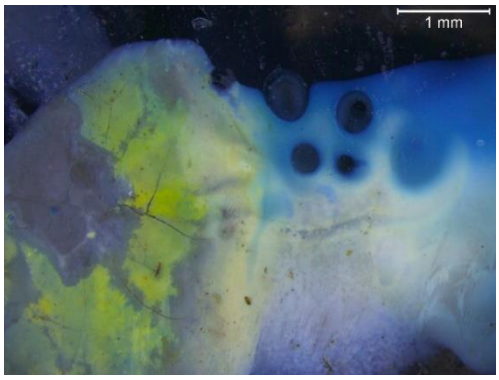	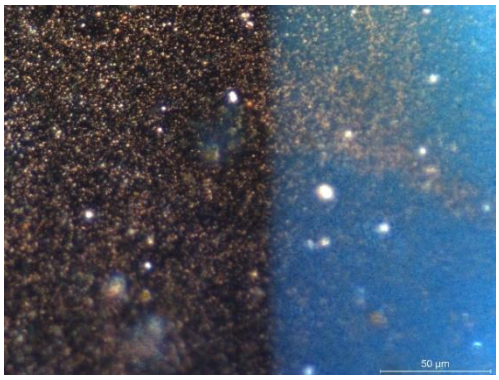
AMBROTYPE B	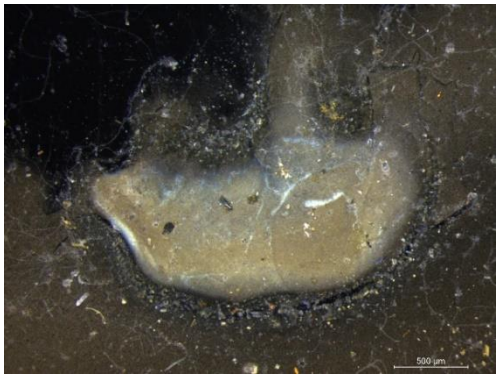	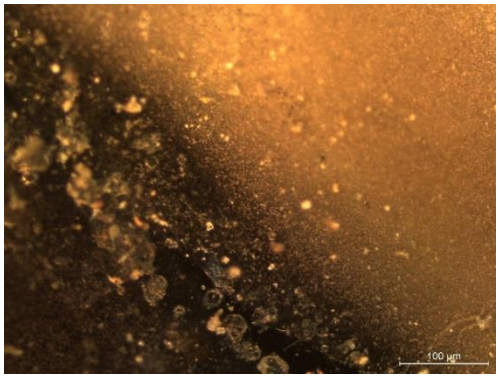

Finally, Table 18 shows the back sides of the objects. On tintype A, some varnish is present as well as a red degradation compound. The back of tintype B is covered in varnish and also displays a red degradation compound similar to the one observed on tintype A. It is interesting to see that the degradation compounds are covered with varnish, suggesting that they were already formed at the time of production.

Table 18: back sides of the tintypes, showing a red degradation compound and varnish layers.

	STEREOMICROSCOPE	DARK FIELD MICROSCOPE
AMBROTYPE A		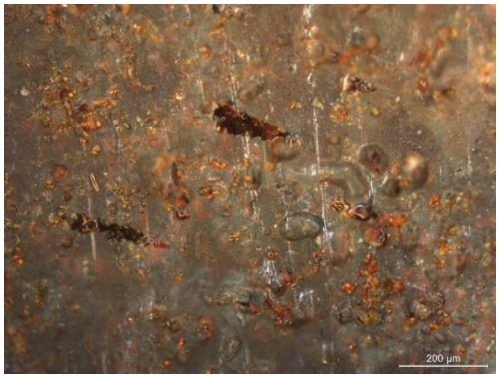
AMBROTYPE B	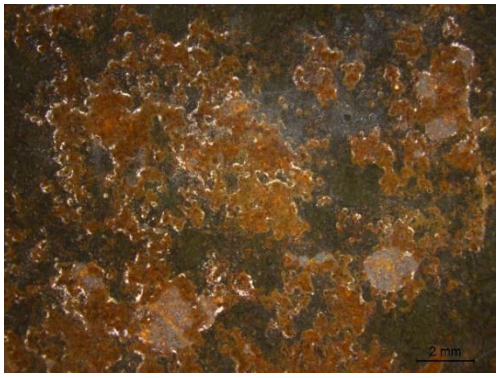	

3.1.3. Scanning electron microscopy-energy dispersive X-ray spectroscopy coupled (SEM-EDS)

- **AMBROTYPES**

The analysed areas on ambrotype A were the interface between a highlight and a dark area (1, Figure 42 A), in order to understand the shape and distribution of the silver particles, which can differ from sample to sample and from dark areas to highlights; an abraded area of the emulsion (2), to understand the morphology of the abrasion and identify the composition of the support; and the right cheek (3), to identify the compound used for colouring. On ambrotype B, the interface between a highlight and a dark area was analysed (1, Figure 42 B), in order to understand the shape and distribution of the silver particles. Also, an area abraded by the frame (3) was analysed as well as the left cheek, to try to identify the red compound (4). Finally, an area including the whitish and bluish degradation aspect mentioned before was analysed as well as an area without image (4).

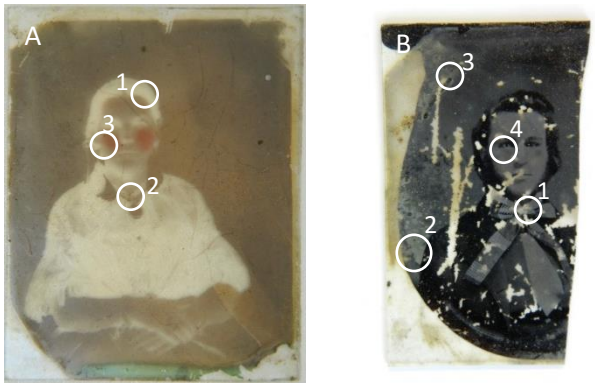

Figure 42: mapping of the analysed areas with SEM-EDS on ambrotypes A and B.

On point 1 of both ambrotypes it was possible to observe the distribution of the image forming particles on the highlight and dark areas and on the interface (Table 19 and Table 20). While on ambrotype A the particles don't show significant differences in size, with an average size of ~2 nm; on ambrotype B, the particles have an average diameter of ~1,5 µm on the highlight area, where they form agglomerates, and ~1 µm on the dark area.

Table 19: VP-SEM images of highlights on ambrotype A (A and B) and on ambrotype B (C and D); dark areas on ambrotype A (E and F) and on ambrotype B (G and H).

HIGHLIGHTS

AMBROTYPE A

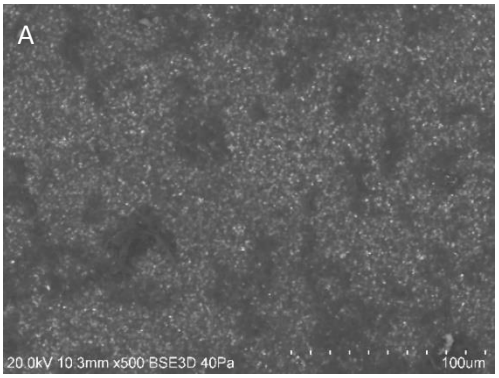

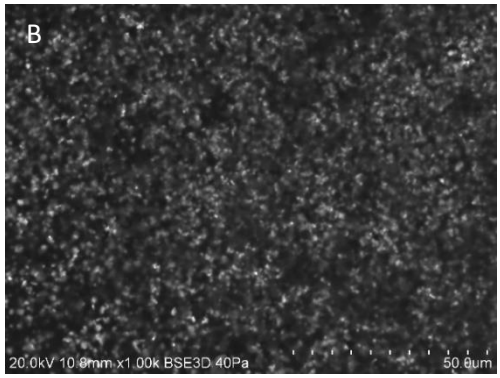

AMBROTYPE B

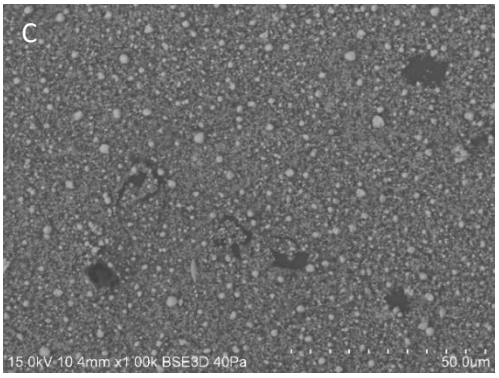

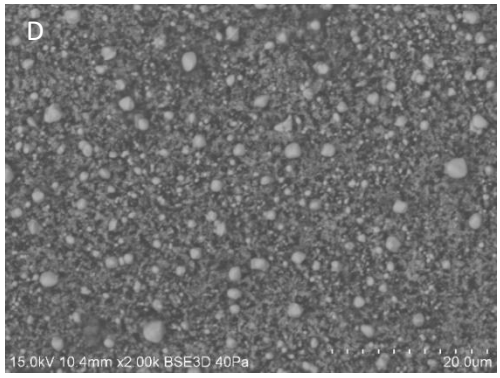

DARK AREAS

AMBROTYPE A

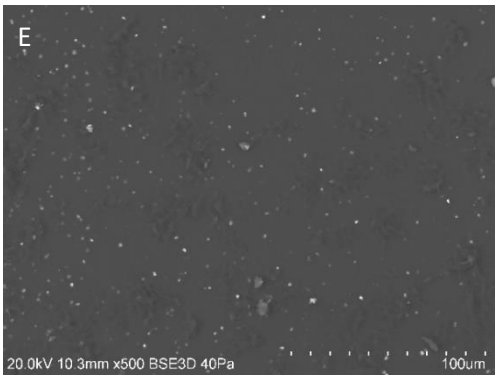

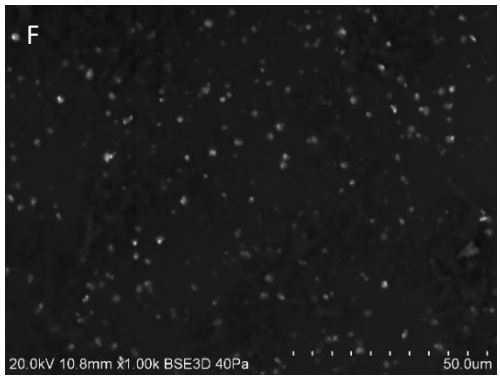

AMBROTYPE B

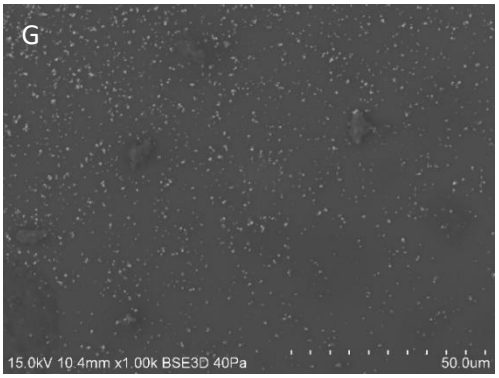

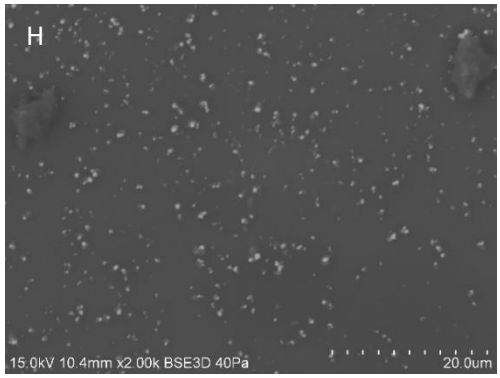

Table 20: VP-SEM images interfaces on ambrotype A (A and B) and on ambrotype B (C and D).

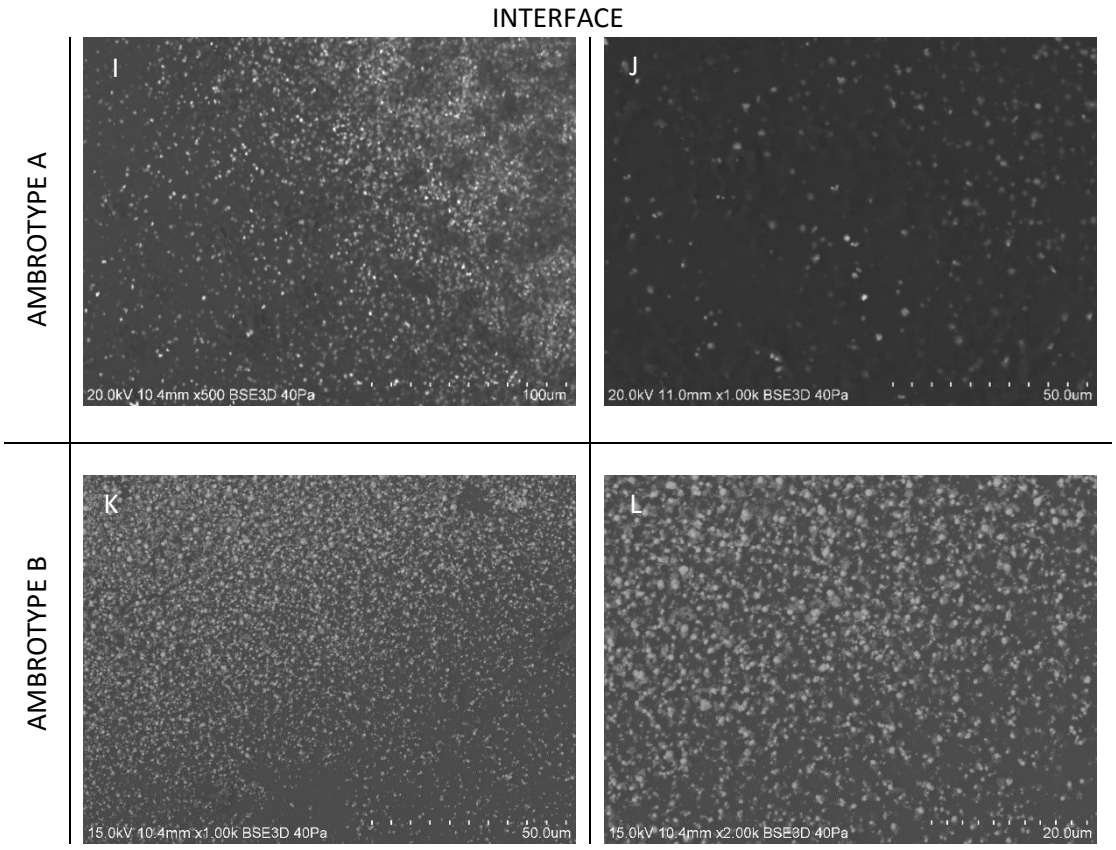

The elemental point analysis on area 1 on ambrotype A (Table 21, 1, a) identified silver (Ag) as the image forming particles and detected the presence of chloride (Cl). This can be related to the use of hydrochloric acid (HCl) or to a process of silver degradation. On area 2 the morphology of the abrasion was observed and the support was confirmed to be a soda-lime-silica (Na-Ca-Si) glass (Table 21, 2, b). On area 3, it was possible to identify the red compound as an iron (Fe) based pigment, probably iron oxide (Table 21, 3, c); and to detect the presence of particles containing barium (Ba) and sulphur (S), which are probably barium sulphate ($BaSO_4$) (Table 21, 3, d). The presence of barium can be related to the use of barium nitrate ($Ba(NO_3)_2$) and ferrous sulphate ($Fe_2(SO_4)_3$) as a developers, which might have not been properly washed and have interacted with each other to form barium sulphate.

Table 21: VP-SEM image of the areas 1, 2 and 3 showing the points analysed (a, b, c and d); elemental point analysis of a particle showing the presence of silver on the image forming particles (a); of the glass surface (b), showing the support to be a soda-lime-silica (Na-Ca-Si) glass; of a particle of the red pigment, probably iron oxide (c); and of a particle containing Ba and S (d).
BSE, backscattered electrons; elemental maps (Fe, Ba, S).

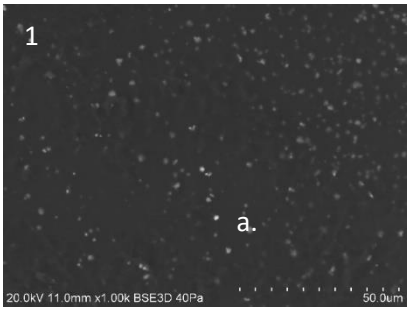

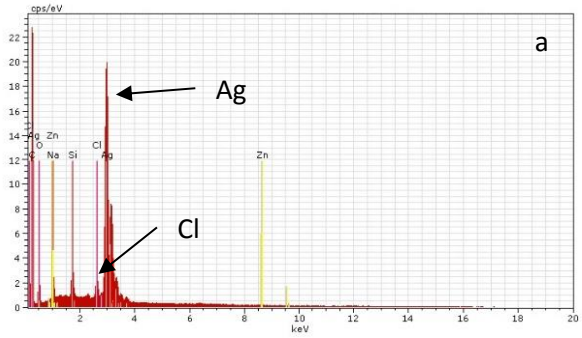

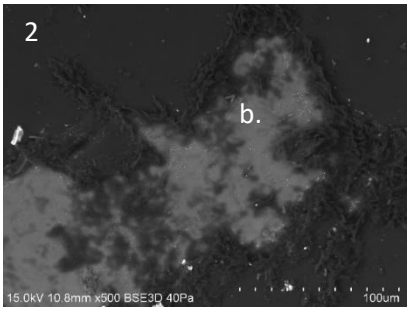

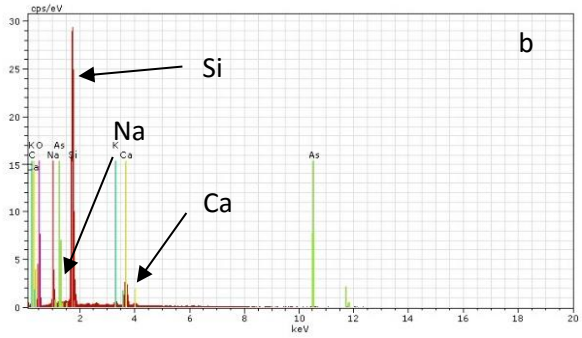

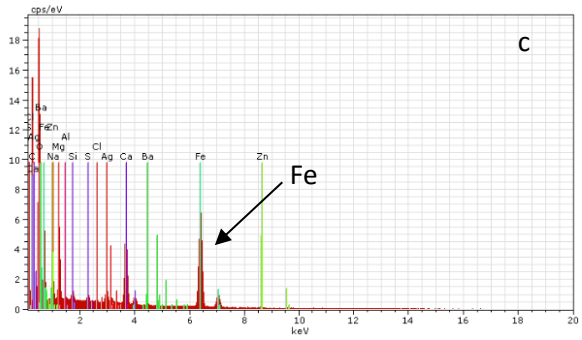

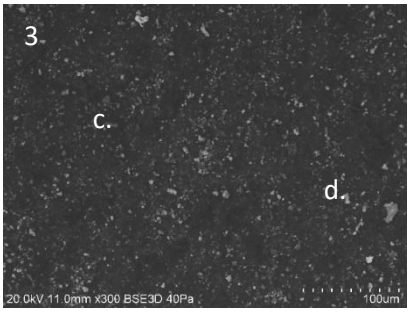

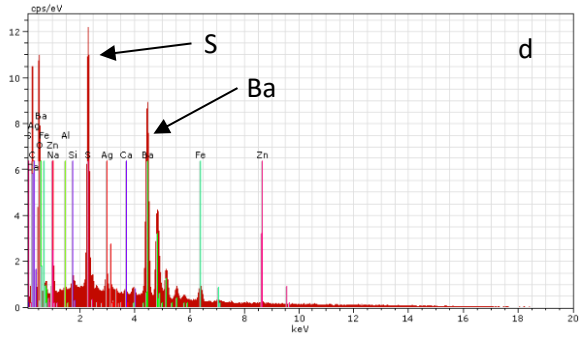

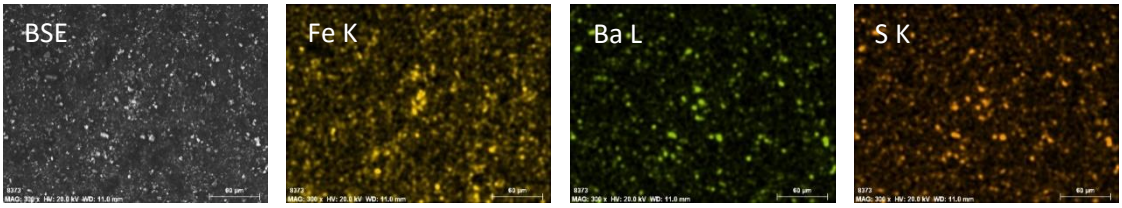

As for ambrotype B, the elemental analysis of an image forming particle on area 1 showed silver (Ag) to be the main element of its composition (Table 22, 1, a). The presence of sulphur (S) was detected as well, which might be related to a degradation process of the silver particles. On area 2 it was possible to characterise the tarnished area, evidencing an enrichment in silver (Ag) and sulphur (S), suggesting the presence of silver sulphide (Ag_2S) as a degradation compound (Table 22, 2, b). The enrichment in silver and sulphur on the degradation compound is evidenced by the elemental maps of the area (Table 22, BSE, Ag, S). This compound was probably formed by the interaction of hydrogen sulphide present in the atmosphere with the image silver particles in the presence of moisture [45]. The detection of silver sulphide particles in the area covered with a thin layer of what appears to be silver mirroring suggests that this silver compound is responsible for it. Elemental point analysis was also done on the dark area, showing that the support is a soda-lime-silica (Na-Ca-Si) glass (Table 22, 2, c). On area 2 an interface between another area was also analysed, showing the presence of silver (Ag) and iodide (I) on a particle (Table 23, 2, d); as well as the presence of sodium (Na) and sulphur (S) on a different particle (Table 23, 2, e). Ag and I suggest the use of silver iodide as the photosensitive material on the collodion solution and Na and S the use of sodium thiosulphate ($Na_2S_2O_3$) as a fixing agent. The presence of these elements was also mapped through elemental maps of the area (Table 23, BSE, Ag, I, S, Na).

Table 22: VP-SEM images of areas 1 and 2 showing the points analysed (a, b and c); elemental point analysis of a particle showing the presence of silver on the image forming particles (a); of a particle on a tarnished area with Ag and S, suggesting the presence of silver sulphide (b); on the dark area, showing that the support is a soda-lime-silica glass (c). BSE, backscattered electrons; elemental maps (Ag, S).

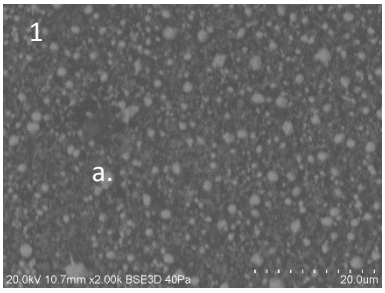

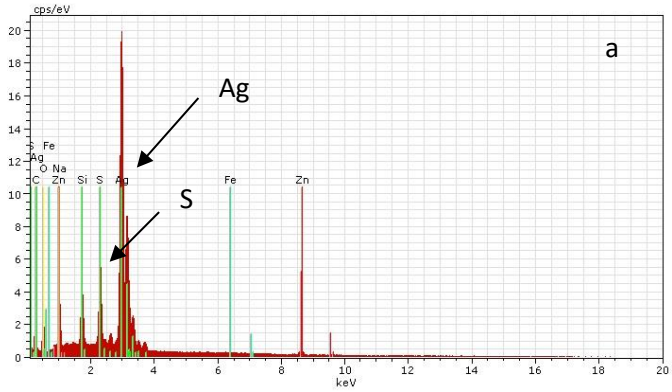

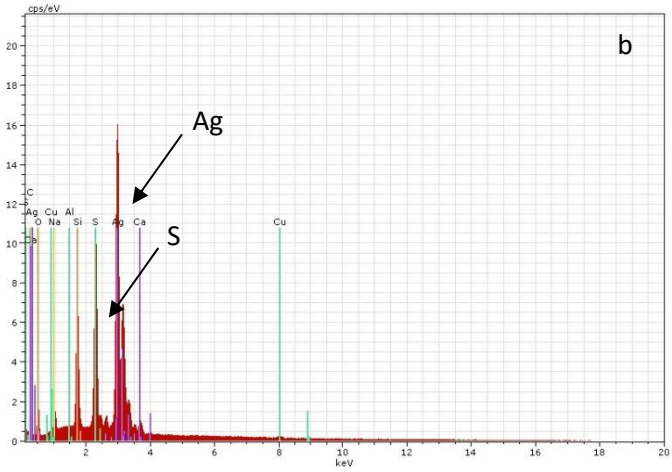

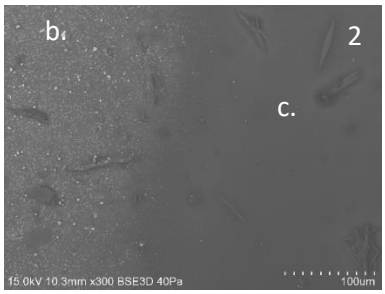

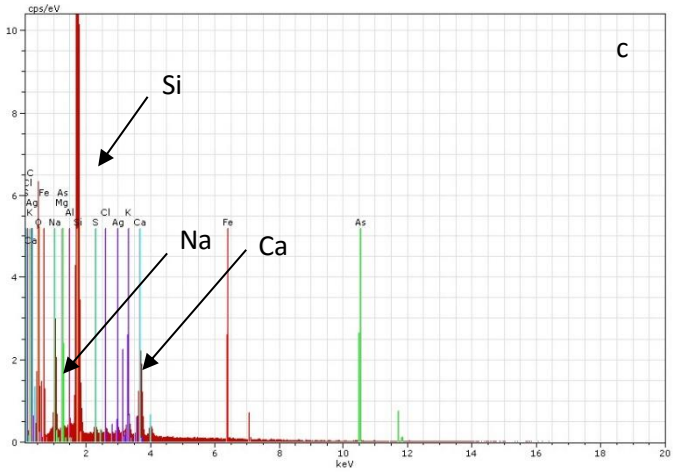

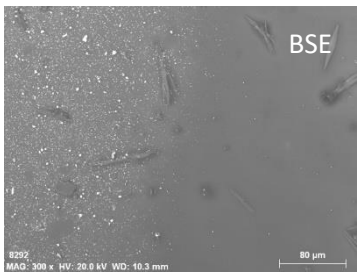

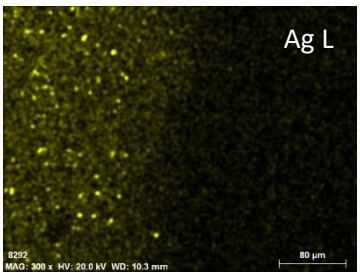

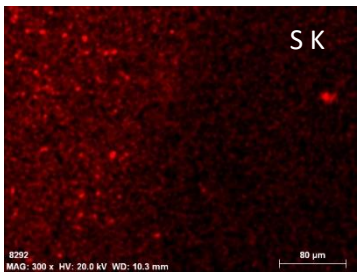

Table 23: VP-SEM images of area 2 showing the points analysed (d and e); elemental point analysis of a particle containing Ag and I (d); and of a particle containing Na and S.
BSE, backscattered electrons; elemental maps (Ag, I, S and Na).

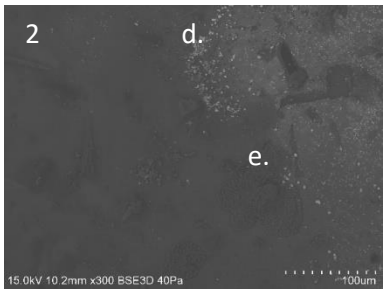

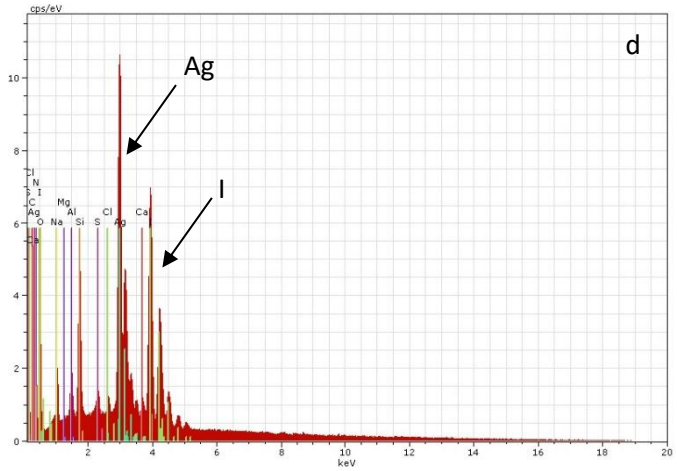

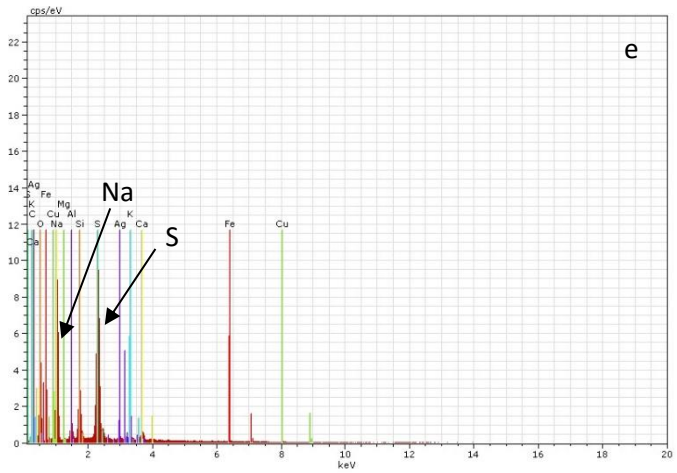

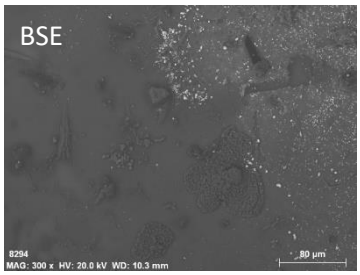

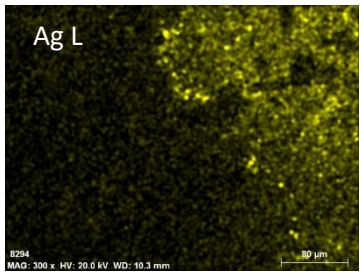

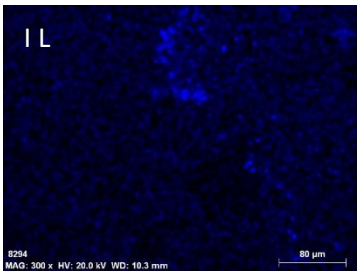

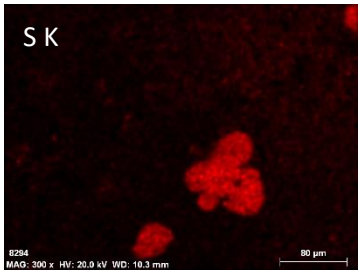

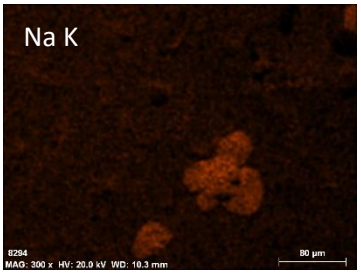

On area 3, the area beneath the brass mat, elemental point analysis on the main degradation compound showed an enrichment in copper (Cu), sulphur (S) and chloride (Cl) and the presence of silver (Ag) and chloride (Cl) on a different particle of the same area (Table 24, 3, a, b). This is can also be verified through the elemental maps (Cu, S, Cl and Ag) of the area (Table 25, BSE, Cu, S, Cl, Ag). The first analysis shows the presence of two copper degradation compounds, probably copper sulphide and copper chloride. This occurrence of local copper corrosion can be linked to the contact with the brass mat. The second analysis can be explained either through the use of hydrochloric acid during the production process or due the degradation process of the silver particles through the formation of silver chloride (AgCl). On point 4, elemental point analysis on the pigment particles revealed the presence of iron (Fe), suggesting that these are iron oxide (Table 25, 4, c).

Table 24: VP-SEM image of area 3 showing the points analysed (a and b); elemental point analysis on a particle containing Ag and Cl (a); and on a particle containing Cu, S and Cl (b).

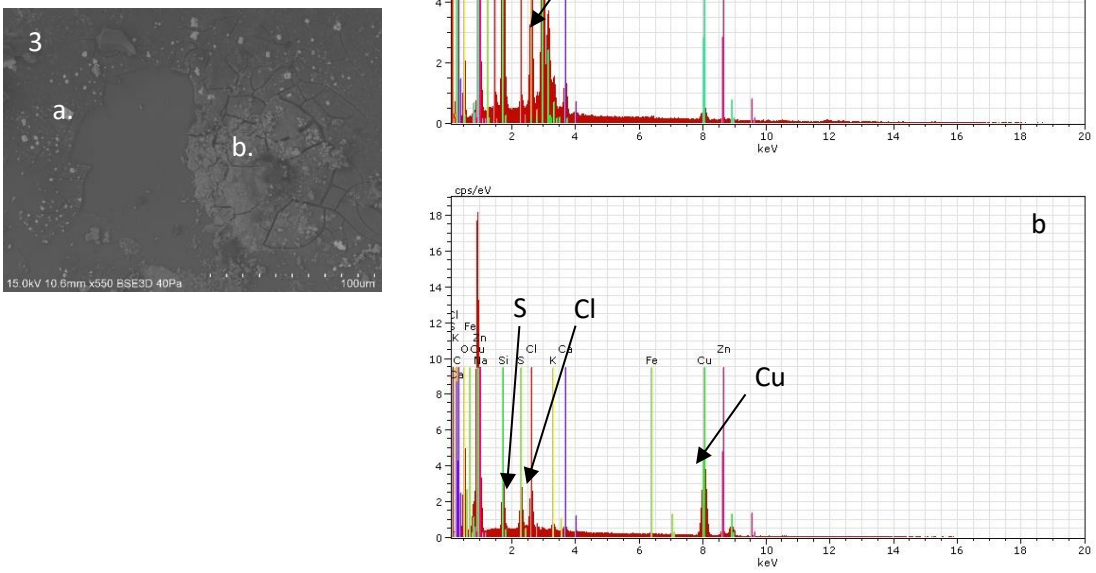

Table 25: BSE, backscattered electrons; elemental maps (Cu, S, Cl and Ag). VP-SEM image of area 4 showing the point analysed (c); elemental point analysis on a pigment particle containing Fe (c).

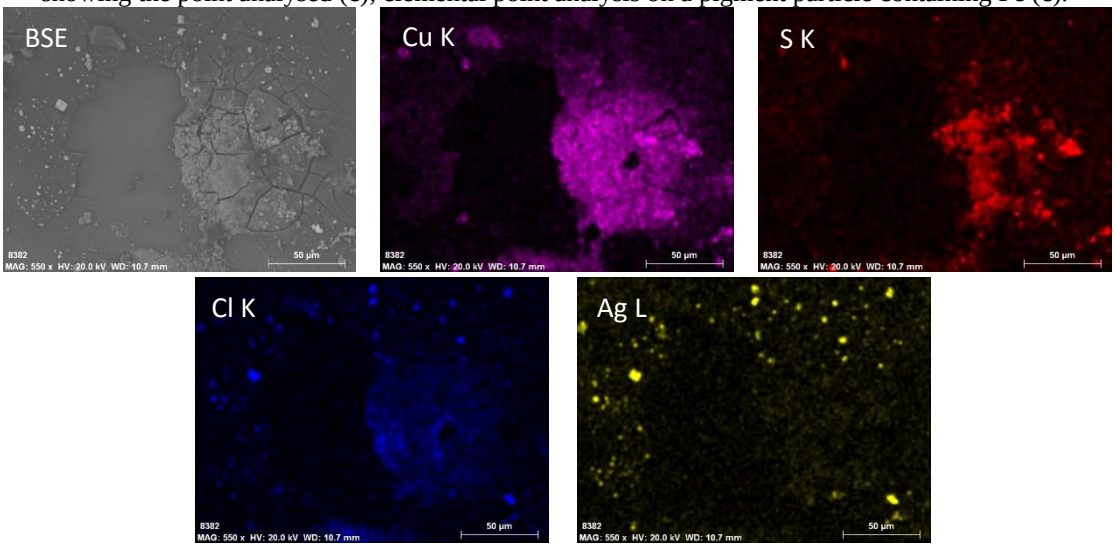

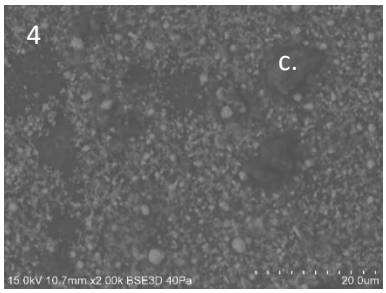

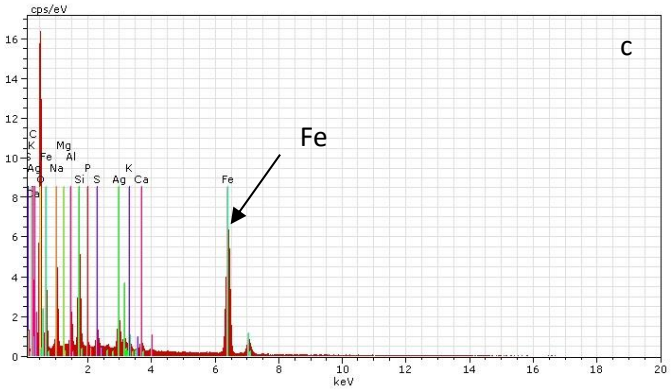

- **TINTYPES**

On tintype A, the areas chosen for analysis were an area of interface between a highlight and a dark area, in order to observe the characteristics of the image forming particles (Figure 43, A, 1); the area with the gold retouch on the woman's hand, to verify the materials used for the effect (Figure 43, A, 2); and an abraded area where the support was exposed (Figure 43, A, 3) in order to identify its composition. On tintype B, the areas chosen for analysis were an area of interface between a highlight and a dark area, in order to observe the characteristics of the image forming particles (Figure 43, B, 1); a *drip line* (Figure 43, B, 2); an abraded area where the support was exposed (Figure 43, B, 3) in order to identify its composition; and an area abraded by the frame with a degradation compound, to analyse its composition (Figure 43, B, 4).

Figure 43: mapping of the areas analysed with SEM-EDS on tintypes A and B.

On points 1 of both tintypes, the highlight area with more silver particles and higher density and the dark area has with fewer particles and lower density was observed (Table 26), as well as the interface between a highlight and a dark area (Table 27). In neither of the tintype the particles show significant differences in size, with an average size of ~2 µm for tintype A and 0,8 µm for tintype B.

Table 26: VP-SEM images of highlights on tintype A (A and B) and on tintype B (C and D); dark areas on tintype A (E and F) and on tintype B (G and H).

HIGHLIGHTS

TINTYPE A

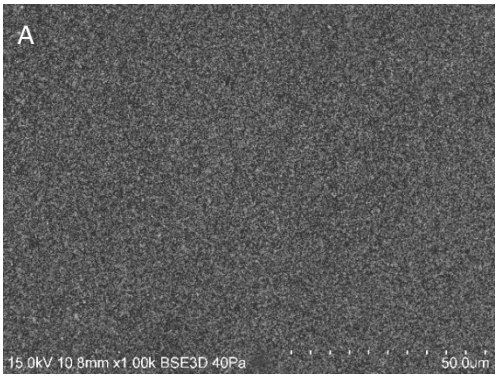

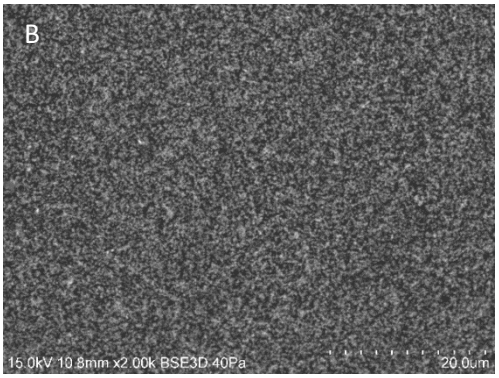

TINTYPE B

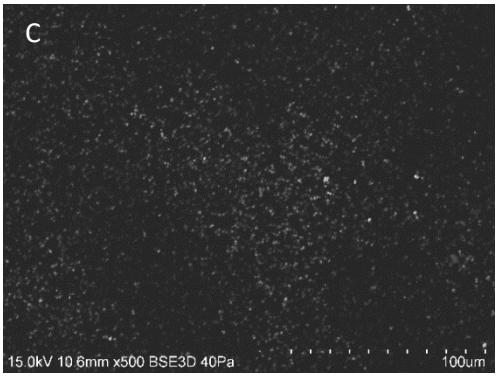

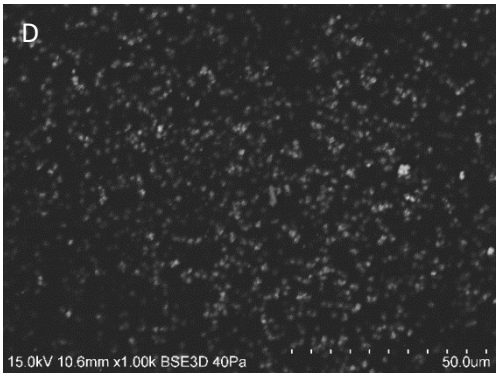

DARK AREAS

TINTYPE A

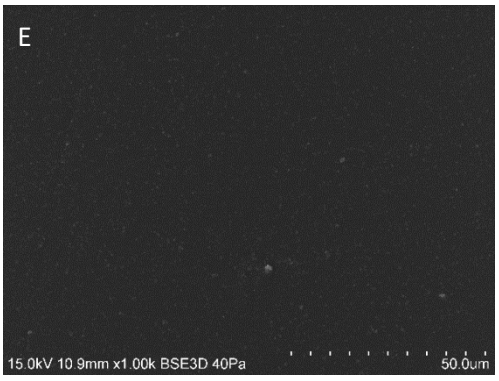

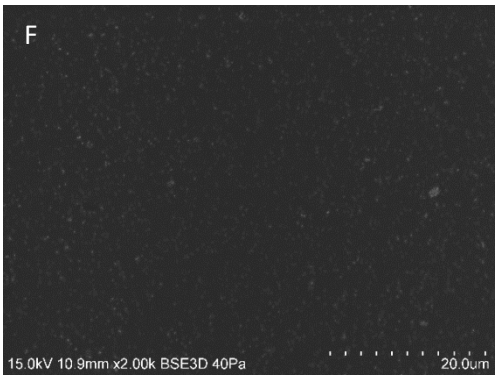

TINTYPE B

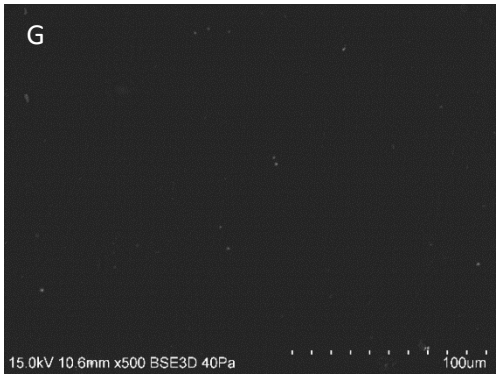

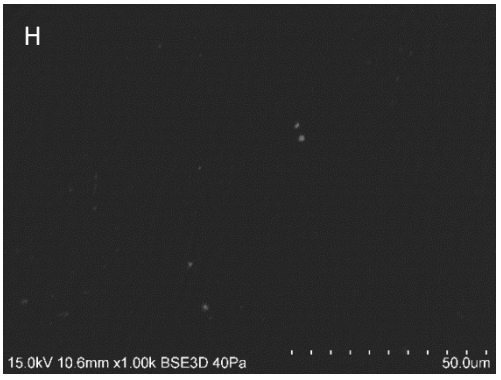

Table 27: VP-SEM images interfaces on tintype A (A and B) and on ambrotype B (C and D).

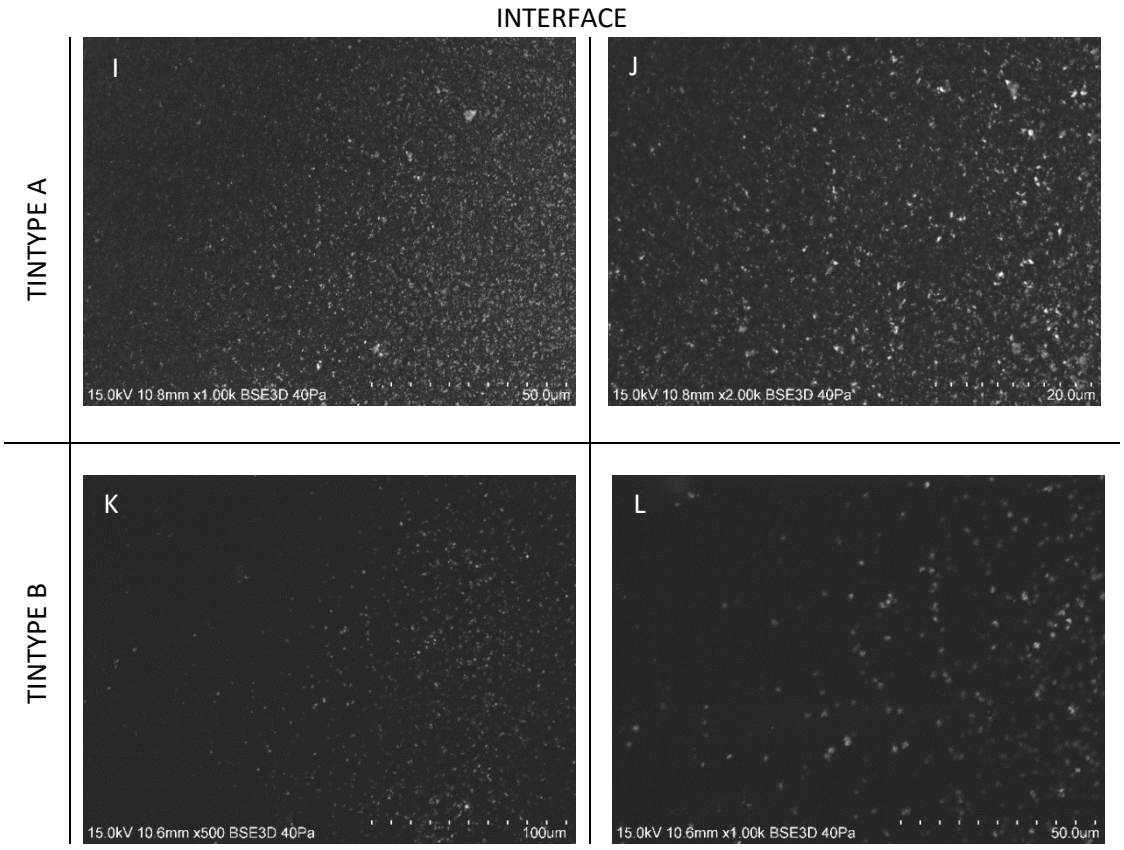

The elemental point analysis of an image forming particle on tintype A shows the presence of silver (Table 28, a). On point 2 a golden particle used on the retouch was analysed confirming the presence of gold (Au) (Table 28, b), and the golden particles were observed with high magnifications (Table 28, i). Elemental point analysis was also done on a particle of a different kind showing the presence of silver (Ag) and sulphur (S), indicating a degradation process of the image forming particles (Table 28, c). This was evidenced by the elemental maps of Au, Ag and S (Table 28, BSE, Au, Ag, S).

Table 28: VP-SEM images of areas 1 and 2 showing the points analysed (a, b and c) and of the golden particles (i); elemental point analysis on a particle containing Ag (a); on a particle containing Au (b); and on particle containing Ag and S (c).
BSE, backscattered electrons; elemental maps (Au, Ag, S).

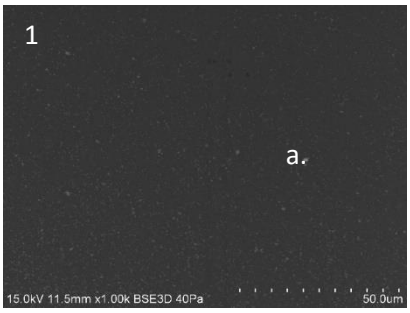

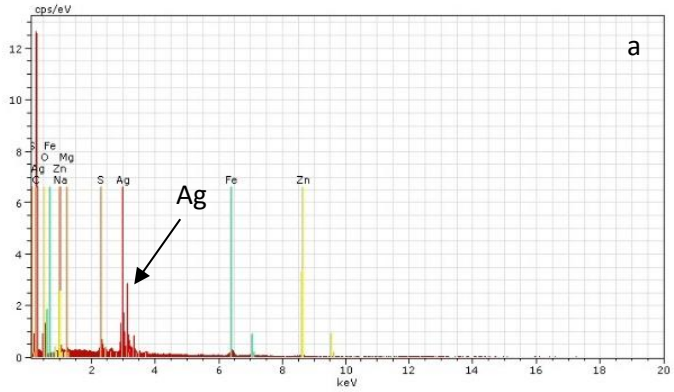

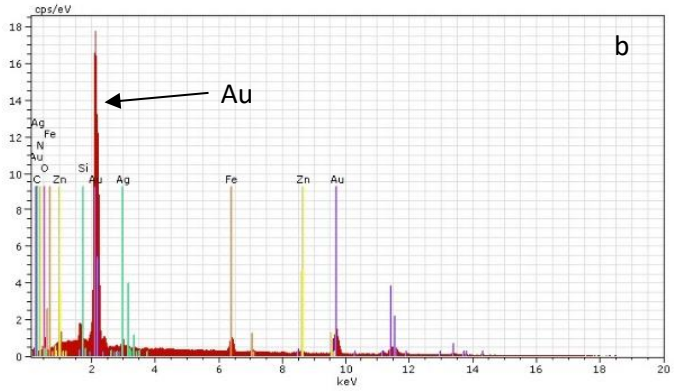

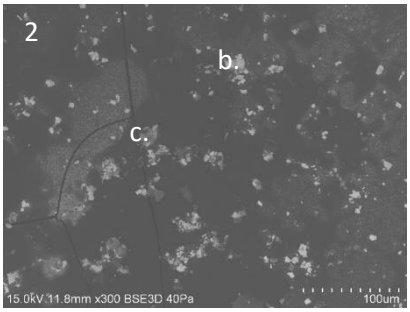

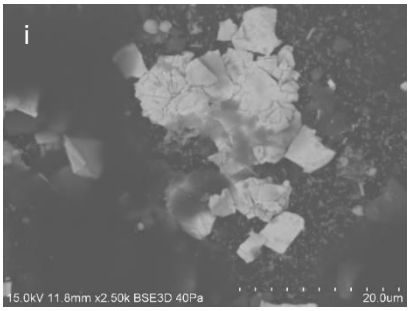

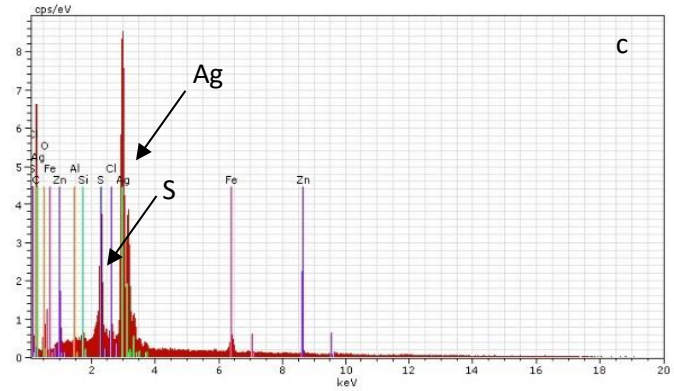

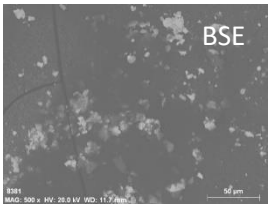

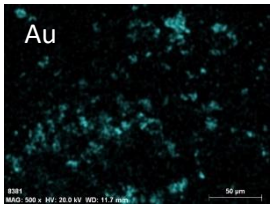

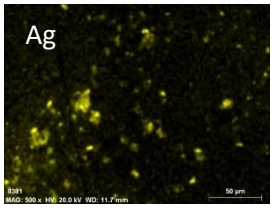

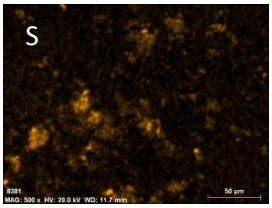

On area 3, it is possible to observe the morphology of the degradation, where a part of the emulsion is missing, exposing the support. Elemental point analysis of the emulsion showed the presence of silver and iodide, which implies that iodides were used in the collodion solution (Table 29, a); and of the support showed that is it composed mostly of iron (Table 29, b). This is corroborated by the elemental maps of Fe, Ag and I of the area (Table 29, BSE, Fe, Ag, I).

Table 29: VP-SEM images of area 3 showing the points analysed (a and b); elemental point analysis on a particle containing Ag and I (a) and on a particle containing Fe (b).
BSE, backscattered electrons; elemental maps (Fe, Ag, I).

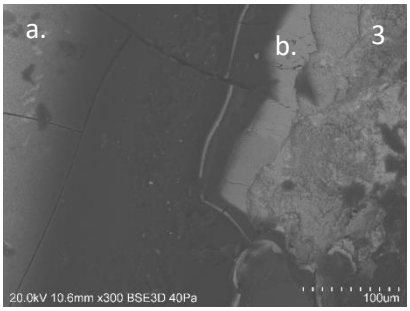

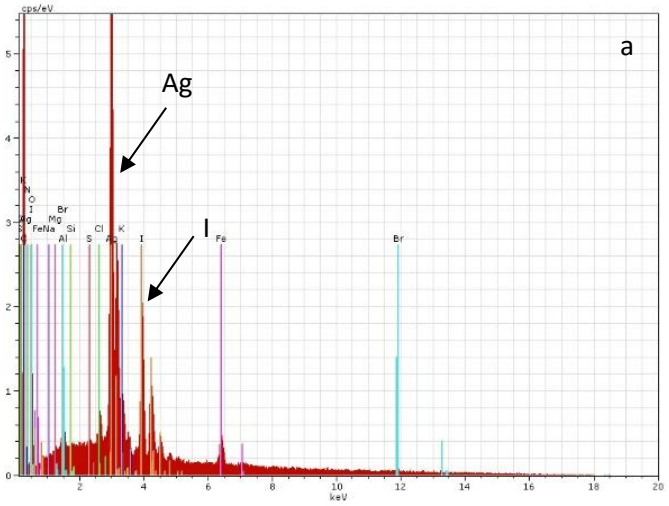

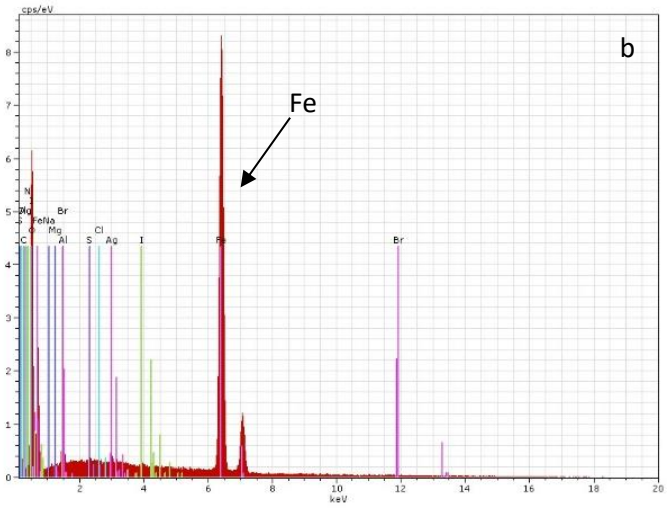

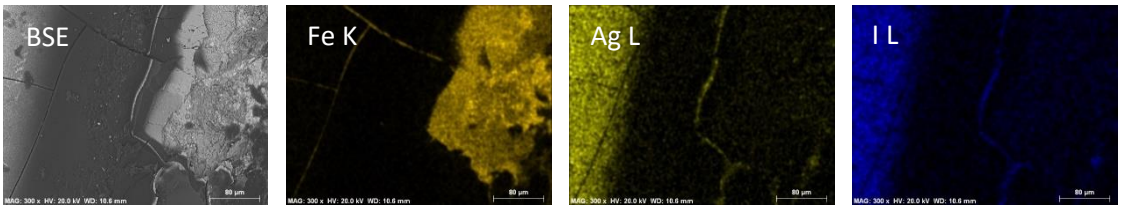

On tintype B, the elemental point analysis of an image forming particle on area 1 showed the presence of silver (Table 30, a). On point 2, the elemental point analysis was done on an accumulation visible and showed the presence of silver (Ag), sulphur (S) and sodium (Na) (Table 30, b). The distribution of these elements can be seen on the elemental maps (Table 30, BSE, Ag, S, Na). The presence of sulphur and sodium along with silver point to the use of sodium thiosulphate as the fixing agent.

Table 30: VP-SEM images of areas 1 and 2 showing the points analysed (a and b); elemental point analysis on a particle containing Ag (a); and on a particle containing Ag, S and Na (b). BSE, backscattered electrons; elemental maps (Ag, S, Na).

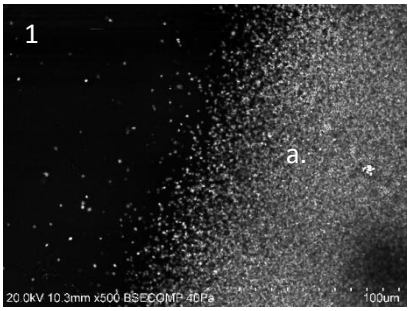

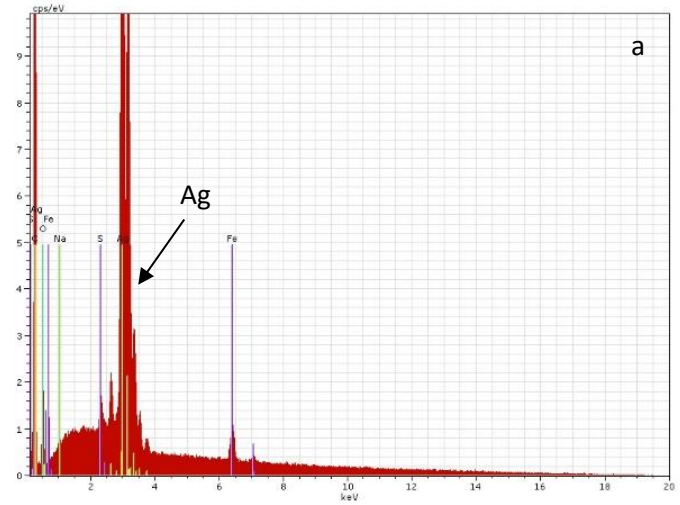

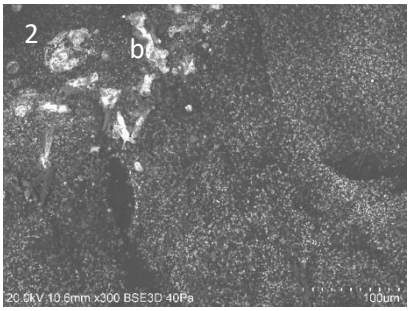

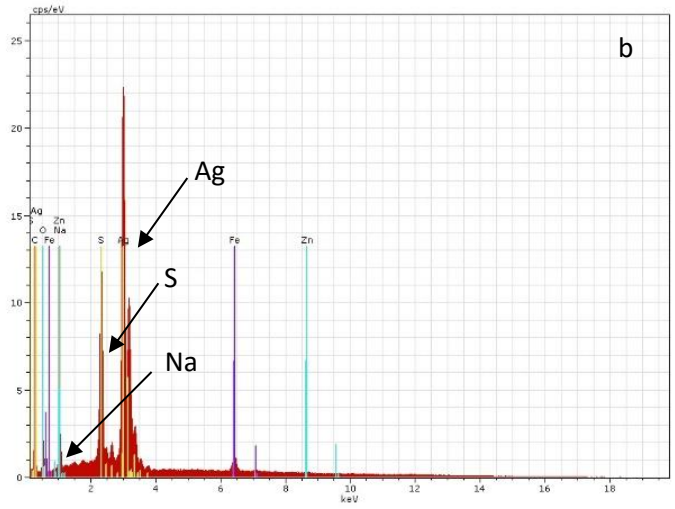

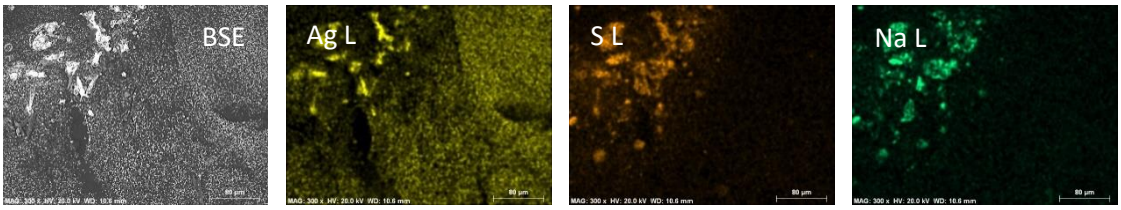

On point 3, it is possible to observe the morphology of the abrasion, where a part of the emulsion is missing, exposing the support (Table 31, 3). Elemental point analysis of the support showed that is it composed mostly of iron (Table 31, a). The elemental maps (Fe and C) of the area confirm the support to be composed of iron and show the presence of a thick layer of an organic layer where there was no abrasion, which is probably due to the presence of a finishing varnish (Table 31, BSE, C, Fe). On area 4, elemental point analysis was done on a particle on an abraded area, on the degradation compound formed by the contact with the brass mat. It showed the presence of copper (Cu) and chloride (Cl), which probably form copper chloride, a copper degradation compound (Table 31, b).

Table 31: VP-SEM images of area 3 showing the point analysed (a); elemental point analysis on a particle containing Fe (a). BSE, backscattered electrons; elemental maps (C, Fe).

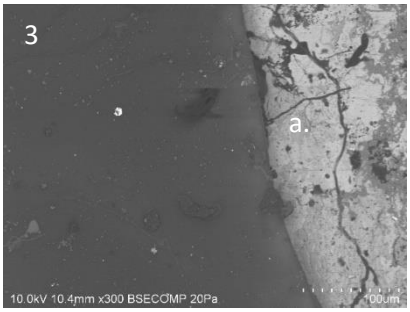

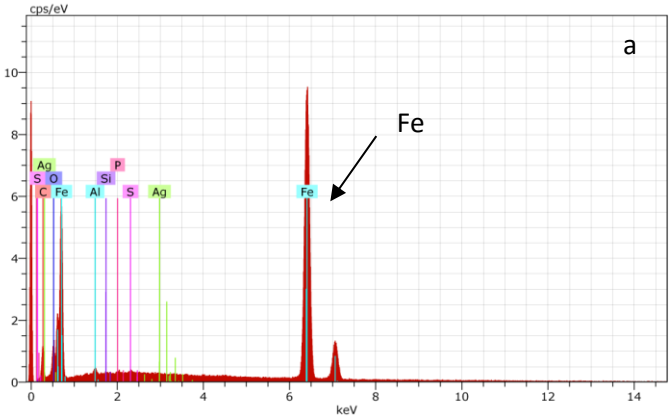

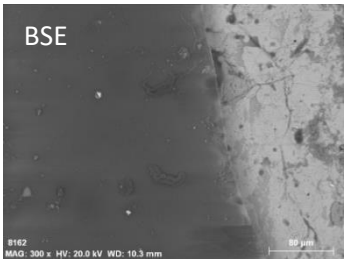

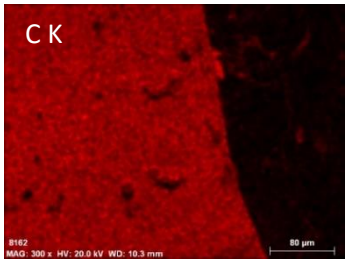

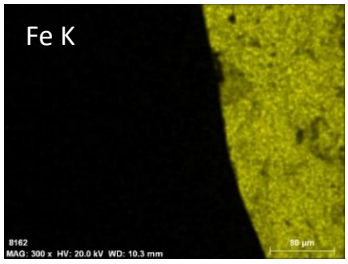

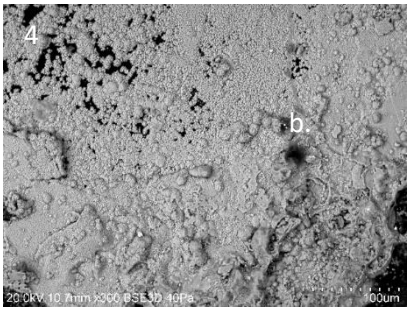

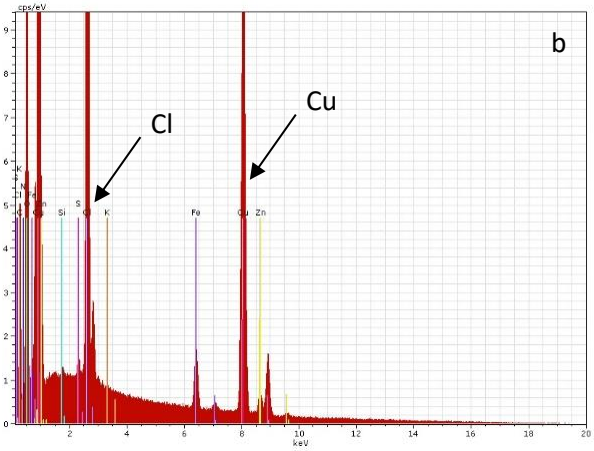

3.1.4. Micro-Fourier transform infrared spectroscopy (µ-FT-IR)

The purpose of the µ-FTIR analysis was to detect the presence of collodion and identify the sources of the varnishes. The presence of collodion can be confirmed by the presence of the characteristic absorption bands of nitrocellulose ($C_6H_7(NO_2)_3O_5$) at 1632-1641 cm^{-1} ,1059 cm^{-1}, 1268-1273 cm^{-1} and 824-833 cm^{-1} [46] [46]. For the identification of the varnish, several characteristic absorption bands need to be present. Namely, the carbonyl band at 1630-1 750 cm^{-1} in the case of sources such as protein, tree resin, insect or oil; or C-H stretches at 2850-2960 cm^{-1} in the case of wax or gum based varnishes [43]. Particular bands will allow to distinguish more specifically the product used for the production of the varnishes. Several areas of the objects' surfaces were analysed with µ-FTIR spectroscopy, including both cheeks, but the results were consistently similar, so only one spectrum of one point of the surface is shown and is considered to represent the all the results.

- **AMBROTYPES**

Both spectra present absorption bands which can be attributed to the presence of collodion: for ambrotype A, 1639 cm^{-1}, 1246 cm^{-1} and 825 cm^{-1}(Figure 43); and for ambrotype B, 1633 cm^{-1}, 1290 cm^{-1} and 825 cm^{-1} (Figure 45)[47]. The other absorption bands are related to the varnish: for ambrotype A, the absorption bands at 2933 cm^{-1}, 2864 cm^{-1}, 1710 cm^{-1}, 1462 cm^{-1}, 1246 cm^{-1} and 1003 cm^{-1} can be attributed to the presence of a natural tree resin, most probably mastic gum; and the ones at 1639 cm^{-1}, 1375 cm^{-1}, 1167 cm^{-1} and 927 cm^{-1} can be attributed to the presence of shellac, a resin from an insect source. In fact, the bibliography mentions the use of coatings produced with a combination of natural resins. Regarding ambrotype B, because the varnishes and the collodion have absorption bands at very close values, 1246 cm^{-1} and 1639 cm^{-1}, and these can be attributed to both and explain some deviation from the standards [43]. The broad band around 3415 cm^{-1} can be explained by the effect of irradiation on nitrocellulose, which leads to the appearance of new absorption bands in this region [48]. The shoulder at 3351 cm^{-1} (O-H) and the absorption band at 1010 cm^{-1} (C-O), along with the weak absorption band at 2933 cm^{-1} (C-H stretch) might indicate the presence of a gum, possibly mastic [43]

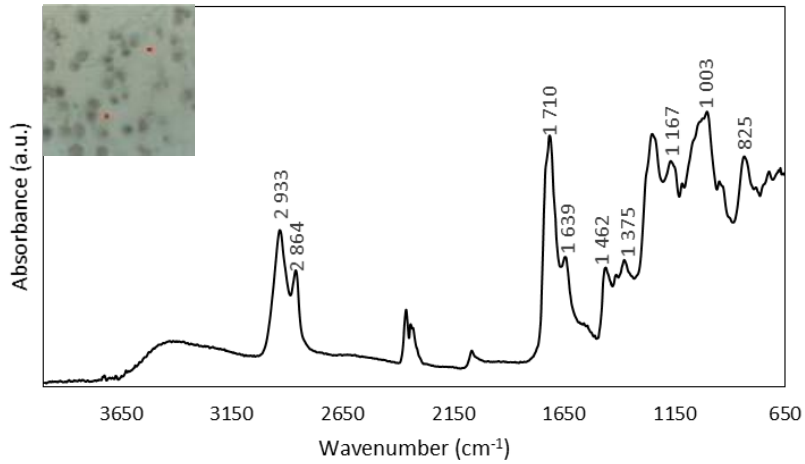

Figure 44: µ-FTIR spectrum of ambrotype A. The inset, detail from the analysed spot.

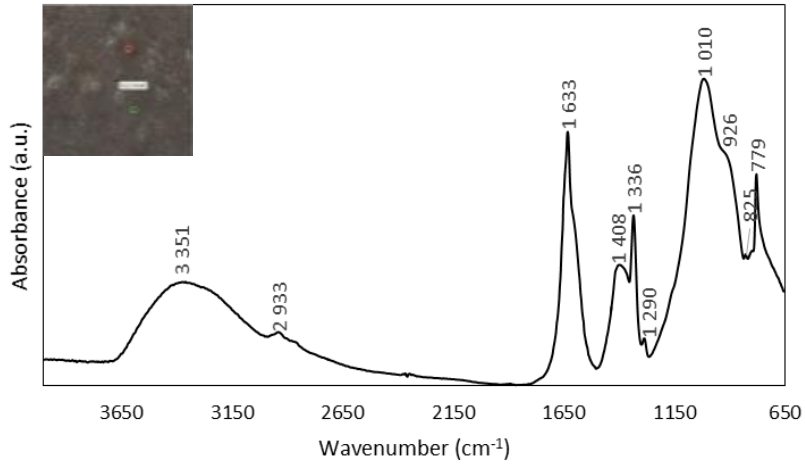

Figure 45: µ-FTIR spectrum of ambrotype B. The inset, detail from the analysed spot.

- **TINTYPES**

Both spectra show absorption bands which confirm the presence of collodion: for tintype A these where at 1643 cm^{-1}, 1278 cm^{-1}, 1059 cm^{-1} and 841 cm^{-1} (Figure 46); and for tintype B at 1641 cm^{-1}, 1273 cm^{-1}, 1059 cm^{-1} and 833 cm^{-1} (Figure 47). Regarding the varnishes, for tintype A the absorption bands at 2933 cm^{-1}, 2862 cm^{-1}, 1375 cm^{-1}, 1110 cm^{-1} and 746 cm^{-1} can be attributed to the presence of shellac and the ones at 1710 cm^{-1}, 1462 cm^{-1} and 1163 cm^{-1} to mastic. Probably, a mixture of both natural resins was used, as mentioned before. Tintype B also shows the presence of shellac, with the absorption bands at 2862 cm^{-1}, 1375 cm^{-1} and 933 cm^{-1}; and mastic, with the peaks at 1454 cm^{-1} and 1705 cm^{-1} [49].

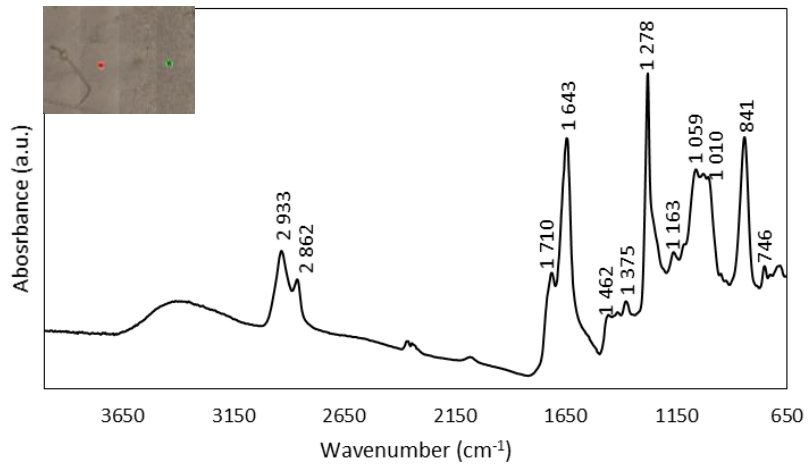

Figure 46: µ-FTIR spectrum of tintype A. The inset, detail from the analysed spot.

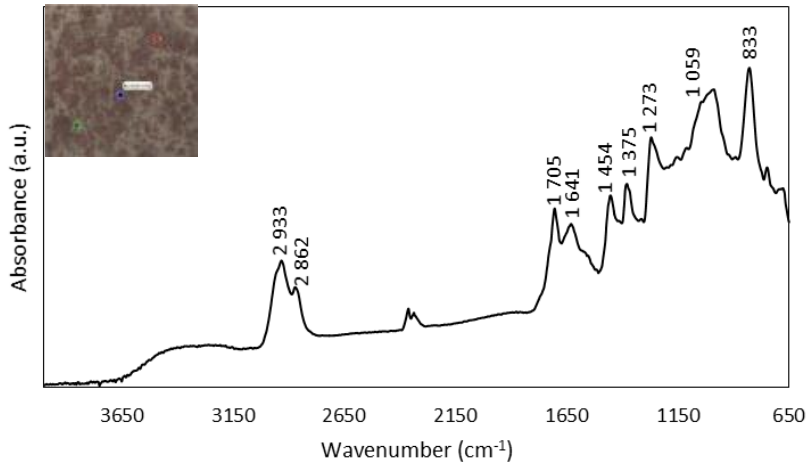

Figure 47: µ-FTIR spectrum of tintype B. The inset, detail from the analysed spot.

3.1.5. Micro-Raman spectroscopy (µ-Raman)

- **AMBROTYPES**

Figure 48, A illustrates the points analysed on ambrotype A: a red painted area (1) and on an area of the image apparently without degradation compounds (2). Several points were analysed, but these two represent the results obtained, because all the others showed similar results. On ambrotype B most analysis did not show any bands, simply fluorescence, so only one spectrum will be presented, as shown on Figure 48, B.

The analysis of point 1 on ambrotype A shows a spectrum with four bands at 222 cm^{-1}, 289 cm^{-1}, 407 cm^{-1} and a smaller one at 606 cm^{-1} (Figure 49, 1). These are probably

related to the red compound used to paint the face of the subjects. Mars red, a synthetic iron oxide pigment (Fe_2O_3), characteristic of the middle of the 19th century has characteristic bands at 224 cm^{-1}, 291 cm^{-1}, 407 cm^{-1}, 494 cm^{-1}, 610 cm^{-1} and 660 cm^{-1}, some of which correspond to the ones observed on point 1 [50]. The spectrum of point 2 shows a peak at 122 cm^{-1} and another at 228 cm^{-1} (Figure 49, 2). Both peaks can be attributed to the presence of AgCl, which has been reported to exhibit peaks at 144 cm^{-1} and 227 cm^{-1}, based on the μ-Raman analysis of a AgCl pattern (appendix I). Similarly, the spectrum of ambrotype B has two absorption bands at 128 cm^{-1} and 224 cm^{-1} (Figure 50), which are also attributed to AgCl.

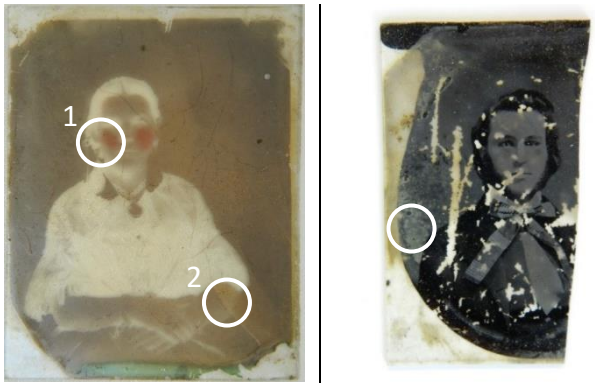

Figure 48: mapping of the areas analysed with μ-Raman spectroscopy on ambrotypes A and B.

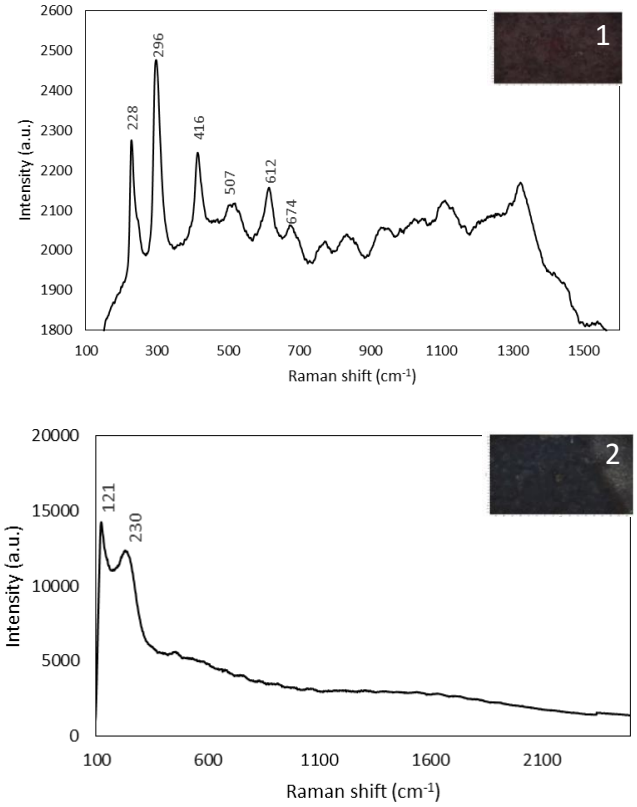

Figure 49: μ-Raman spectrum of ambrotype A (areas 1 and 2).
The insets, details from the analysed spots.

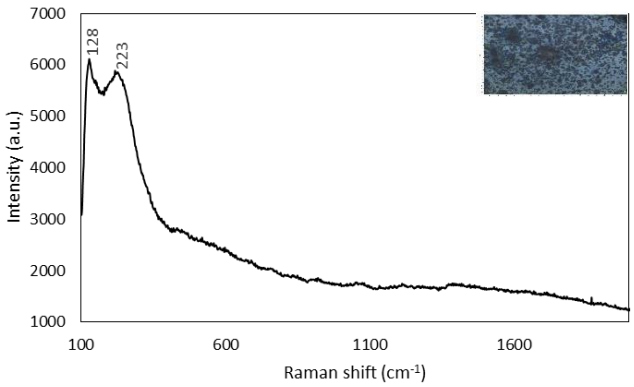

Figure 50: µ-Raman spectrum of ambrotype B. The inset, detail from the analysed spot.

- **TINTYPES**

Figure 51 illustrates the points analysed on the tintypes. Several points were analysed on the surface of tintype A, but most gave spectra without peaks due to the emission of high levels of fluorescence, probably related to the presence of a thick layer of varnish on the surface of the object. However, one point gave a spectrum with a peak at 119 cm^{-1} (Figure 52), which can be related to the presence of Ag_3 clusters [51]. The analysis of tintype B produced two spectra with significant peaks. One with a peak at 122 cm^{-1} (Figure 53, 1), which can be related to the presence of Ag_3 clusters [51]. And the other with peaks at 128 cm^{-1} and 249 cm^{-1} (Figure 53, 2), which can be assigned AgCl, as mentioned before.

Figure 51: mapping of the areas analysed with µ-Raman spectroscopy on tintypes A and B.

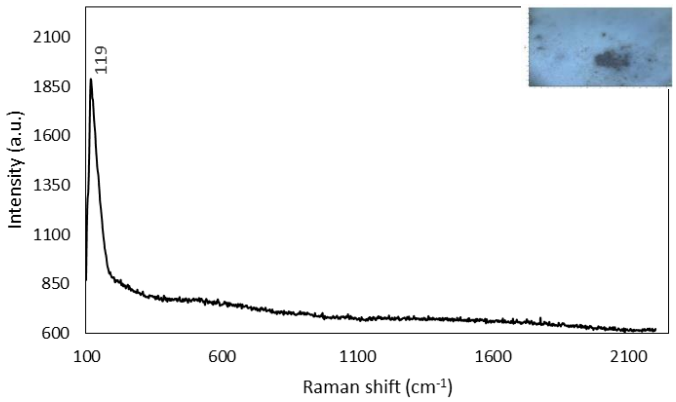

Figure 52: µ-Raman spectra of tintype A. The inset, detail from the analysed spots.

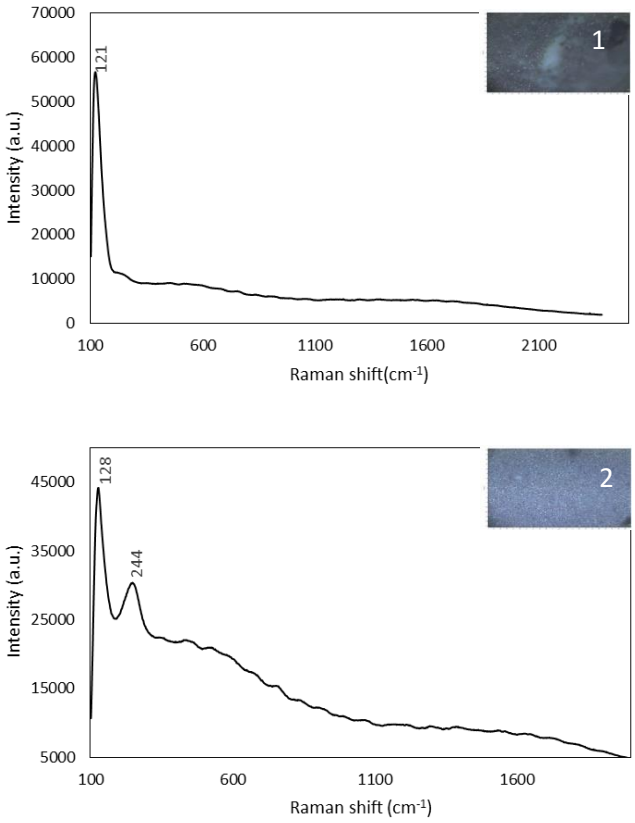

Figure 53: µ-Raman spectra of tintype B (areas 1 and 2). The insets, details from the analysed areas.

3.1.6. Micro X-ray diffraction (μ-XRD)

The objects were analysed on several points, but most produced identical results. So, only some will be shown and considered representative of all the analyses done. Mainly, it was expected to detect the presence of metallic silver, as the image forming particles, and some silver degradation compounds, if any. Also, perhaps some compounds related to the production process and to the composition of supports could be detected, especially on the tintypes, as they have a metallic support and therefore are easily detected through diffraction. Finally, the four brass mats were analysed and it was expected to detect the presence of copper and zinc, as they are made out of brass.

- **AMBROTYPES**

The μ-XRD analysis of ambrotype A also revealed the presence of metallic silver (Ag) and silver iodide (AgI) (Figure 54). Silver iodide is related to its use as a photosensitive material, as mentioned before. The presence of these compounds was also detected on the EDS point analysis. The analysis of ambrotype showed only the presence of silver nitrate ($AgNO_3$) (Figure 55). The results of this analysis have poor resolution, so the match to silver nitrate cannot be made with certainty. This compound, however, was typically used in the production process [8].

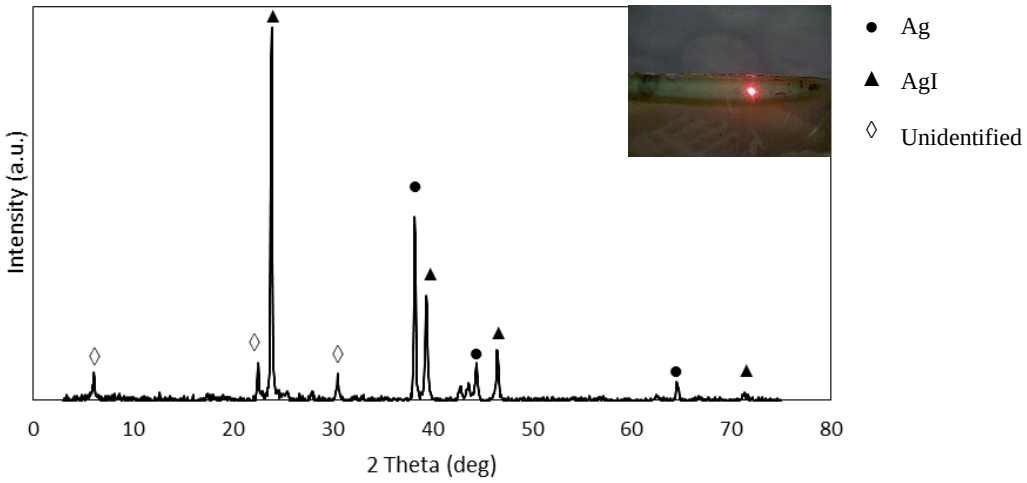

Figure 54: μ-XRD diffractogram of the analysis of ambrotype A. The inset, detail of the analysed spot.

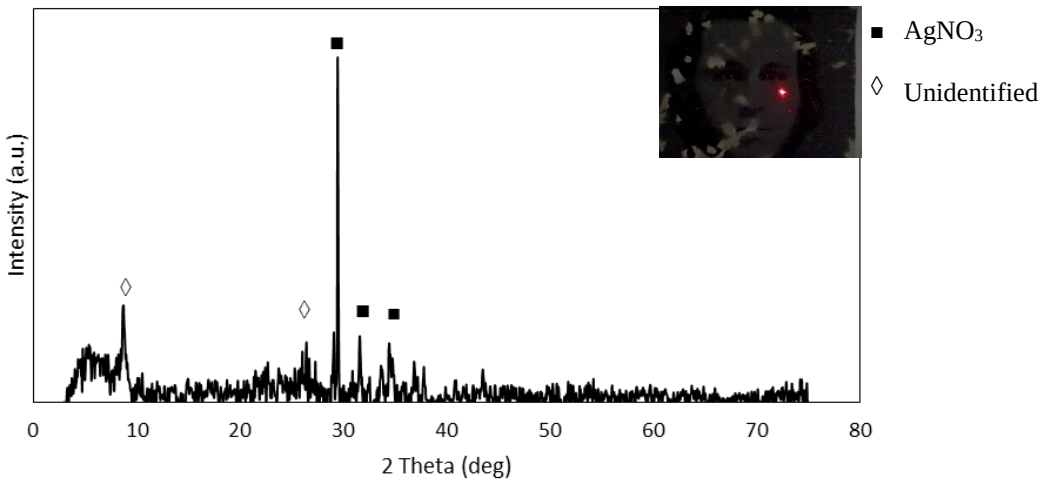

Figure 55: μ-XRD diffractogram of the analysis of ambrotype B. The inset, detail of the analysed spot.

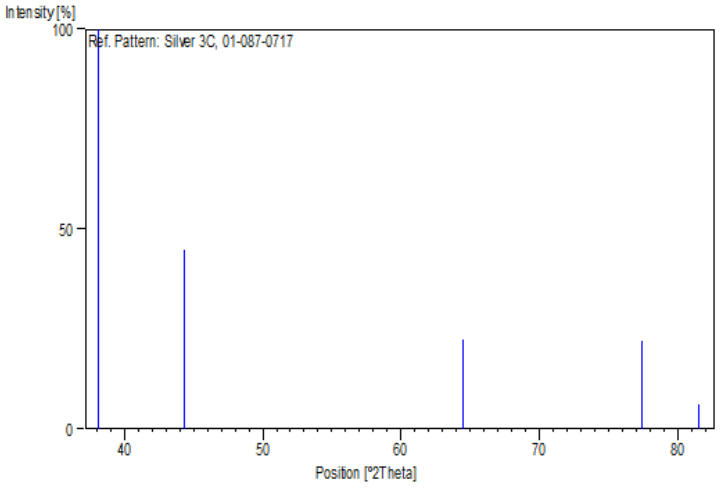

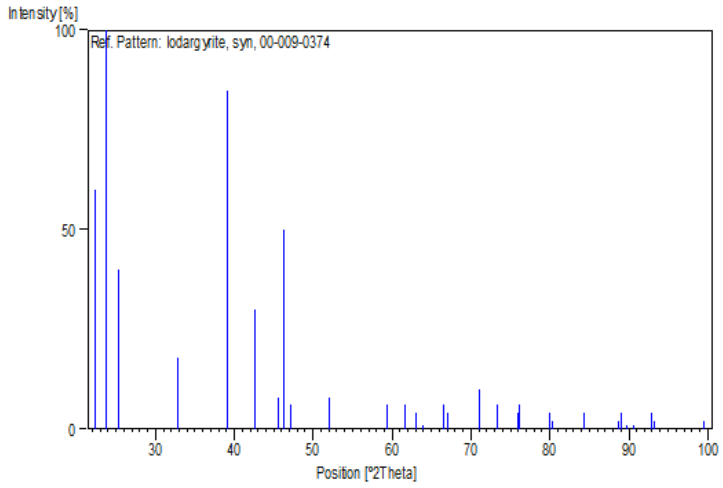

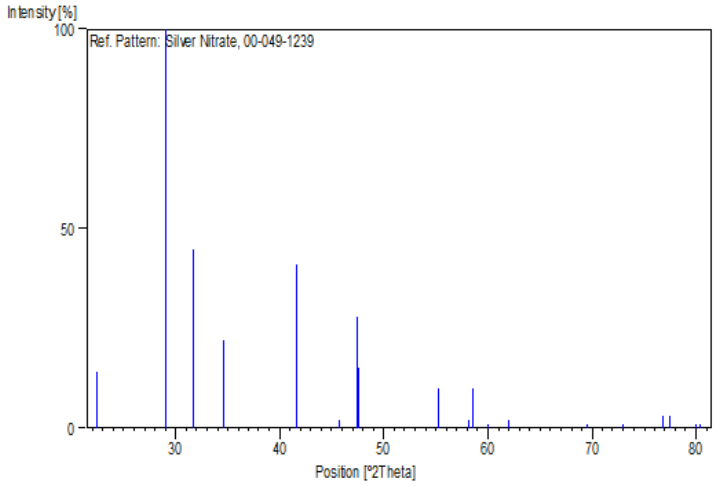

Figure 50: stick patterns of Ag (reference code: 01-087-0717), AgI (reference code: 00-009-0374) and $AgNO_3$ (reference code: 00-049-1239).

- **TINTYPES**

The μ-XRD analysis of tintype A (Figure 56) detected silver iodide (AgI), magnetite (Fe_3O_4), hematite (Fe_2O3) and wuestite (FeO). On tintype B, silver iodide and magnetite were also detected, along with metallic silver, present on the image forming particles. The presence of silver iodide is related to the production process, as mentioned before, and was also detected on the EDS analysis of both tintypes. The presence of magnetite, hematite and wuestite is related to the degradation of the support due to the oxidation of iron.

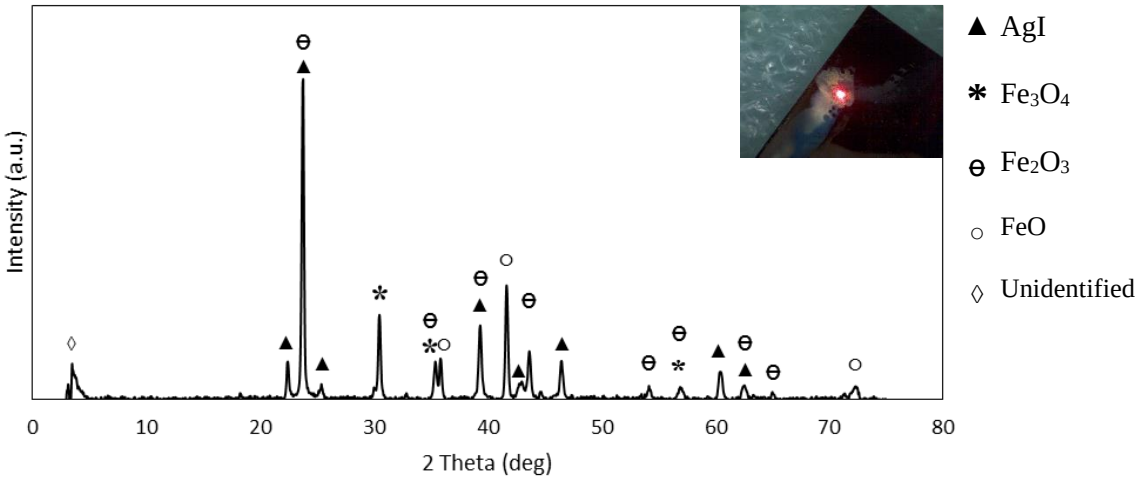

Figure 56: μ-XRD diffractogram of the analysis of tintype A. The inset, detail of the analysed spot.

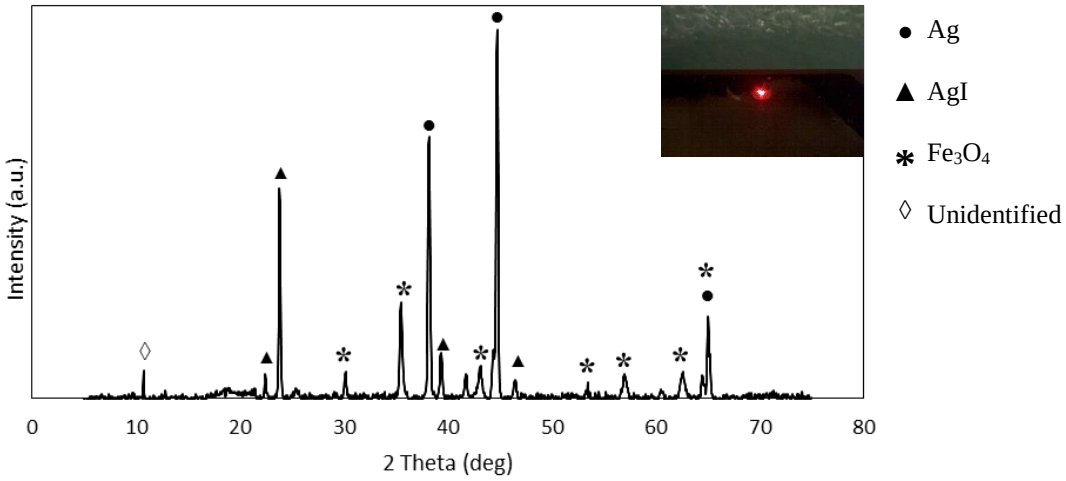

Figure 57: μ-XRD diffractogram of the analysis of tintype B. The inset, detail of the analysed spot.

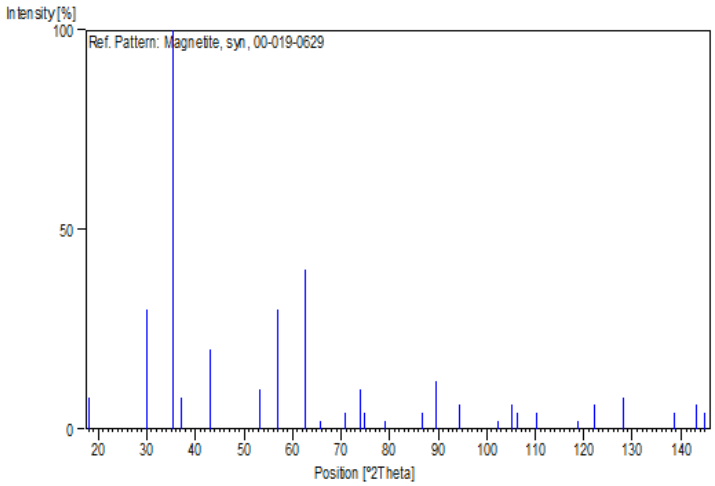

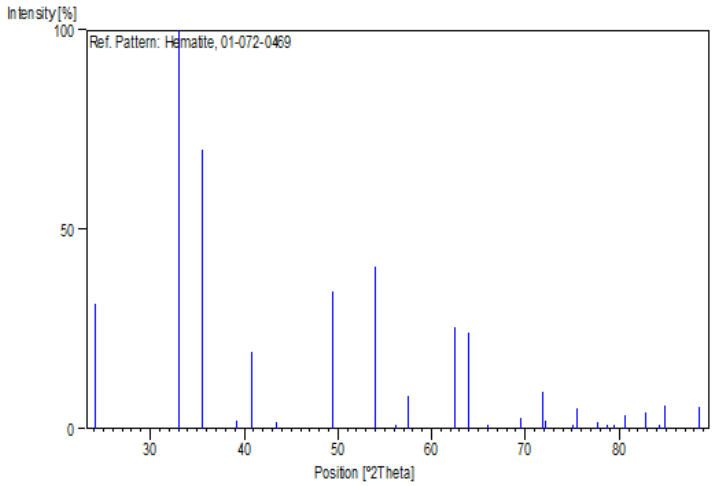

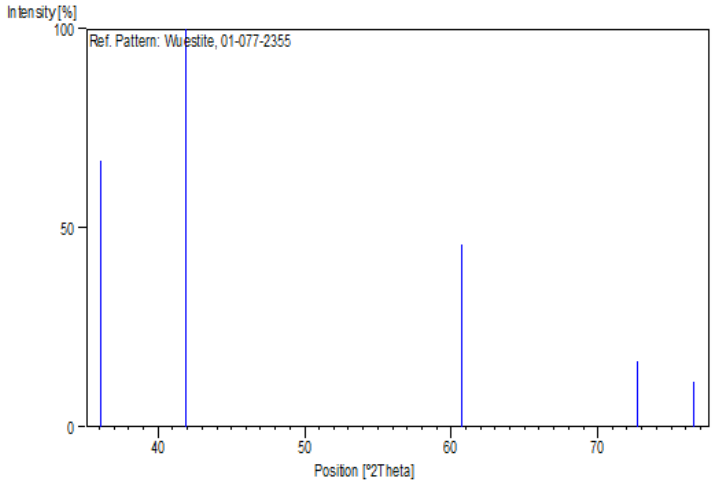

Figure 50: stick patterns of magnetite (reference code: 00-019-0629), hematite (reference code: 01-072-0469) and wuestite (reference code: 01-077-2355).

- **BRASS MATS**

The μ-XRD analysis of the four brass mats revealed the presence of copper and zinc, as expected for brass samples (Figure 58 and Figure 59).

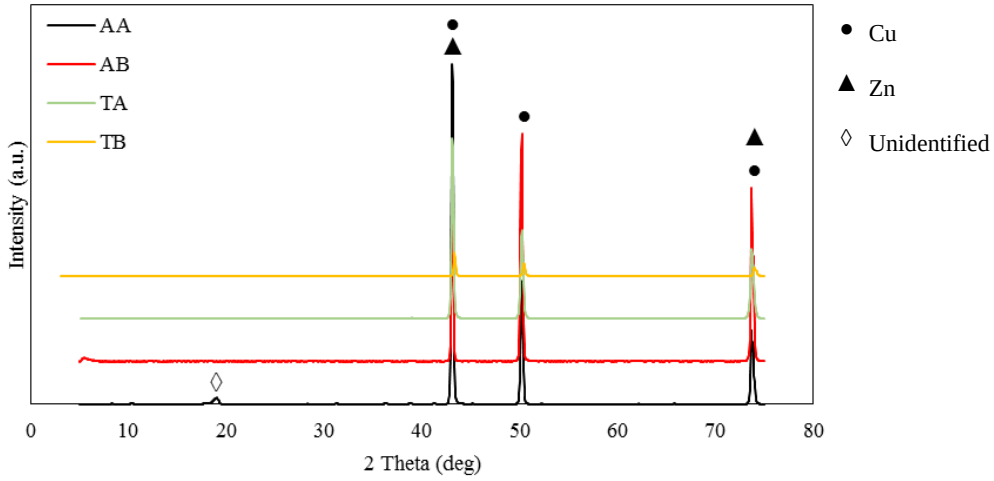

Figure 58: μ-XRD results of the analysis of the four brass mats.

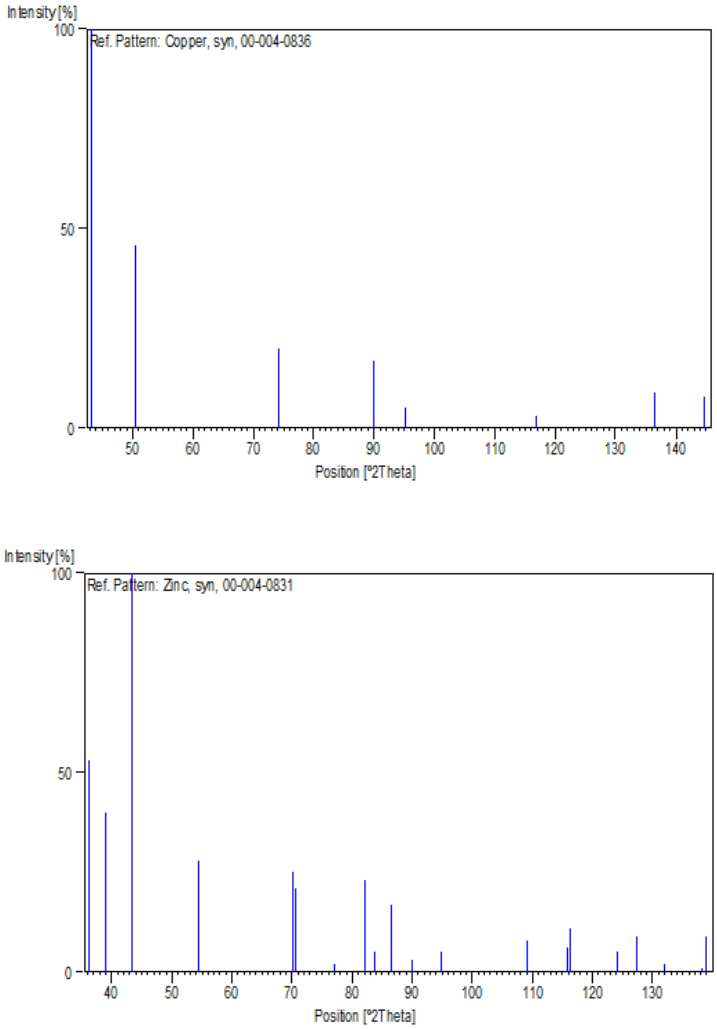

Figure 59: stick patterns of Cu (reference code: 00-004-0836) and Zn (reference code: 00-004-0831).

CHAPTER 4: CONCLUSIONS

The purpose of this study was to characterize both chemically and physically two ambrotypes and two tintypes, in order to understand their degradation pathologies and investigate their production methods cross-checking the analytical data with information from technical manuals of the time. The motivation to this study was based on the fact that the data regarding chemical and physical analysis on tintypes and ambrotypes is very scarce, and the expectation was to contribute with data for further studies on the field.

The results obtained with technical photography were particularly helpful in demonstrating the surface morphologies with the raking light and the distribution of the varnish layers and some degradation compounds with the UV radiation, which disclosed aspects not observable with the other modes. Also, the transmitted light mode displayed the abrasions and gaps on the ambrotypes. OM was essential to observe the surfaces with detail, especially the retouches and degraded areas. It showed aspects that were not noticeable with the naked eye, particularly the red pigments present on the cheeks and lips of one of the ambrotypes. OM was useful not only for the physical characterization of the objects but also to select the areas to be analysed with SEM-EDS.

SEM-EDS was the most insightful technique and the one used most extensively. It allowed to observe the image forming particles, particularly their highlights with more particles, sometimes forming agglomerates, the dark areas with fewer and scattered particles, and the interface between these on which a gradual transition between the two forms of particle morphology and distribution can be seen. Regarding the chemical analysis, the elemental point analysis conjugated with the elemental maps provided an illustration of the areas with retouches, allowing to identify the red pigments as iron based and one retouch on the jewellery made with gold. Also, areas with traces of elements that can be linked to the production process – silver and iodide, that could be related to the use of silver iodide as the photosensitive material; with barium and sulphur, which can be related to the use of ferrous sulphate and barium nitrate as developers; or with sodium and sulphur, that can be related to the use of sodium thiosulphate. Also, elemental point analysis conjugated with the elemental maps also provided insight into degradation compounds containing silver and sulphur or chloride, typical silver degradation compounds, or copper and sulphur which can be related to the interaction of the brass mats with the compounds on the surface of the object. Finally, it provided the identification of the image forming particles as silver and the supports – soda-lime-silica glasses in the case of the ambrotypes and iron in the case of the tintypes.

By µ-FT-IR analysis the presence of collodion was confirmed and the sources of the varnishes were identified, specifically mixtures of mastic and shellac or only one of the two. Through µ-Raman spectroscopy it was possible to detect the presence of silver and silver chloride and to identify the red pigment used in one of the ambrotypes as Mars red. Finally, with µ-XRD diffraction the existence of silver, silver iodide and silver chlorate was shown as well as the presence of iron oxides on the tintypes, particularly magnetite, hematite and wuestite.

Overall, the aims have been achieved as an extensive characterization of the objects was done providing results regarding the chemical and physical aspects, related both to degradation patterns and the production methods used in their making. The hope is that this study can serve as a case for further research, either thru what was achieved and uncovered either thru mistakes that should be avoided on this kind of studies in order to achieve better and more promising results.

REFERENCES

[1] G. B. Romer, “Fundamentals of the Conservation of Photographs,” 2010. [Online]. Available: www.getty.edu/conservation. [Accessed March 2016].

[2] M. Roosa, “Care, Handling, and Storage of Photographs,” *International Preservation Issues*, vol. 5, 2004.

[3] G. T. Eaton, “The Photographic Process,” in *Photographic Chemistry in black-and-white and colour photography*, New York, Morgan & Morgan, 1965, pp. 7-10.

[4] S. Fujita, “Fundamentals of Photography,” in *Organic Chemistry of Photography*, New York, Springer, 2004, pp. 1-103.

[5] F. Frey and S. Clarke, Care of Photographs, Amsterdam: European Commission on Preservation and Access, 2003.

[6] N. Rosenblum, A World History of Photography, Washington DC: Library of Congress Cataloging - Publication Data, 1997.

[7] R. Taft, Photography and the American Scene: A Social History, 1839-1889, New York: Dover Publications, Inc., 1938.

[8] M. F. Valverde, Photographic Negatives: Nature and Evolution of Processes, Rochester: George Eastman House, 2005.

[9] N. Burgess, “The Ambrotype Manual Part II: Practical Details of the Ambrotype Process,” in *The Photograph and Ambrotype Manual: A Practical Treatise*, New York, Hubbard, Burges & Co, 1861, pp. 125-234.

[10] M. Osterman and G. B. Romer, “History and the Evolution of Photography,” in *The Focal Encyclopedia of Photography: Digital Imaging, Theory and Applications, History and Science*, M. R. Peres, Ed., Oxford, Elsevier, 2007, pp. 23-177.

[11] L. Pavão, Conservação de Colecções de Fotografia, Lisboa: Dinalivro, 1997.

[12] C. W. Abney, Photography with emulsions: a treatise on the theory and practical working of gelatine and collodion emulsion processes, New York: Scovill Manufacturing Co., 1882.

[13] R. W. H. Burbank, “Chapter VI: The Old Collodion Process, Wet Plates,” in *The Photographic Negative written as a practical guide*, New York, Scovill Manufacturing Co., 1888, pp. 50-65.

[14] J. Towler, The Silver Sunbeam, New York: Joseph H. Add, 1864.

[15] J. M. Reilly, Care and Identification of 19th century photographic prints, Rochester: Eastman Kodak Compan, 1986.

[16] E. Carretti, "Non-invasive physicochemical characterization of two 19th century English ferrotypes," *Journal of Cultural Heritage*, vol. 10, p. 501–508, 2009.

[17] E. M. Eastabrooke, The Ferrotype and How to Make it, New York: The Antony and Scovill Company, 1880.

[18] P. Maurice, "Ambrotypes: Positively Capturing the Past," *Material History Review*, vol. 38, no. Fall, pp. 50-64, Fall 1993.

[19] K. Whitman, The History and Conservation of Glass Supported Photographs, Rochester: George Eastman House, 2007.

[20] T. Sutton, A Treatise on the Positive Collodion Process, London: Bland & Long, 1857.

[21] 1000 Photo Icons: George Eastman House, Koln: Taschen, 2002.

[22] H. L. Smith, "Photographic pictures on japanned surfaces". Ohio, U.S.A. Patent 14,300, 19 February 1856.

[23] A. K. P. Trask, Practical Ferrotyper, Philadelphia: Benerman & Wilson, 1872.

[24] C. Pfeiffer, "A Descriptive analysis of Ten Painted Tintypes from the George Eastman House Collection," Theses and Dissertations, Paper 1494, Ryerson University, Toronto, 2012.

[25] S. Kasher, America and the Tintype, New York: International Center of Photography, 2008.

[26] P. C. Duchochois, The Photographic Image: a theoretical and practical treatise, New York: Press of William R. Jenkins, 1891.

[27] H. O. Klein, Collodion Emulsion, London: Penrose & Co., 1905.

[28] A. Chipman, J. N. Weber and J. L. Mass, "Inexcusable but appropriate: the technical analysis of hand-painted tintypes from the Smithsonian National Museum of American History and the Winterthur/University of Delaware program in Art Conservation Collections," in *PMG Winter Meeting*, Ottawa, 2011.

[29] H. Henisch and B. Henisch, The Painted Photograph 1839-1914 Origins, Techniques, Aspirations, University Park, PA: The Pennsylvania University Press, 1996.

[30] S. H. Ferguson, "In Living Color: Process and Materials of the Hand Colored Daguerreotype," *The Daguerreian Annual*, pp. 13-18, 2008.

[31] S. Burns, Forgotten marriage: The painted tintype & the decorative frame 1860-1910, New York: The Burns Press, 1995.

[32] H. M. Heden, “Improvement in ferrotype plates”. Worcester, Massachusetts Patent 100291, 1 March 1870.

[33] M. Gillet, C. Garnier and F. Flieder, “Glass Plate Negatives: Preservation and Restoration,” *Restaurator,* vol. 7, no. 2, p. 49–80, 1986.

[34] G. D. Pietro, “Silver mirroring on silver gelatin glass negatives,” Universität Basel, Basel, 2002.

[35] C. E. Rogge, “The varnished truth: The recipes and reality of tintype coatings,” *Journal of Cultural Heritage,* no. 15, p. 57–63, 2014.

[36] L. M. Duncan, “A Technical Study of Five Ruby Ambrotypes,” Winterthur/ University of Delaware Program in Art Conservation, Delaware, 2009.

[37] M. C. Christensen, “FT-IR Techniques for studying the composition and degradation of photographic materials,” Department of Conservation of The National Museum of Denmark, Denmark.

[38] G. Marucci, A. Monno and I. D. v. d. Werf, “Non invasive micro-Raman spectroscopy for investigation of historical silver salt gelatin photographs,” *Microchemical Journal,* no. 117, p. 220–224, 2014.

[39] I. Martina, R. Wiesinger, D. Jembrih-Simbürger and M. Schreiner, “Micro-Raman characterisation of silver corrosion products: instrumental set up and reference database,” *e-preservation science,* vol. 9, pp. 1-8, 2012.

[40] F. S. N. K. A. G. S. Silvia A. Centeno, “The formation of chlorine-induced alterations in daguerreotype image particles: a high resolution SEM-EDS study,” *Applied Physics,* no. 105, p. 55–63, 2011.

[41] C. B. Tragni, “The Use of Ultraviolet-Induced Visible Fluorescence for Examination of Photographs,” George Eastman House, Rochester, 2005.

[42] Y. Leng, Materials Characterization: Introduction to Microscopic and Spectroscopic Methods, Singapore: John Wiley & Sons, 2008.

[43] M. R. Derrick, D. Stulik and J. M. Landry, “Spectral Interpretation,” in *Infrared Spectroscopy in Conservation Science*, The Getty Conservation Institute, 1999, pp. 82-129.

[44] J. Hannavy, Ed., Enciclopedia of Nineteenth-Century Photography, vol. 1, New York: Routledge, 2008, pp. 278, 1093, 1421.

[45] T. Blanton, S. Misture, N. Dontula and S. Zdzieszynski, “In situ high-temperature X-ray diffraction characterization of silver sulfide, Ag2S,” *Powder Diffraction* , vol. 26, no. 2, pp. 114-118, 2011.

[46] D. C. Stulik and A. Kaplan, The Atlas of Analytical Signatures of Photographic Processes: Silver Gelatin, Los Angeles: The Getty Conservation Institute, 2013.

[47] M. McCormick-Goodhart, “Research on Collodion Glass Plate Negatives: Coating Thickness and FTIR Identification of Varnishes,” *Topics in Photographic Preservation,* vol. 3, pp. 135-150, 1989.

[48] S. Berthumeyriea, S. Collina, P.-O. Bussierea and S. Therias, “Photooxidation of cellulose nitrate: New insights into degradation mechanisms,” *Journal of Hazardous Materials,* vol. 272, p. 137–147, 2014.

[49] M. Derrick, “Fourier Transform Infrared Spectral Analysis of Natural Resins Used in Furniture Finishes,” *Journal of the American Institute for Conservation,* vol. 28, no. 1, pp. 43-56, 1989.

[50] I. M. Bell, R. J. Clark and P. J. Gibbs, “Raman spectroscopic library of natural and synthetic pigments (pre ~1850 AD),” *Spectrochimica Acta Part A,* vol. 53, pp. 2159-2179, 1997.

[51] E. Liang, C. Engert and W. Kiefer, “Surface-enhanced Raman scattering of halide ions, pyridine andcrystal violet on colloidal silver with near-infrared excitation: low-wavenumber vibrational modes,” *Vibrational Spectroscopy,* vol. 8, pp. 435-444, 1995.

[52] P. Maurice, “Snippets of History: The Tintype and Prairie Canada,” *Material Cultural Review,* vol. 41, Spring 1995.

[53] C. Johnston, “The Cochineal,” November 2004. [Online]. Available: https://www.ischool.utexas.edu/~cochinea/html-paper/c-johnston-04-hand-coloring.html. [Accessed March 2016].

[54] M. R. Peres, Ed., The Focal Enciclopedia of Photography, Burlington: Elsevier, 2007.

[55] B. Lavédrine, A Guide to the Preventive Conservation of Photograph Collections, Los Angeles: Getty Publications, 2003.

[56] H. Gernsheim, “The Collodion Period,” in *The History of Photography: from the camera obscura to the beginning of the modern era*, Oxford, Oxford University Press, 1969, pp. 231-242.

[57] G. B. Wilmot, “The Raman Spectra and Structure of Silica and the Soda-Silica Glass,” Massachusetts Institute of Technology, Massachusetts, 1951.

[58] C. McCabe, “Preservation of 19th-Century Negatives in the National Archives,” *Journal of the American Institute for Conservation,* vol. 30, no. 1, pp. 41-73, 1991.

[59] A. Shugar, K. Lough and J. J. Chen, “Characterization of a Surface Tarnish Found on Daguerreotypes Revealed under Shortwave Ultraviolet Radiation,” *Materials Research Society*, vol. 1656, 2014.

[60] P. Ravines, K. G. Baum, N. A. Cox, S. Welch and M. Helguera, “Multimodality imaging of Daguerreotypes and development of a registration program for image evaluation,” *Journal of the American Institute for Conservation,* vol. 53, pp. 19-32, 2014.

[61] A. Casoli and S. Fornaciari, “An analytical study on an early twentieth-century Italian photographs collection by means of microscopic and spectroscopic techniques,” *Microchemical Journal,* no. 116, p. 24–30, 2014.

[62] A. C. Neiva, M. A.Marcondes, H. P. F. Pinto and P. A. D. Almeida, “Analysis of photographs and photo-paintings by energy-dispersive X-ray fluorescence spectroscopy,” *Radiation Physics and Chemistry*, no. 95, p. 378–380, 2014.

[63] A. Vila and S. A. Centeno, “FTIR, Raman and XRF identification of the image materials in turn of the 20th century pigment-based photographs,” *Microchemical Journal,* no. 106, p. 255–262, 2013.

[64] B. Cattaneo, D. Chelazzi, R. Giorgi, T. Serena, C. Merlo and P. Baglioni, “Physico-chemical characterization and conservation issues of photographs dated between 1890 and 1910,” *Journal of Cultural Heritage,* no. 9, pp. 277-284, 2008.

APPENDICES

APPENDIX I: reference μ-Raman spectra

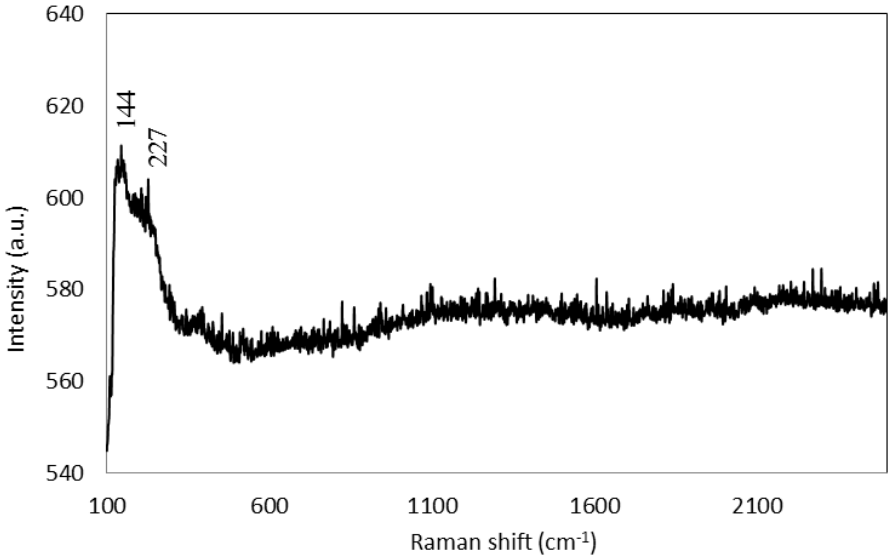

AgCl Raman standard spectrum

APPENDIX II: diffraction peaks

Ambrotype A		
	Ag	AgI
2 Theta		
23.9		23.7
30.5		32.7
38.3	38.2	
39.4		39.2
44.4	44.3	
46.5		46.3
64.5	64.5	
71.4		71.0

Ambrotype B	
	$AgNO_3$
2 Theta	
29.5	28.9
31.6	31.6
34.6	34.6

Tintype A				
	AgI	Fe_3O_4	Fe_2O_3	FeO
22.4	22.3			
23.8	23.7		24.1	
25.4	25.4			
30.4		30.0		
35.4		35.4	35.6	
35.8				36.0
39.3	39.2		39.2	
41.7				41.9
42.7	42.6			
43.7		43.0	43.5	
46.4	46.3			
54.3			54.0	
57.5		57.0	57.5	
60.4	59.3			
62.5	63.0		62.4	
65.0			64.0	
72.4				72.7

Tintype B			
	Ag	AgI	Fe_3O_4
2 Theta			
22.4		22.3	
23.8		23.7	
30.1			30.0
35.5			35.4
38.1	38.1		
39.4		39.2	
43.1			43.0
44.7	44.3		
46.5		46.3	
53.4			53.4
57.0			57.0
62.7			62.5
65.0	64.5		65.7

Brass mats		
	Cu	Zn
2 Theta		
43.0	43.3	43.2
50.2	50.4	
73.9	74.1	73.9